Transformation of Human Melanocytes and Mechanisms of Melanoma Metastasis

by

Piyush B. Gupta

B.S. Mathematics & Biological Chemistry
University of Chicago, 1999

SUBMITTED TO THE DEPARTMENT OF BIOLOGY IN PARTIAL FULFILLMENT OF THE REQUIREMENTS FOR THE DEGREE OF

DOCTOR OF PHILOSOPHY IN BIOLOGY
AT THE
MASSACHUSETTS INSTITUTE OF TECHNOLOGY

FEBRUARY 2006

Signature of Author: _____
Department of Biology
November 15, 2005

Certified by: _____
Robert A. Weinberg
Professor of Biology
Thesis Supervisor

Accepted by: _____
Stephen P. Bell
Professor of Biology
Chairperson, Graduate Committee

Transformation of Human Melanocytes and Mechanisms of Melanoma Metastasis

by

Piyush B. Gupta

Submitted to the Department of Biology on November 15, 2005 in Partial Fulfillment of the Requirements for the Degree of Doctor of Philosophy in Biology

ABSTRACT

While a fundamental feature of human melanoma is its tendency to metastasize to numerous organs throughout the body, very few animal models recapitulate this essential aspect of the disease. In the work described, it is demonstrated that human dermal melanocytes, transformed by the introduction of the SV40ER, hTERT, and RasG12V genes, form primary tumors that are invasive and highly metastatic to secondary sites in the body. Moreover, the anatomical sites of metastasis exhibited by the melanoma cells created in this manner are analogous to those observed in human patients. The introduction of an identical set of genes into human epithelial and fibroblast cell types results in localized tumor formation in the absence of metastasis. These observations indicate that part of the metastatic proclivity of melanoma is attributable to lineage-specific factors expressed in melanocytes but not in other cell types. Analysis of microarray data from human nevi reveals that Slug, a master regulator of neural crest cell specification and migration, correlates in its expression pattern with other genes that are important for neural crest cell migration during development. Moreover, Slug is required for the metastasis of the transformed melanoma cells. These findings indicate that melanocyte-specific factors present prior to neoplastic transformation can play a pivotal role in governing melanoma's progression.

Thesis Supervisor: Robert A. Weinberg
Title: Professor of Biology, MIT; Member, Whitehead Institute for Biomedical Research

Acknowledgments

I have benefited immensely from the insight and support of a great many individuals during my Ph.D. tenure. It is not an exaggeration to state that the work described in this thesis could not have been completed without their assistance. First and foremost, I am indebted to my Ph.D. adviser, Dr. Robert. A. Weinberg, for being an inexhaustible source of support, guidance, and wisdom. I am very fortunate to have been profoundly influenced in innumerable ways, both tangible and intangible, as a consequence of his mentorship over the years. Perhaps I am most grateful for the inspiration that I have drawn from our many scientific discussions.

I am thankful to the members of my thesis committee for providing helpful insights and important external perspectives on my work on a periodic basis. I am particularly grateful to Dr. Philip Sharp for encouraging my interests in bridging the world of mathematics and molecular biology at a critical juncture in my graduate career. Without his support it is quite likely that my current path would have been different from the one I find myself on today.

I thank Homayoun Vaziri, Scott Dessain and Akira Orimo for the many philosophical discussions we have enjoyed together. I thank Sheila Stewart for her irrepressible optimism and enthusiasm. I am grateful to Bill (Ante Sven) Lundberg for introducing me to the world of laboratory experiments, technique, and design. I am also grateful to many members of the Weinberg laboratory who have provided valuable technical advice and reagents, including (but not limited to) Sendurai Mani, Charlotte Kuperwasser, Scott Dessain, Ittai Ben-porath, Jing Yang, Akira Orimo, and Elinor Eaton. Thanks are due as well to Tony Chavarria and Ferenc Reinhardt for their expert

assistance with animal experiments, and to Jeanne Winston for the dedication and attention with which she addressed the lab's tissue culture needs.

There are many collaborators that have been instrumental in making possible the work described in this thesis. I have tried to acknowledge these individuals as appropriate throughout the text of the thesis. I would like to extend a special thanks to Charlotte Kuperwasser, with whom I have collaborated with on several projects, for the energy, dedication and integrity with which she approached our joint scientific work. I am grateful to Dr. Stephen Naber for is generosity in examining countless histology slides and for his kind encouragement along the way.

I would like to thank Betsey Walsh in the Biology Office for her dedication to helping we students navigate the many administrative requirements associated with graduate study; her attentiveness has saved me (as I am sure it has many others) from administrative quagmires on many an occasion over the years. I also thank Christine Hickey and Maria Pavao for providing helpful administrative assistance closer to my lab home-base.

I would like to especially thank my close friend Chuck who has provided me with support, advice and motivation that was invaluable for my success.

Finally, I would like to thank the members of my immediate family; my parents, Suman and Sudhir, my brother, Gaorav (Pankaj) and my sister, Namita, for their continued support and interest in my work and other activities. I am also grateful to my maternal grandparents, Banwari Lal & Santosh Gupta, for their unwavering support and wisdom.

The difficulty with constructing boundaries is that they have no true existence outside of the mind and therefore are indicative of nothing more than a perceived reality. Nonetheless, it is a fact that this thesis is finite, both in space and in time. Being a subset of a finite entity, this current subsection shares in this unfortunate quality. It is in this spirit that I close, acknowledging my awareness that the finite space and time allotted to this section has enabled me to thank only a very small minority of the many people to whom I truly owe an enormous debt of gratitude. To those I've not mentioned, I say this: you know who you are. As do I.

Table of Contents

Chapter 1

Introduction

To the force within us that appeals to a higher truth and to all those that live their lives in accordance with that force. Melanoma is a highly aggressive disease that frequently spreads to numerous organs in the body. There are currently no effective therapies for treating melanoma, once it has spread. This work describes the establishment and characterization of a novel model of human metastatic melanoma and elucidates one mechanism by which melanoma is intrinsically predisposed to spread.

Melanocytes

Melanoma arises from the neoplastic transformation of a highly specialized cell type called the melanocyte. Human eyes, hair and skin obtain their coloration via pigment deposition and synthesis by this highly specialized cell type. Skin, which is the largest and most prominent epithelial organ, is routinely faced with unique challenges by virtue of its constant exposure to toxic elements found in the environment. The deposition of pigments, or melanins, by melanocytes confers protection from one ubiquitous external stressor: ultraviolet radiation (UV) damage resulting from sun exposure (Chedekel and Zeise 1988). In the skin, melanocytes are in the minority, being outnumbered ~30-35-fold by keratinocytes. Located at or immediately below the basal epithelial layer of the skin, melanocytes project dendritic processes that ramify apically through the keratinocyte layers and transfer packets of melanins to adjacent keratinocytes via organelles called melanosomes (Kanitakis 2002). Once transferred, melanosomes exhibit an apical peri-nuclear distribution in the recipient keratinocytes (Boissy 2003), strongly suggesting that their primary function is to confer protection to keratinocytes from DNA damage due to sun exposure.

While melanocytes express E-cadherin and readily form heterotypic adherens junctions with neighboring keratinocytes, they are incapable of forming homotypic junctions (Jouneau et al. 2000). The molecular basis for this self-aversion is unknown. In principle, this phenomenon could be due to the lack of an essential cofactor for adherens junction formation within the melanocyte. However, E-cadherin transfection into NIH3T3 cells suffices to induce their self-association, indicating that it may be more likely that there are unique membrane proteins that specifically repel melanocytes from one another. Thus, despite expressing E-cadherin and forming adherens junctions, melanocytes are neither epithelial nor mesenchymal cells and are perhaps best viewed as an intermediate cell type exhibiting properties of both. In fact, in addition to expressing the epithelial marker, E-cadherin, melanocytes express the mesenchymal marker, vimentin (Si et al. 1993).

Dermal melanocytes differentiate from a remarkable cell population that is transiently present during embryogenesis, called the neural crest (Dupin and Le Douarin 2003). Neural crest cells, which are unique to the vertebrate evolutionary lineage, are specified bilaterally on the dorsal-lateral sides of the neural tube. Ultimately, the neural crest cells give rise to a number of differentiated cells types in adult tissues, including dermal melanocytes, glial cells, schwann cells, and many others (Christiansen et al. 2000b). A feature that these cells manifest during the normal course of development is a unique ability to migrate from regions adjacent to the neural tube, where they are originally specified, to distant regions in the embryo (Christiansen et al. 2000a). Many of the phenotypes that neural crest cells exhibit during their migration, as well as the

extracellular and intracellular factors that regulate these tightly controlled migrations, have also been implicated in the cancer cell invasion and metastasis.

Phenotypic characteristics shared by both neural crest cell migration and cancer cell invasion include: (1) a switch from E-cadherin expression to N-cadherin expression, (2) the stimulation of migration by extracellular fibronectin, (3) an expression of members of the Snail superfamily of transcription factors (which includes Slug and Escargot), which functionally mediate the invasive behavior, (4) the functional role of rho family GTPases in mediating invasive behavior, and (5) induction of matrix metalloproteinase expression. In light of these and other striking similarities, the mechanisms by which neural crest cells migrate during normal development have been of significant interest to cancer researchers, since these mechanisms may provide a unifying perspective on the seemingly diverse devices that cancer cells utilize to acquire metastatic competence.

In addition to having consequences for our understanding of metastasis in general, the characteristic migratory ability displayed by the normal precursors of dermal melanocytes is of relevance to our understanding of the metastatic properties of cutaneous melanoma in particular. The factors underlying the clinical course of this disease, which frequently displays malignant behavior, remain a complete mystery. It has been proposed that the proclivity for metastatic behavior demonstrated by cutaneous melanoma may be attributable in part to the uniquely migratory properties that neural crest cells display during development. However, this hypothesis has been difficult to evaluate experimentally, in large part due to the uncharacterized genomic variations present in laboratory tumor models, making it impossible to determine which tumor

phenotypes are due to genomic differences and which phenotypes are due to epigenetic or differentiation-specific differences. Many of the experiments described in this thesis use a novel model of human melanoma to address the validity of this hypothesis.

Melanoma

A significant amount is known about the genomic aberrations that are present in cutaneous human melanoma. Since melanomas arising in other organs often have very different characteristics, I focus here on cutaneous melanoma. Melanoma is an example of a sporadic cancer that often exhibits deletions of p21 locus on chromosome 9, which harbors the *INK4* loci (Pollock et al. 2001b). In cases with a familial history, missense mutations are often observed at the *INK4a* locus, a subset of which segregate with the disease (Pollock et al. 2001a). In this regard, it is interesting to note that nonsense mutations are very rarely observed in familial cases, whereas nonsense mutations have been observed in over 50% of cultured melanoma lines that have altered the wildtype INK4a sequence. Deletions at this locus frequently encompass both *INK4a/ARF* and *INK4b*. The functional role of p16, which regulates the pRb tumor suppressor pathway, in melanomagenesis has been experimentally demonstrated using mouse models (Chin et al. 1997; Tolleson et al. 2005; Ackermann et al. 2005a; Bardeesy et al. 2001b; Chin et al. 1999; Tietze and Chin 2000; Chin 2003) . While convincing experimental evidence has accumulated implicating *INK4a/ARF* in tumor suppression, the evidence for a role of INK4b is significantly weaker. Nevertheless, there remains a lingering possibility that the INK4b gene product might also be relevant in suppressing melanoma due to its co-deletion with the INK4a/ARF locus and the observation that p15INK4b-deficient mice display a weakly tumor-prone condition. However, it would seem more likely that the

co-deletion of the INK4b locus is a reflection of the physical structure of the neighboring genome, where deletion of both loci is more readily accomplished than the deletion of INK4a/ARF alone.

The p16 and ARF proteins play diverging roles in melanomagenesis in mice and man, with the former being more important for human melanoma and the opposite holding true in the mouse (Chin 2003). Point mutations have been characterized in melanoma-prone families that only disrupt the p16 protein (leaving p19ARF intact), providing strong evidence that this protein is the key tumor suppressor in humans at this locus, and that the concomitant loss of the p14ARF protein, while certainly beneficial, is not a requirement. In contrast, mice that are null for p19ARF exhibit a tumor susceptibility condition that closely phenocopies that of mice doubly null for both INK4a and p19ARF, suggesting that p16 provides little additional benefit in the murine context. In support of this notion, melanomas that arise in mice expressing a mutant allele of *H-ras* under control of a melanocyte-specific promoter on a p53-deficient background fail to exhibit disruptions at the INK4a locus, with demonstrably normal p16 protein activity. These findings reveal an important fundamental difference between the pathogenetics of melanoma in humans and mice. Along the same line, mice in which the INK4a/ARF locus has been deleted do not contract melanoma with any appreciable frequency, again demonstrating a significant difference between mice and humans.

It is worth noting that there are other significant differences in the biology of normal melanocytes between humans and mice. For example, while melanocytes are interspersed throughout the basal layer of the epidermis in human skin, melanocytes in mice are only present within hair follicles embedded in the dermis, with none in the

epidermis. Thus, "black" mice have a black hair color but skin that is wholly devoid of pigment. These observations, of which more of the same sort can be made, highlight some fundamental differences between humans and mice in the biology of melanocytes and pathobiology of melanoma and provide a compelling rationale for the importance of developing human cell-based models of melanoma.

For some years, there was a debate over the prevalence of *ras* mutations in melanoma, with estimates ranging from 5-25% (Reifenberger et al. 2004; van, V et al. 1989; Omholt et al. 2002). It was later discovered that a significantly higher frequency of mutations were found in melanoma cell lines (~24%) than in melanoma cells that had never been cultured (~5%) (Gorden et al. 2003). In spite of these uncertainties, a role for the Ras-MAPK pathways was unambiguously demonstrated by the observation that activating *BRAF* mutations frequently occur in human melanoma tumors, with frequencies approaching 60% (Shinozaki et al. 2004; Yazdi et al. 2003b). Moreover, *BRAF* mutations are essentially mutually exclusive with mutations in *NRAS* (Papp et al. 2005; Omholt et al. 2003a; Goydos et al. 2005), indicating functional redundancy with respect to tumorigenesis (there is evidence to suggest that N-Ras mutations may be more prevalent among metastatic nodules, suggesting a potentially independent contribution to progression beyond that provided by B-RAF). Quite remarkably, the frequency of BRAF mutations in normal nevi was also ~60% (Yazdi et al. 2003a; Kumar et al. 2004), indicating that while MAPK pathway activation may be important for nevus formation, the subsequent development of melanoma requires additional oncogenic lesions. Consistent with this notion is the finding that MAPK phosphorylation is observed in early stage human melanomas (Omholt et al. 2003b; Cohen et al. 2002). Also in support of this

idea is the observation that the expression of mutant Ras under a melanocyte-specific promoter is able to provoke melanoma formation in mice that lack the INK4a locus (Bardeesy et al. 2001a; Ackermann et al. 2005b).

An effect of cell culture on the selection of particular mutations was discovered for melanoma in a second significant context; stabilizing mutations in the beta-catenin gene were observed in 20-25% of cultured melanoma lines but rarely observed in human tumors (Rubinfeld et al. 1997). Nevertheless, there is clinical evidence to support a role for the Wnt pathway in human melanoma, as a focal pattern nuclear beta-catenin staining has been observed in approximately one-third of human melanoma tumors (Rimm et al. 1999).Activation of the canonical Wnt pathway may be associated with progression, since nuclear beta-catenin is observed more frequently in vertical growth phase melanomas relative to radially growing melanomas and in metastatic tumors compared to primary melanomas (Demunter et al. 2002a). While APC deletions in melanoma are rare, a recent report has indicated that APC promoter methylation occurs in ~17% of primary melanomas. However, the signals responsible for the activation of beta-catenin in melanoma are not yet fully characterized. In addition to canonical Wnt signaling, Wnts that do not signal via beta-catenin have also been implicated in both neural crest cell and melanoma biology. Experiments with disheveled mutants that decouple canonical and non-canonical Wnt signaling have revealed that while beta-catenin activity is essential for neural crest specification, subsequent migration of the neural crest is regulated by Wnt11, which does not require beta-catenin activation (De et al. 2005). However, there is also evidence to suggest that beta-catenin-mediated signaling is important for the delamination of premigratory neural crest cells (Burstyn-Cohen et al. 2004).

Interestingly, non-canonical Wnts have also been implicated in the motility and invasiveness of melanomas (Weeraratna et al. 2002).

Chapter 2

Generation and Characterization of Melanoma Cells[1]

[1] Unless stated otherwise, the work in this thesis is my own personal contribution. Collaborative efforts are indicated as appropriate in either the text or as footnotes. The work in this chapter has appeared in a published manuscript (Piyush B. Gupta, Charlotte Kuperwasser, Jean-Philippe Brunet, Sridhar Ramaswamy, Wen-Lin Kuo, Joe W. Gray, Stephen P. Naber, Robert A. Weinberg. **The melanocyte differentiation program predisposes to metastasis following neoplastic transformation.** *Nature Genetics.* (2005) Oct;37(10):1047-54).

Introduction

Previous work has elucidated a series of intracellular signaling pathways whose simultaneous perturbation suffices to convert a variety normal primary human cell types to a neoplastic state (Hahn et al. 1999b; Elenbaas et al. 2001a; Lundberg et al. 2002). Using this approach, researchers have experimentally generated cancers derived from primary human fibroblasts, mammary, lung and prostate epithelial cells, embryonic kidney cells and neuronal cells. This has been accomplished by the introduction of genetic elements that (a) disrupt the p53 and pRb tumor suppressor pathways, (b) maintain telomere length, (c) constitutively activate the Ras pathway, and (d) perturb a (currently uncharacterized) subset of the functions of the PP2A phosphatase. The modifications (a, b) together allow human cells to proliferate indefinitely in culture, and (c, d) drive the immortalized cells into a tumorigenic state. The constellation of genetic elements originally used in these experiments to perturb the four pathways indicated above included the Simian Virus 40 Early Region (SV40ER), which encodes the Large T (LT; (a)) and small t (st; (d)) oncoproteins, the catalytic subunit of the human telomerase holoenzyme (hTERT; (b)), and an oncogenic allele of *H-ras* (c). Experiments in which substitutions have been made of these various genetic elements have demonstrated that it is the perturbation of the intracellular pathways indicated (a-d) above and not the particular choice of genetic elements that is relevant for transformation (Boehm et al. 2005)

One proposed explanation for the intrinsic proclivity of melanoma for metastasis is based on the derivation of dermal melanocytes from the embryonic neural crest cell population. Thus, it has been suggested that molecular pathways that mediate neural

crest cell migration may be latent in the melanocyte lineage and are activated following neoplastic transformation. The question of whether factors associated with the melanocyte cell type of origin can influence melanoma's metastatic behavior has been difficult to address experimentally. In fact, since established cancer cell lines harbor numerous uncharacterized genomic alterations, it is impossible to determine whether any phenotypic differences between tumors arising from these cell lines are due to differences in oncogenic lesions or a consequence of differences in originating cell types. Therefore, to examine the effects of cell type-specific factors on melanoma phenotypes (including metastatic behavior), it is essential to devise a method that controls for phenotypic variations arising from differences in oncogenic lesions.

To effectively control for oncogene-specific differences in tumor phenotypes I exploited the transformation scheme described above, which makes possible the neoplastic transformation of primary human cells through the introduction of a defined set of genetic elements. Since this procedure generates cancer cell lines transformed with an identical set of genes, variations in tumor phenotypes arising from genetic differences between cancer cell lines are effectively minimized. A variety of human cell types transformed in this manner generate localized tumors in the absence of metastasis. In this chapter, I contrast the properties of melanoma cell lines that were generated from primary melanocytes via the introduction of defined genetic elements with other cancer types generated in an identical manner.

Retroviral transduction of primary human melanocytes and tumor formation

Primary human foreskin melanocytes at passage 3 were purchased from the Yale Tissue Culture Core facility. These cells exhibited hallmarks of melanocytes in culture.

Some of these unique characteristics include: (1) black pigmentation, visible under phase-contrast microscopy or upon centrifugation, (2) a highly differentiated morphology having 2-3 dendritic processes per cell, and (3) a highly refractile cell body. In order to passage these cells, which undergo a p16-mediated growth arrest after 14-16 population doublings (PDs), I introduced the SV40ER into the primary cells using retroviral infection. At this stage of genetic modification, the melanocytes lost their apparent pigmentation and highly differentiated morphology. The ability of LT to induce de-differentiation has been established in several different systems (Prince et al. 2001; Diamandopoulos et al. 1976; Bond et al. 1996), and in particular it has been demonstrated that LT-mediated immortalization of murine melanocytes is accompanied by de-pigmentation (Prince et al. 2001). Following the SV40ER, I introduced the hTERT cDNA, which resulted in immortalized melanocytes that proliferate indefinitely in culture. At this point, the melanocytes did not display any features associated with neoplastic transformation; these cells failed to generate either anchorage-independent colonies in soft agar culture (Figure 2) and also were incapable of forming tumors in immunocompromised animals *in vivo* (Figure 3).

I subsequently introduced an oncogenic Ras protein (RasG12V) into the immortalized melanocytes, yielding Mel-STR cells[2]. Introduction of oncogenic RasV12

[2] A note on the nomenclature used in this thesis for experimentally generated cancer cell lines. Cell type is indicated by a 2- or 3-letter abbreviation, such as Mel for melanocyte, MEC for mammary epithelial cell and BJ for foreskin fibroblasts. This is immediately followed by a hyphen and then several letters in capital corresponding to the introduced genetic elements, and listed from left to right in the temporal order of retroviral infection. The letters correspond to: S=SV40ER, T=hTERT, R=RasV12, M=TPR-Met, H=HGF, G=GFP, and V=empty vector. For example, Mel-STM is the cell line created by sequentially introducing SV40ER, hTERT, and TPR-Met into primary melanocytes. As another example, Mel-SVV corresponds to the cell line created by introducing SV40ER and then two empty vectors into primary melanocytes.

Figure 1 (a) Signaling pathways implicated in melanoma formation *in vivo* in humans and using murine models. (b) Schematic depiction of the sequential retrovirus infection protocol used to transduce primary human cells. (c) Western blots of retrovirus-transduced primary human melanocytes, showing expression of the LT, Ras, and TPR-met proteins in primary and engineered cell lines.

(a)

Signaling Pathways Implicated in Melanocyte Transformation

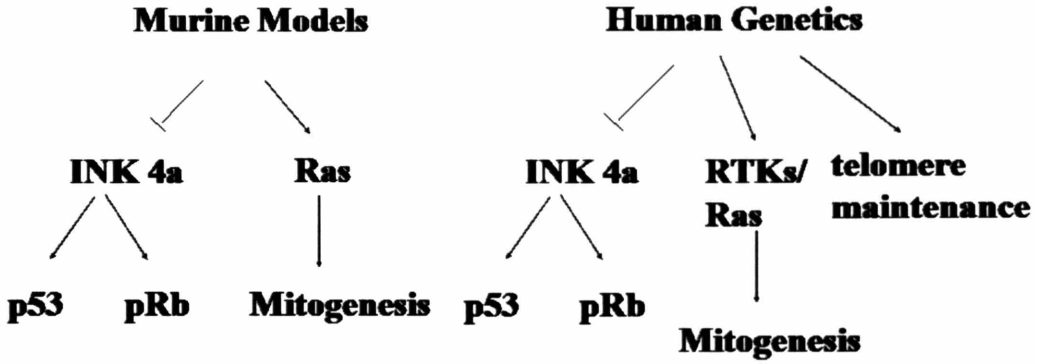

(b)

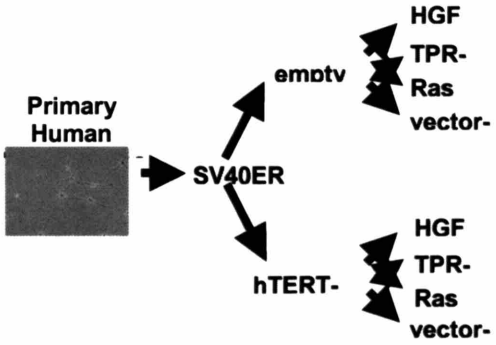

(c)

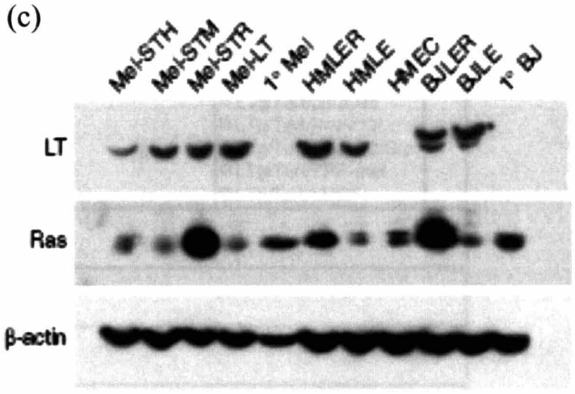

Figure 2 Anchorage-independent colony formation assays of engineered melanocyte (Mel) cell lines. (a) Assays were performed in triplicate for each cell line shown and a representative field photographed. (b) Quantification of soft agar colony formation experiment in (a). Error bars indicate standard errors about the mean. Expression of the SV40ER and hTERT, together with either RasV12 or TPR-met is required for efficient colony formation in suspension culture.

(a)

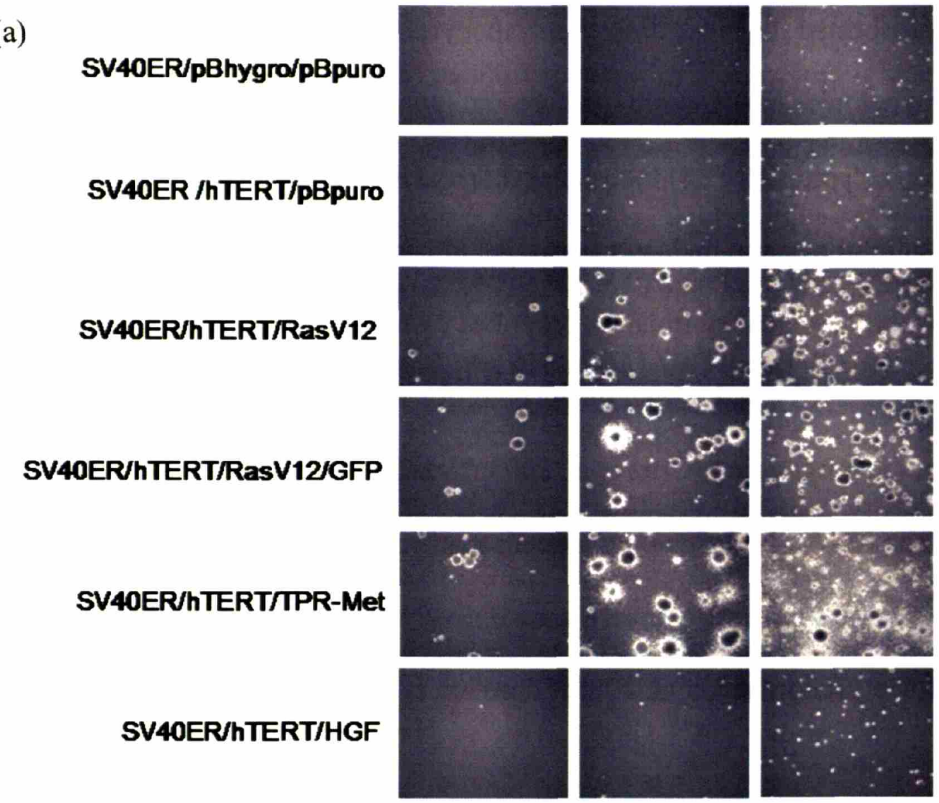
SV40ER/pBhygro/pBpuro
SV40ER /hTERT/pBpuro
SV40ER/hTERT/RasV12
SV40ER/hTERT/RasV12/GFP
SV40ER/hTERT/TPR-Met
SV40ER/hTERT/HGF

(b)

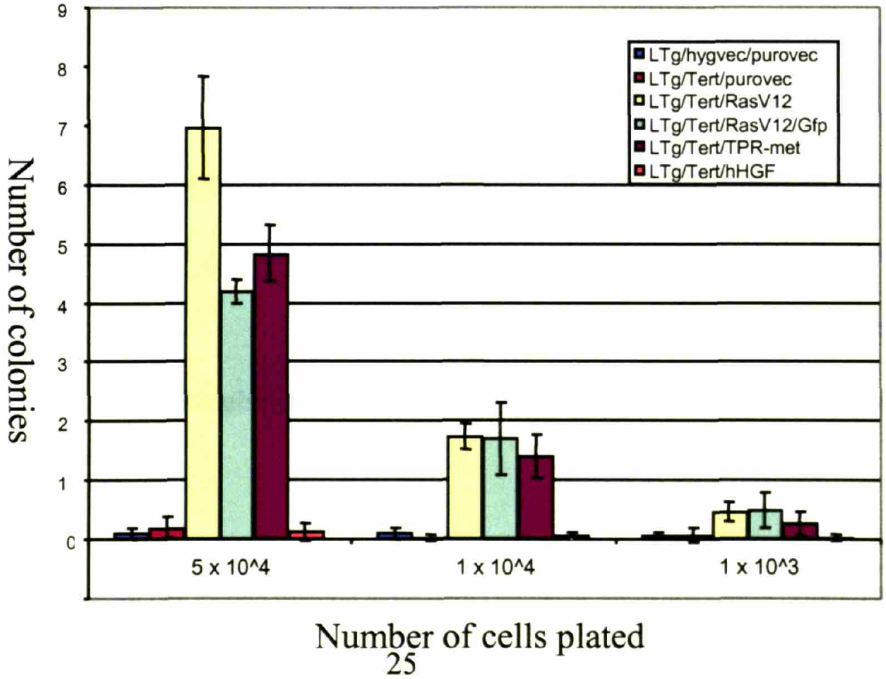
LTg/hygvec/purovec
LTg/Tert/purovec
LTg/Tert/RasV12
LTg/Tert/RasV12/Gfp
LTg/Tert/TPR-met
LTg/Tert/hHGF
Number of colonies
0
1
2
3
4
5
6
7
8
9
5 x 10^4
1 x 10^4
1 x 10^3
Number of cells plated

efficiently transformed the immortalized melanocytes cells, as demonstrated by their ability to form colonies in suspension culture and tumors *in vivo* (Figures 2, 3). Several tyrosine kinase receptors (RTKs) that signal (in part) through the Ras-MAPK pathway have also been implicated in melanomagenesis. In particular, melanoma cell lines frequently exhibit autocrine stimulation provoked by hepatocyte growth factor (HGF) secretion (Li et al. 2001), and c-Met, the receptor for HGF, is frequently upregulated during melanoma progression (Cruz et al. 2003; Natali et al. 1993). To test whether activation of the HGF-c-Met signaling loop also suffices to provide the proliferative signal for transformation, I introduced a constitutively active form of the c-Met receptor (termed TPR-Met) (Giordano et al. 1989; Giordano et al. 1997) into the immortalized human melanocytes.

TPR-met was able to substitute for RasV12 in enabling the melanocytes to become transformed, as indicated by the ability of these Mel-STM cells to form colonies in suspension *in vitro* and tumors *in vivo* (Figures 2, 3). In contrast, ectopic over-expression of HGF, which should generate a c-Met autocrine growth-stimulatory loop, failed to transform the immortalized melanocytes (Figure 2). Hence, while HGF over-expression increased the *in vitro* proliferation of the melanocytes (data not shown) and increased survival of minute colonies in soft agar (Figure 2), tumor formation was not observed *in vivo*.

Histology and immunohistochemistry of Mel-STR melanomas[3]

[3] The pathological evaluation of the generated melanoma primary tumors and metastases was conducted by Dr. Stephen P. Naber of the Tufts-New England Medical Center and the Department of Pathology at Tufts University School of Medicine.

Examination of histological sections of primary tumors generated by the Mel-STR and Mel-STM cells revealed growths exhibiting characteristics of high-grade, well-vascularized, epithelioid, amelanotic melanomas (Figure 3). Clinical tumor samples are routinely diagnosed as melanomas by immunohistochemical staining for melanoma-specific markers as well as the absence of staining for cytokeratins. Indeed, the Mel-STR tumors stained positively for the melanoma markers MART-1 and vimentin, and lacked

Figure 3 **a**, Table of primary tumor formation; **b**, Tumor growth curves in vivo of transformed melanoma cell lines; **c**, Hematoxylin & eosin staining, and MART-1 and pan-cytokeratin immunostainings of histological sections prepared from engineered subcutaneous mammary epithelial cell (MEC-STR) and melanoma (Mel-STR) tumors.

(a)

		Mel-STR	***Mel-STV***	***MEC-STR***	***BJ-STR***
1° Tumor		93/93	0/12	21/21 (S) 20/20 (O)	21/21

(b)

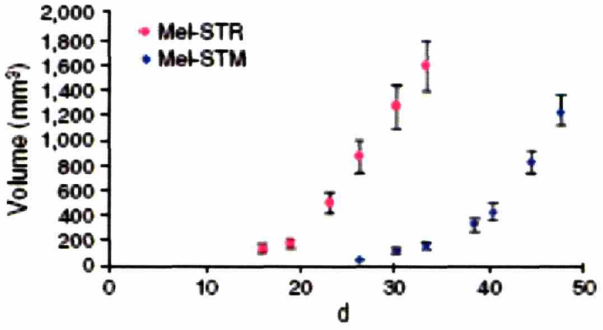

(c)

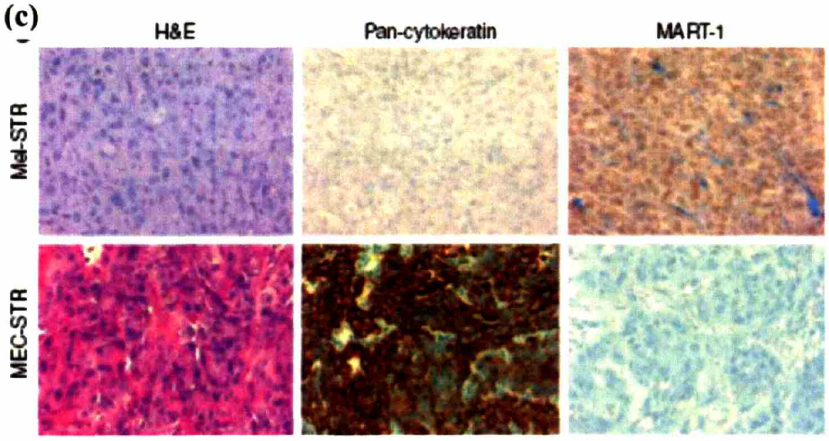

Figure 4 Immunohistochemical staining of subcutaneous Mel-STR melanomas. Tissue sections of paraffin-embedded tumors were stained with beta-catenin and E-cadherin antibodies to examine the integrity of adherens junction components *in vivo*. Mel-STR melanomas neither expressed E-cadherin protein nor exhibited membranous beta-catenin staining, which was instead weakly cytoplasmic and nuclear. Large T antigen staining of the tumor sections revealed individual melanoma cells that had invaded into the overlying dermis, indicating the locally invasive nature of these tumors. Hematoxylin & Eosin stained sections are also shown.

High Magnification: (400x)

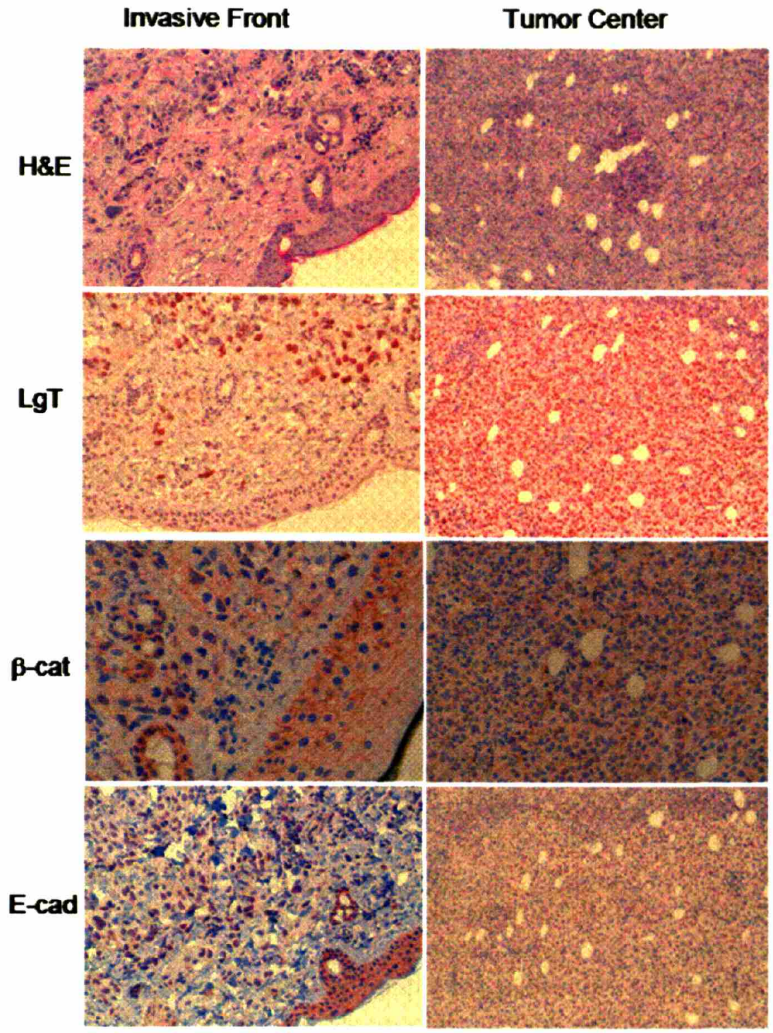

Low Magnification: (40x)

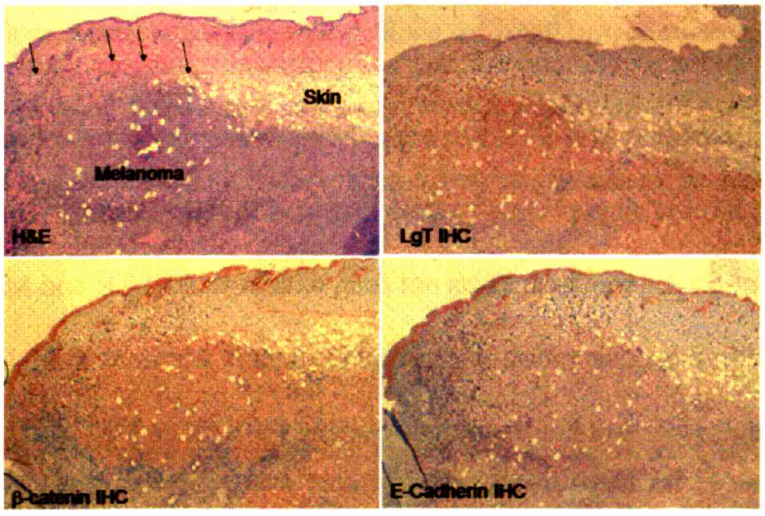

expression of cytokeratins (Figure 3). In contrast, human mammary epithelial cells transformed through the introduction of the identical set of genes (MEC-STR cells) were negative for MART-1 expression and stained positively for cytokeratins (Figure 3).

As discussed in Chapter 1, the disruption of adherens junctions frequently accompanies melanoma progression (Demunter et al. 2002b; Kageshita et al. 2001). To examine whether adherens junctions were intact in Mel-STR melanomas, I used immunohistochemistry to stain melanoma tumor sections for E-cadherin and β-catenin expression. I observed that the Mel-STR melanomas, unlike normal melanocytes, did not express E-cadherin, and exhibited weak membranous and cytoplasmic staining for β-catenin (Figure 4). Since the Mel-STR cells were injected subcutaneously rather than within the dermis, it is important to mention that this staining pattern might be dependent upon the tumor cell microenvironment.

Staining for the SV40 LT antigen revealed that there were a significant number of regions in the tumors that contained cells that did not express the LT protein and were therefore recruited stromal cells of murine origin (Figure 4). Histological examination revealed that these latter cells were frequently associated with regions of inflammation and necrosis and were composed largely of neutrophils (data not shown). LT staining also demonstrated that Mel-STR tumors growing within the subcutaneous space frequently exhibited single cells invading upwards into the dermis. This observation was unique to Mel-STR tumors, and was not seen with both BJ-STR and MEC-STR tumors. Consistent with this observation, ulceration frequently occurred in Mel-STR tumors at relatively small sizes, but not in animals bearing BJ-STR or MEC-STR tumors. These

findings indicated that the Mel-STR tumors were locally invasive, and it was natural to ask whether these melanomas were also capable of metastasizing to distant organs.

Transformed melanoma cells form metastatic tumors *in vivo*

I undertook an extensive anatomical analysis at necropsy of the organs in melanoma-bearing mice in order to determine whether macroscopically visible metastases develop in mice following subcutaneous injection of Mel-STR melanoma cells. To facilitate visualization of metastases in these animals, I used Mel-STR cells into which the green fluorescent protein (GFP) sequence had been introduced using retrovirus infection (Mel-STRG cells). Mice were sacrificed when they appeared moribund, which occurred in the majority of mice approximately 6-8 weeks after the initial injection of transformed cells.

I observed numerous mice with widespread metastatic dissemination. Metastatic nodules were observed in 92% of mice bearing Mel-STR tumors, most commonly in the lungs (92%) and lymph nodes (29%), as well as in the liver (27%), spleen (22%), and small bowel (12%) (Figure 5; Table 1). There were no consistent, apparent differences in the histologies of metastatic growths relative to the corresponding primary tumors. In cases where mice bore metastases in the liver, spleen, or small bowel, metastatic burden was also invariably present in the lungs. This observation suggested the possibility that lung metastases may serve to further disseminate additional metastases to other organs in these animals[4].

[4] Additional experimental observations that support this interpretation are discussed in Chapter 3 of this thesis. In brief, the resection of primary tumors at an early stage of growth results in the formation of metastases in the lungs, albeit fewer in number and size relative to what would be expected if the primary

Figure 5 Primary Mel-STR melanomas give rise to widespread metastases *in vivo*. Immunocompromised NOD/SCID mice were injected subcutaneously with $5x10^5$ GFP-labeled Mel-STR cells. Organs were harvested at necropsy and were immediately visualized for GFP epifluorescence, or fixed for subsequent paraffin embedding. Images of whole-organs (a,c,e,g) and H&E-stained sections (b,d,f,h) were captured of lungs, livers, spleens, and small intestines taken from representative metastasis-bearing mice. Dashed lines demarcate tumor cell regions. M, metastasis; OP, organ parenchyma; CE, colonic epithelium; BV, blood vessel; LN, lymph node; Intest, small bowel. Arrows in h indicate a front of melanoma cells invading from the outside surface of the small bowel, through the *muscularis propria,* into the colonic epithelium.

---

tumor had never been resected. In these animals, in which the primary tumors had been resected, metastases were only observed in the lungs and not in any other organs. This finding is consistent with the notion that lung tumor burden facilitates metastatic dissemination to other visceral organ sites.

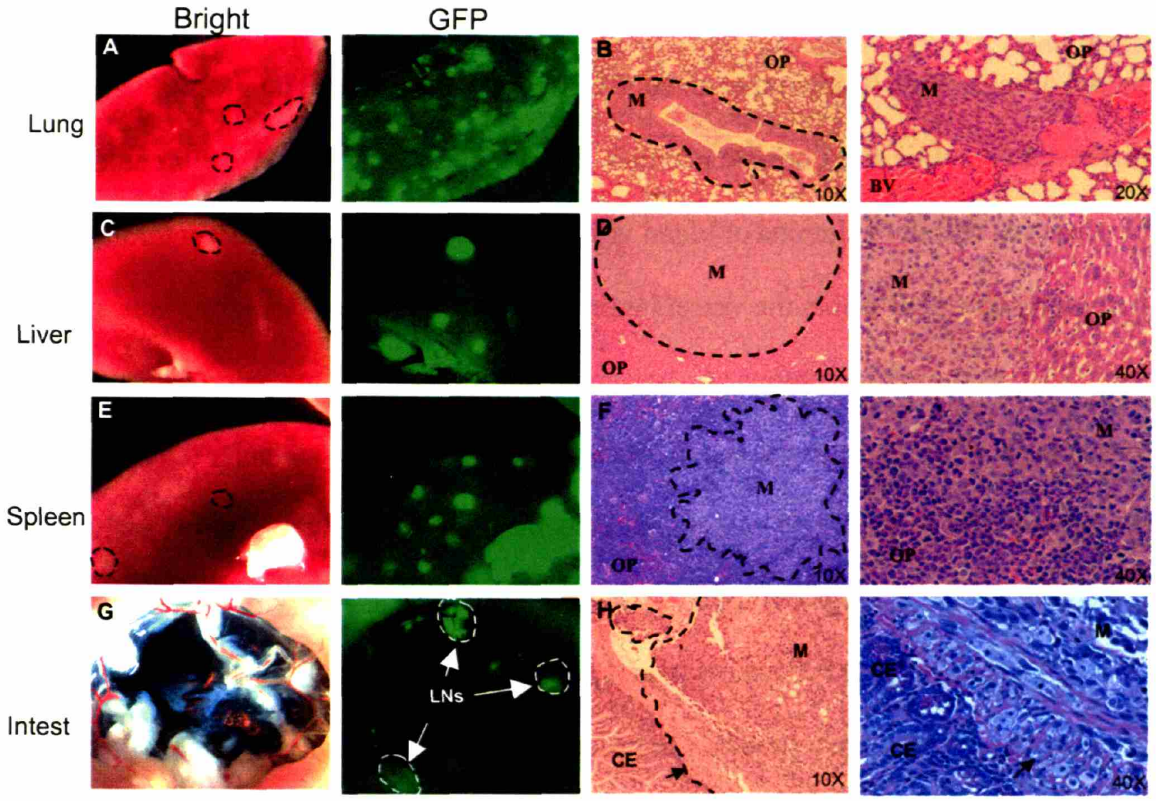
Bright
GFP
Lung
Liver
Spleen
Intest
A
B
C
D
E
F
G
H
OP
M
BV
CE
LNs
10X
20X
40X

Histological examination of metastasis-bearing lungs revealed that metastatic melanomas frequently encapsulated and grew along the lung vasculature (Figure 5). This type of growth in the lungs has been demonstrated previously using a syngeneic mouse model of melanoma (Cameron et al. 2000). Metastasis-associated lung vessels invariably displayed vasculitis and fibrinoid necrosis. In certain cases, melanoma cells could also be observed within the lumina of blood vessels. In such cases, tumor fibrin thrombi were frequently observed within the vessel lumina. Together, these observations indicated a significant host clotting response to melanoma cells within the lung parenchyma and vasculature. The vascular association of metastatic growths, in particular the presence of melanoma cells within blood vessels, suggests that the Mel-STR tumors are capable of disseminating to the lungs through a hematogenous route.

The lymph node metastases mentioned above were located adjacent to the growing tumor mass, most probably representing nodes that were associated with the lymphatic drainage from the site of implantation. In a subset of mice, I also observed Mel-STR metastases in the axillary lymph nodes of the animals. Notably, in cases of axillary lymph node metastasis, the growths were observed exclusively (8/8 cases; Table 1) on the side of the mouse ipsilateral to the original site of injection. Since this pattern of growth parallels the flow of the lymphatic fluid, it is reasonable to conclude that the melanoma cells reached the axial lymph nodes through a lymphatic rather than hematogenous route. Taken together with the discussion in the previous paragraph, these observations suggest that the subcutaneous Mel-STR melanomas are capable of metastasizing to various degrees using both lymphatic and hematogenous vessels.

Table 1 Primary tumor formation and secondary metastasis. Incidence of tumor formation and metastasis in mice subcutaneously injected with melanocyte (Mel-STR), mammary epithelial cell (MEC-STR) and fibroblast (BJ-STR) cells engineered to express the SV40ER, hTERT and RasV12. Also shown are melanocytes expressing the SV40ER, hTERT and a vector control (Mel-STV). S,O indicate subcutaneous and orthotopic injections, respectively. NA, not applicable.

1º Tumor		***Mel-STR***	***Mel-STV***	***MEC-STR***	***BJ-STR***
		93/93	0/12	21/21 (S) 20/20 (O)	21/21
Metastasis	***Any organ***	85/93	NA	1/21 (S) 0/21 (O)	0/21
	Lung	85/93	NA	1/21 (S) 0/21 (O)	0/21
	Liver	25/93	NA	0/21 (S,O)	0/21
	Spleen	21/93	NA	0/21 (S,O)	0/21
	Small bowel	11/93	NA	0/21 (S,O)	0/21
	Lymph nodes	27/93	NA	0/21 (S,O)	0/21

Figure 6 Gross morphology of Mel-STR metastasis-laden organs. Photographs of livers (**a**,**b**) and spleens (**d**,**e**) harboring numerous metastases in mice bearing subcutaneous Mel-STR primary tumors. Liver (**c**) and spleen (**f**) from a tumor-free control mouse are also shown.

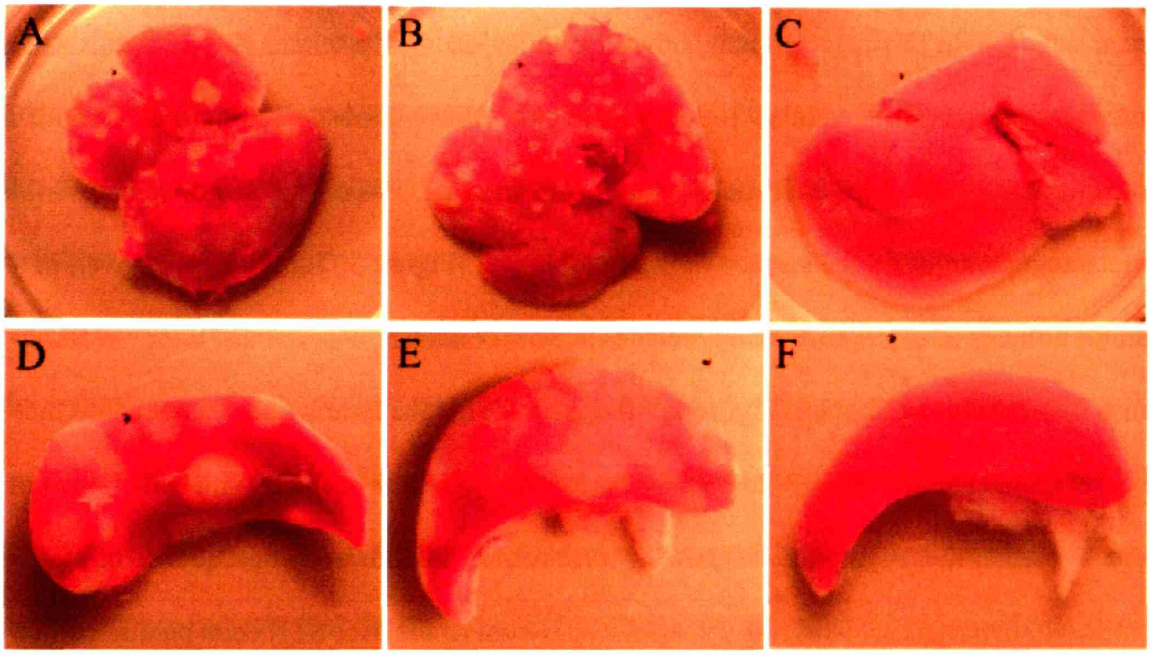
A
B
C
D
E
F

Intestinal metastases are a rare occurrence for human cancers that arise outside of the peritoneal cavity. Such metastases, which occur on the topologically internal (non-luminal) surface of the intestines, are most usually discovered upon laparoscopic examination. In this respect, melanoma is peculiar, as it has a tendency to metastasize to the small bowel (Elsayed et al. 1996; Phillips et al. 1987). I observed that this behavior is recapitulated in the Mel-STR melanoma model, and that 11% of injected mice had visible metastatic nodules on the surface of the small bowel (Figure 5; Table 1). Moreover, in a small number of cases, metastatic melanoma cells could be observed that were invading into the small bowel lumen (Figure 5). It appeared that the lymph nodes adjacent to the bowel metastases were GFP-labeled, indicating the presence of melanoma cells. It is not clear whether these lymph node growths were responsible for or a consequence of the intestinal metastases. Thus, the metastatic spectrum of the Mel-STR cells paralleled to a remarkable extent that observed in human melanoma patients.

In stark contrast to these observations, metastatic nodules were very rarely observed in mice bearing subcutaneous fibroblast (BJ-STR) or mammary epithelial cell (MEC-STR) tumors (Table 1) (Elenbaas et al. 2001b; Hahn et al. 1999a). In addition, in the rare cases that metastases were observed, they were exclusively found in the lungs of the animals. Since melanocytes and BJ fibroblasts normally reside within the skin, it could be argued that the subcutaneous space is a more hospitable environment for melanoma cells and transformed fibroblasts than for transformed mammary epithelial cells. To address this issue, MEC-STR cells were injected into the fourth inguinal

mammary gland. This orthotopic site of injection did not enable the resultant mammary tumors to metastasize.

Discussion

The experiments in this chapter indicate that primary human melanocytes, transformed using a defined set of oncogenes, generate melanomas that are highly metastatic when introduced subcutaneously into mice. In fact, the melanomas created in this manner metastasize to many of the same organs as do melanomas in patients, indicating that these cells represent a useful model with which to study the disease. Unlike many other metastatic xenograft models currently in use, the melanomas described here are metastatic without prior selection *in vivo* for metastatic variants.

Since the primary melanocytes, fibroblasts, and mammary epithelial cells were all transformed *in vitro* through the introduction of an identical set of genes, the observations in this chapter indicate that the unique ability of transformed melanocytes to efficiently form metastatic nodules was a consequence of their pre-existing differentiation program. However, despite the use of an isogenic transformation protocol, there remained the formal possibility that the Mel-STR cells were not metastatic following their genetic manipulation in culture, and that tumor evolution *in vivo* was responsible for the generation and subsequent selection of clonal variants with novel genomic aberrations, the latter of which were responsible for the metastatic phenotype.

The rapidity with which metastases formed in the Mel-STR tumor-bearing animals, together with the high penetrance of the metastatic phenotype, strongly argued against such a scenario and supported the notion that the Mel-STR cells were capable of forming metastases without requiring further genetic modification *in vivo*. Nevertheless,

given its importance for interpreting these results, I conducted additional experiments that specifically address this issue. These experiments are described in Chapter 3,.

Materials and Methods

Tissue culture and Cells

Primary human melanocytes, derived from neonate foreskin, were obtained from Clonetics Laboratories and the Yale Cell Culture Core Facility (New Haven, CT). Primary melanocytes were maintained in MGM-3 medium (Clonetics). Immortalized and transformed melanocyte cell lines were grown in Dulbeccos' Modified Eagle Medium (DMEM), with 5% FBS (hereafter referred to as Mel-STR medium). Foreskin fibroblast (BJ)-derived cell lines were previously described [12] and maintained in DMEM:M199 (4:1), supplemented with 10% heat-inactivated fetal calf serum. Human mammary epithelial (HMEC)-derived cell lines were generated as previously described [13] and grown in DMEM:F12 (1:1) supplemented with EGF (10 ng/ml), insulin (10 μg/ml), hydrocortisone (1 μg/ml), and 5% calf serum.

To generate the immortalized melanocyte cell line Mel-ST, primary melanocytes were infected with pBABE-LTg-zeo, and pBABE-hTERT-hygro. These immortalized melanocytes were subsequently infected with pBABE-RasV12-puro, pBABE-TPR-met-puro, or pBABE-HGF-puro, to generate Mel-STR, Mel-STM, and Mel–STH cells, respectively. GFP-labeled cells were infected with the pWZL-GFP-blast vector. For a detailed description of these various plasmids, refer to the retrovirus vectors section below.

Retrovirus vectors and infections

Retroviral constructs for human HGF and mutant c-Met receptor (TPR-met) were generated by cloning the full-length cDNA of human HGF or TPR-met (provided by G. Vande Woude) into the pBABE-hygromycin vector system (S.A.Mani) (Morgenstern and

Land 1990). To facilitate increases expression of these genes, I subcloned the HGF and TPR-met genes into the pBABE-puromycin vector using flanking BamHI/EcoRI sites. Other pBABE-based used for these studies vectors included LTg-zeocin (Elenbaas et al. 2001a), hTERT-hygromycin (Counter et al. 1998), and RasV12-puromycin (S. Lowe, Cold Spring Harbor Laboratories). PWZL-based vectors (Morgenstern and Land 1990) used were RasV12-blasticidin (which I subcloned from pBABE-RasV12-puromycin using BamHI/SalI sites) and GFP-blasticidin (gift from A. Orimo).

Amphotropic retroviruses were created by transient cotransfection of DNA into 293T cells. 6cm plates were cotransfected with 1 μg of appropriate packaging plasmid (pCL-10A1 (Imgenex) for moloney-based infections and DHR8.1:VSVG (9:1) for lentiviral infections) and 1 μg of carrier vector using FuGene 6 (Roche). Viral supernatants were harvested at 48 hrs post-transfection, passed through a 0.4μm filter, and supplemented with 8 μg/ml polybrene (Sigma) prior to infection.

Western blotting

Western blotting was performed using standard protocols. In brief, total protein was extracted from cells using an extraction buffer of 50mM Tris, 100mM NaCl, 5mM EDTA, 1%NP40 detergent in the presence of protease inhibitors (Roche). Cell pellets were homogenized in 5 volumes of this extraction buffer and maintained on ice for 30 minutes. Cellular debris was removed by aspirating the lysate supernatant following centrifugation for 20' at 13,000 rpm on a table-top centrifuge at 4 degrees Celsius. Fifty to one hundred micrograms of total protein was loaded on a gel for SDS-PAGE analysis. Following electrophoresis, proteins in the gel were electroblotted to Immobilon-P

polyvinylidene difluoride (PVDF) membranes. Membrane blots were probed for at least one hour at room temperature in primary and secondary antibodies with three washes in phosphate-buffered saline + .05% Tween following antibody incubations. Following antibody incubations and washes, the PVDF membranes were treated according to the manufacturer's protocol using the Pierce ECL Dura detection kit and exposed to film to visualize HRP-conjugated secondary antibodies. Primary antibodies used were against Large T antigen (Pab101, Santa Cruz), Ras (C-20; Santa Cruz), Slug (G-18; Santa Cruz), and ß-actin (Abcam). Goat anti-mouse (115-035-146) and goat anti-rabbit (111-035-144) HRP-conjugated secondary antibodies were purchased from Jackson Immunoresearch.

In vivo growth curves and metastasis experiments

Athymic nude mice were purchased from Taconic Laboratories (NCR nude, nu/nu). NOD/SCID mice were bred and maintained in-house. All mice were housed in a specific pathogen-free facility and were administered autoclaved food and water *ad libum*. For *in vivo* tumor experiments, 10^6 cancer cells were resuspended in 200ul of medium and injected subcutaneously into 10-12wk old male NOD/SCID mice or 8wk old irradiated athymic nude mice. Nude mice received 400 rad of γ-radiation using a dual ^{137}Cesium source one day prior to injection. For tumor growth curve experiments, mice were monitored bi-weekly and tumor diameters were measured using precision calipers. For *in vivo* metastasis experiments, primary tumors were permitted to grow for ~7-8 weeks or until they reached a diameter of 2cm.

Soft agar assays

Soft agar assays were performed in 6cm tissue culture plates in triplicate. For each dish, 4 mL of 0.6% agarose containing 1x DME and 10% IFS was used as the bottom layer. This layer was maintained at 50 degrees Celsius until immediately prior to pouring, following which it was allowed to solidify at room temperature. Following stabilization of the bottom agarose layer, the desired number of cancer cells were diluted into 0.6% agarose containing 1x DME and 10% IFS and poured on top of the solid bottom agarose layer. Plates were maintained for 3 weeks in a tissue culture incubator, with weekly additions of 1ml culture medium to prevent agarose gel dehydration.

Immunohistochemistry

Immunohistochemistry was performed on formalin-fixed, paraffin-embedded tissues. Five micron sections were de-paraffinized, rehydrated through a graded alcohol series and subjected to antigen retrieval procedures for immunohistochemistry, as described previously [40]. Sections were incubated in mouse monoclonal antibodies against MART-1 (Ventana), pan-cytokeratin (Ventana), human E-cadherin (1:50 Santa Cruz), human β-catenin (1:50, Santa Cruz) or Large T antigen (Pab101, Santa Cruz 1:50). Immunocomplexes were visualized using the ABC peroxidase method (Vector Laboratories, Burlingame, CA). Sections were counterstained with hematoxylin.

Chapter 3

Metastatic Competence of Mel-STR Melanomas[5]

[5]The work in this chapter has appeared in a published manuscript (Piyush B. Gupta, Charlotte Kuperwasser, Jean-Philippe Brunet, Sridhar Ramaswamy, Wen-Lin Kuo, Joe W. Gray, Stephen P. Naber, Robert A. Weinberg. **The melanocyte differentiation program predisposes to metastasis following neoplastic transformation.** *Nature Genetics.* (2005) Oct;37(10):1047-54). Part of the work in this chapter was performed in collaboration with other investigators, as detailed in footnotes 6 and 8 of this chapter.

Introduction

As discussed in Chapter 2, primary human melanocytes, fibroblasts, and mammary epithelial cells were all transformed to a neoplastic state following retroviral transduction with SV40 LT and st, hTERT, and RasV12. Remarkably, melanoma cells experimentally generated in this manner were uniquely capable of forming tumors that could metastasize with high frequency to secondary organ sites. Since identical genetic lesions were used to transform these various cell types, it follows from these observations that the pre-existing differentiation state of melanocytes was capable of influencing the metastatic behavior of melanoma cells following melanocyte transformation.

The short latency with which metastases were seen after introduction of the Mel-STR melanoma cells into mice, together with the large number of microscopic and macroscopic metastases observed, suggested that many cells in the polyclonal population of transformed melanocytes already possessed the ability to form metastases prior to their introduction into murine hosts. Nonetheless, it remained formally possible that metastasis only occurred *in vivo* after rare metastasis-prone cells arose within the primary tumor cell population[6]. Since these considerations have significant consequences for the interpretation of the results of the previous chapter, further experiments were conducted to specifically address this possibility.

---

[6] If rare clonal variants that arise in primary tumors *in vivo* are to succeed in forming metastases with high penetrance across animals, it must also be postulated either (1) that the clonal variants provide an advantage that results in their selection within the primary tumor microenvironment or (2) that there is a high likelihood that a rare cell (and its progeny) within a primary tumor that is capable of metastasizing will, in fact, do so. The apparently inefficient nature of the metastatic process would suggest that possibility (2) is unlikely. These issues are considered in detail in the discussion section of this chapter.

Figure 7 Two fundamentally distinct models of Mel-STR metastatic sufficiency.

Model I

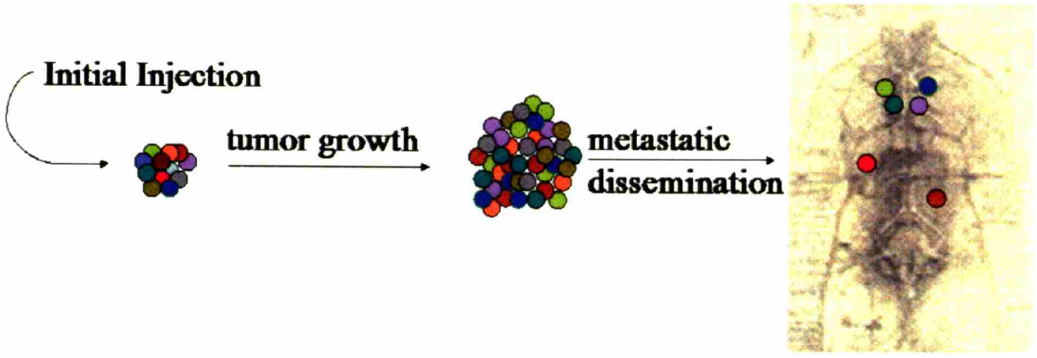

- The introduced genes, together with the pre-existing melanocyte epigenetic program, are sufficient to enable the cells to be metastatic upon injection into the mouse

Model II

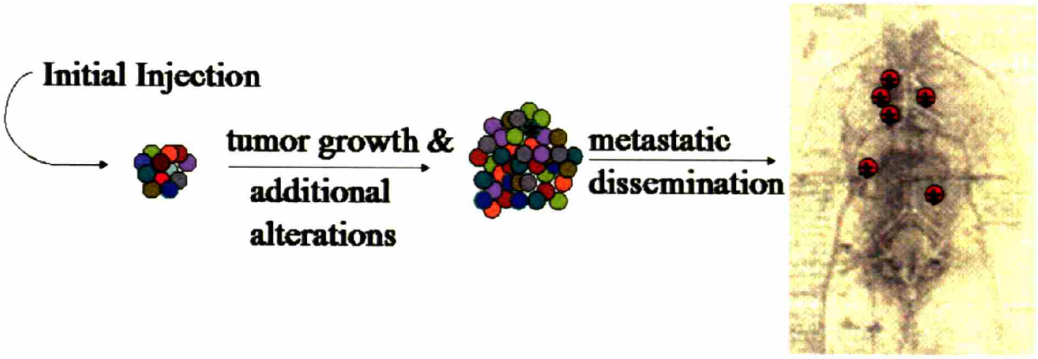

- Additional genetic or epigenetic alterations are required (either in vitro or in vivo) that enable the cells to be metastatic upon injection into the mouse

I used three approaches to address this problem: (1) clonal analysis of metastatic nodules using Southern blotting, (2) comparative genomic hybridization to assay for DNA copy number alterations, and (3) tumor resection experiments to determine the stage of tumor growth at which metastases are seeded into secondary organs. The results from each of these experiments are described below.

Clonal analysis of metastatic nodules

I decided to analyze the distribution of cell clones among the disseminated metastases arising in single animals *in vivo*. The reasoning here was that if rare (epi)genetic alterations were required *in vivo* prior to the acquisition of metastatic potential, all of the metastatic growths in any given animal would derive from a single clonal variant present in the primary tumor, or from a relatively small number of such variants. Alternatively, if a significant number of clones in the primary tumor were capable of seeding metastases at the moment of injection, this should be manifested by clonal heterogeneity among the metastases within the animal. Because retrovirus infection leads to quasi-random insertion of proviral sequences into host cell genomes, Southern blot analysis could be used to identify the ancestral clone(s) from which the various Mel-STR populations were derived.

Individual metastatic nodules arising in single Mel-STR-injected mice were micro-dissected and the tissue fragments were subsequently dissociated into single cells by enzymatic treatment. The heterogeneous cell populations (comprised of both metastatic human tumor cells and murine stromal cells) were plated on tissue culture dishes and the melanoma cells were selected using a drug marker that had previously introduced by retroviral infection into the tumor cells during the initial transformation

Figure 8 (a) Schematic depiction of the Southern blotting experimental design. (b) Southern blot analysis of the metastases arising in single Mel-STR-injected mice. Lanes were loaded with BamHI-cleaved genomic DNA extracted either from organs (#305Lu, Pr, LN), from the parental Mel-STR cell line (Parental, #305CL) immediately prior to injection, or from Mel-STR cells that were isolated from individual metastatic nodules *in vivo* and expanded in culture (L1-4, V1-5). Arrows indicate independent insertion sites. BamHI cleaves once within the vector provirus, upstream of the probed retroviral GFP sequence. GFP probe specificity in lanes exhibiting smears was confirmed by digesting the extracted DNAs with EcoRI, which cleaves twice within the vector provirus and collapses the smears into a single internal 880bp fragment independent of provirus integration site. Genomic integrity in samples exhibiting smears was also confirmed by probing EcoRI-digested DNA for an endogenous 1 kb region upstream of the SNAIL gene, revealing a single intact 10.7 kb band without detectable degradation. HindIII digestion of the extracted DNAs recapitulated the results observed with BamHI cleavage (data not shown). L, lung; V, liver; LN, lymph node; CL, parental Mel-STR cell line; Pr, primary tumor lysate; Lu, whole-lung lysate

(a)

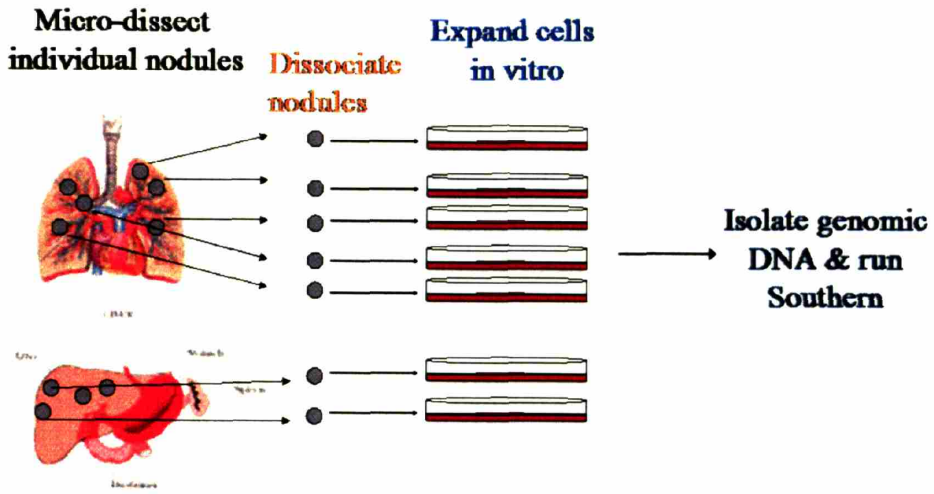
Micro-dissect individual nodules
Dissociate nodules
Expand cells in vitro
Isolate genomic DNA & run Southern

(b)

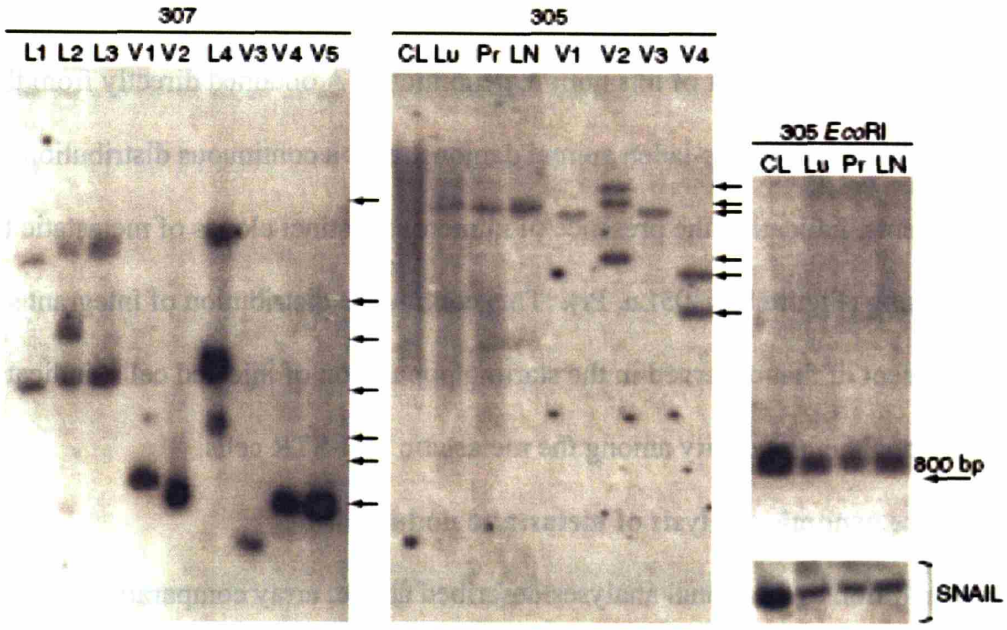
307
L1 L2 L3 V1 V2 L4 V3 V4 V5
305
CL Lu Pr LN V1 V2 V3 V4
305 EcoRI
CL Lu Pr LN
800 bp
SNAIL

process. This experimental procedure produced pure tumor cell populations, each of which was derived (theoretically) from a single metastatic nodule *in vivo*. I therefore isolated genomic DNA from each of the metastatic nodule-derived tumor cell populations and performed Southern blot analysis, probing for GFP provirus sequence.

The continuous distribution in the sizes of cleaved DNA fragments derived from the parental transformed cells demonstrated the extensive polyclonality of the Mel-STR population immediately prior to injection *in vivo* (Figure 8). Upon examination of metastatic Mel-STR nodules, at least 8 distinct clones were present among the metastases of two animals that had been injected with the same polyclonal population of transformed melanocytes (Figure 8, #305,7). Since these various clones were identified through examination of a small number of nodules relative to the total metastastic burden, it is apparent that a large number of additional cell clones were present among the metastases of these animals. In support of this notion, genomic DNA obtained directly from the entire lung of one metastasis-laden animal demonstrated a continuous distribution of DNA fragments, indicating the presence of numerous distinct clones of metastatic tumor cells in the lung (Figure 8, #305Lu, Pr). This continuous distribution of integrant sizes was reminiscent of that observed in the starting population of injected cells, indicating extensive clonal heterogeneity among the metastatic Mel-STR cells.

Comparative genomic analysis of metastatic nodules

In addition to the clonal analyses described above, array comparative genomic hybridization (CGH) was used to directly interrogate the genomes of metastatic nodules to determine whether alterations in DNA copy number were observed relative to the

Figure 9 Whole genome array CGH performed on DNA harvested from Mel-STR metastatic nodules isolated from the liver, heart, and spleen of a single metastasis-laden animal. No significant genome copy number alterations are observed in any of the metastatic nodules relative to the parental primary tumor obtained from the same animal. Data are displayed as log2 (CY3/CY5 intensity ratios) from pter to qter with chromosome 1 on the left and chromosomes 22 and X on the right.

S373B_Liver13v14T

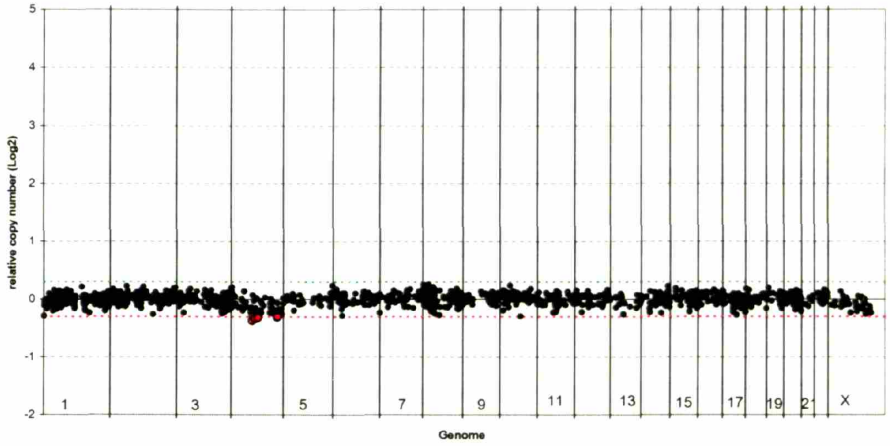

S529A_Heart3v14T

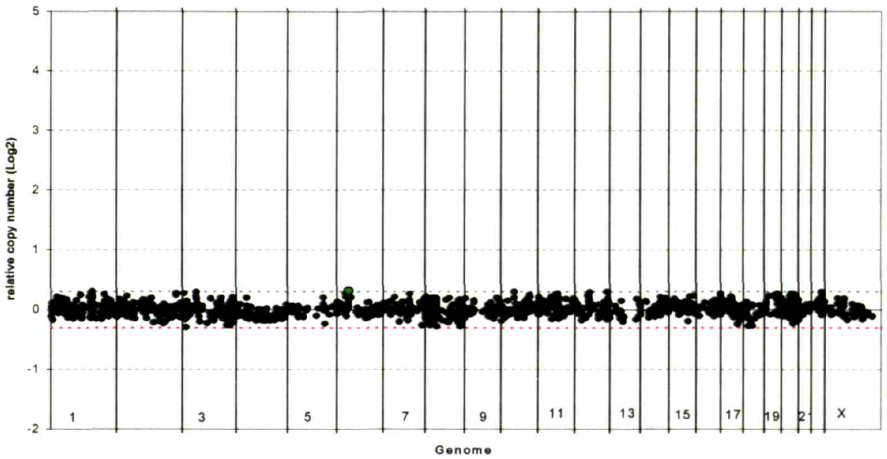

S373A_Spleen1v14T

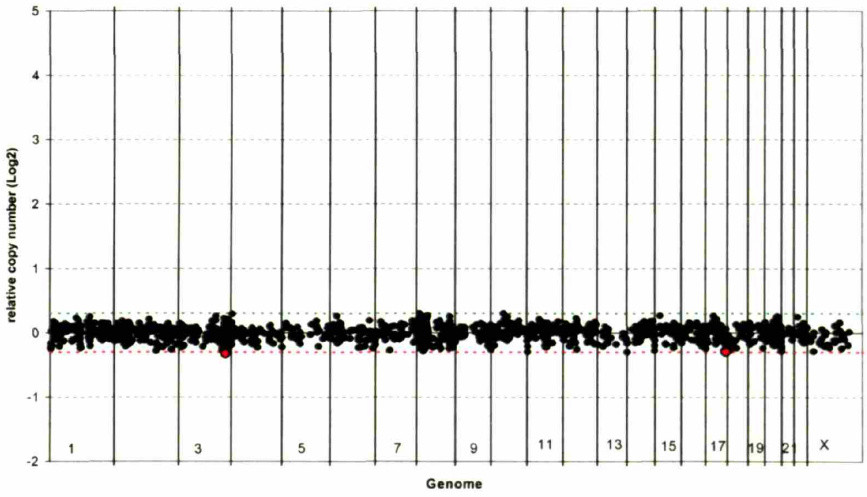

primary tumors[7]. While a positive result in these experiments (i.e., the detection of consistent alterations between metastases and primary tumors) would be a strong indicator of selection for metastasis-competent clones, a negative result from these experiments would not eliminate the possibility that subtle recurrent genomic alterations, such as point mutations, within the genomes of metastatic cells were contributing to their metastatic ability.

Genomic DNA was isolated, as described above, from the metastatic nodules present in various organs of a single metastasis-laden mouse and subjected to array CGH analysis, with genomic DNA from the primary tumor of the same animal used as the reference DNA. There were no significant alterations in DNA copy number observed in six independent nodules isolated from three different organs, relative to the primary tumor DNA. This result indicates that within the level of resolution afforded by the array CGH assay, genomic alterations sustained at the site of primary tumor growth that resulted in DNA copy number changes were not responsible for enabling Mel-STR cell metastasis.

Mel-STR tumors rapidly seed metastatic cells to secondary organs

To further examine the metastatic phenotype of the transformed melanoma cells, the stage of tumor growth at which metastatic Mel-STR cells were seeded into secondary organs was determined[8]. Accordingly, primary Mel-STR tumors from age-matched

---

[7] The array CGH experiments were performed in collaboration with Wen-Lin Kuo and Joe Gray at Lawrence Livermore National Laboratories and UCSF.

[8] While metastases were observed in animals bearing subcutaneous Mel-STR melanomas at approximately 7-8 weeks following injection, it was quite possible that metastatic cells were seeded into the circulation from the primary tumors at a far earlier time. In principle, these cells might lodge within the parenchyma of secondary organs at an earlier time point and require an incubation period to form visible metastatic nodules, which would be in part responsible for the observed metastatic latency.

Figure 10 (a) Schematic depiction of protocol for tumor resection experiment. Mice were injected subcutaneously with Mel-STR cells and the primary melanomas surgically resected at the indicated times. All mice were sacrificed at 48 days post-injection. (b) The fraction of mice with visible lung metastases upon necropsy is indicated. (c) are representative melanoma-burdened lungs from mice whose primary melanomas were excised at day 18 or day 28 after injection, respectively. Arrows indicate individual metastatic nodules.

(a)

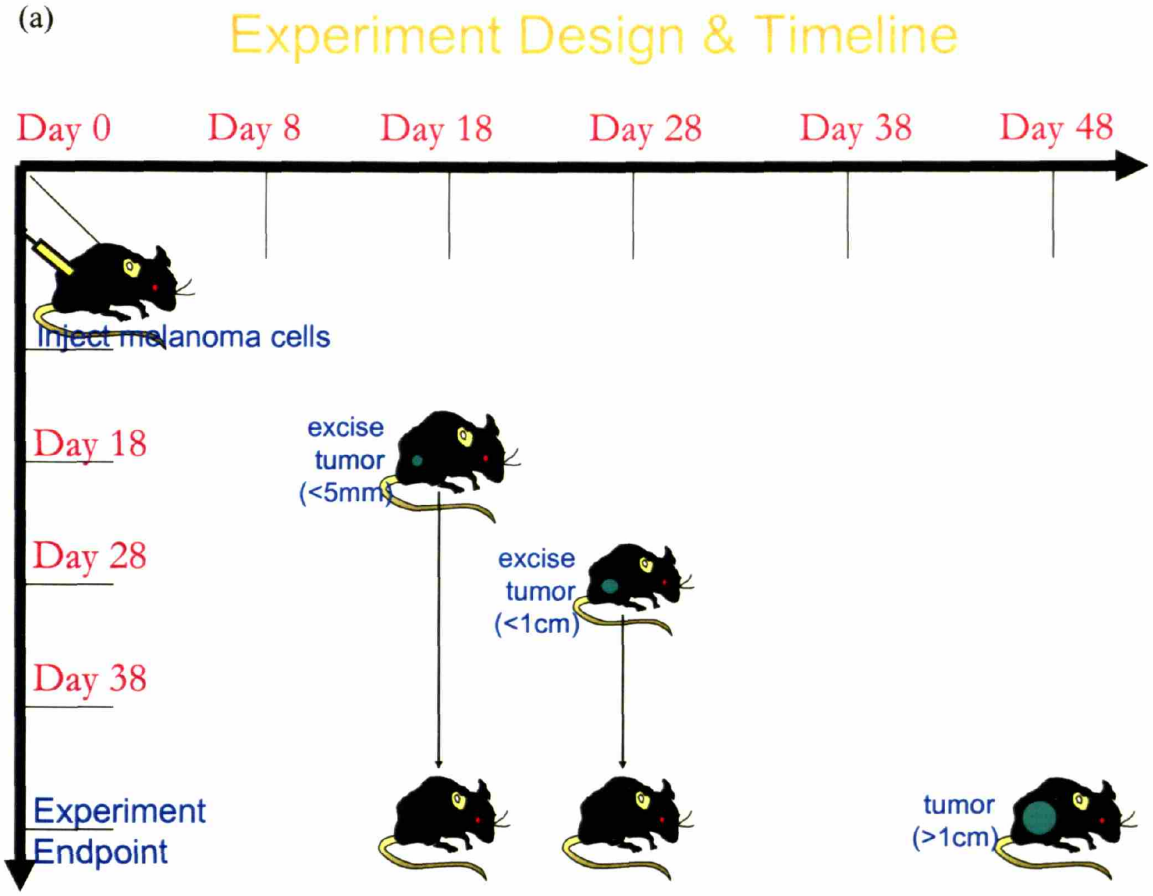

(b)

Resection (day)	Occurrence of metastasis
18	7/7
28	3/3
44	2/2

(c)

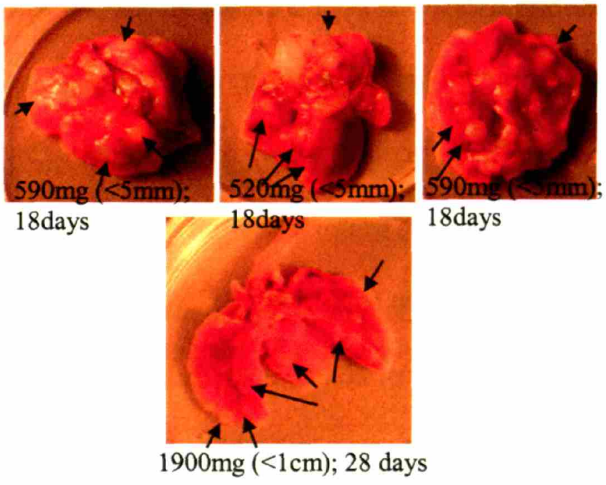

cohorts of mice were surgically resected[9] at specific times after injection (18, 28 or 44 days), and the mice were examined for macroscopically visible metastatic growths at the endpoint of the experiment (44 days). To ensure full resection of the primary melanomas, a 0.5cm margin of skin was removed during the surgery and subjected to histological examination, confirming the absence of melanoma cells in the adjacent skin (data not shown). These studies revealed that mice in each experimental cohort, even those in which the primary tumors were removed only 18 days after injection (mean weight = 400mg), exhibited numerous macroscopically visible metastatic nodules in the lungs of the animals at the endpoint of the experiment (Figure 9). Similarly, mice whose primary tumors were surgically resected 28 days after injection (mean weight = 600mg) also developed extensive lung metastases (4/4).

Estimation of the frequency of metastasis-enabling alterations

Under the assumption that the ability to metastasize is acquired by the Mel-STR melanoma cells after injection into the host animal, it is possible to estimate a conservative lower bound on the frequency with which such an alteration must occur in order to give rise to our observed data.

Let N_0 be the number of tumor cells that survive the initial subcutaneous injection. The results of the tumor resection experiments indicate that numerous metastatic cells have already been seeded in the lungs within the 18 days after the initial injection. Thus, the total number of elapsed cell divisions prior to seeding metastasis depends on N_0 and N_f, where N_f is the number of cancer cells in the tumor mass at the time of surgical

[9] The tumor resection surgeries were performed by Charlotte Kuperwasser, currently at Tufts University, Boston MA.

resection. Given the size of the primary tumors at the time of resection, we can estimate that $N_f = 10^7$. Therefore, $\alpha = \log_2 (N_f/N_0)$, where α is the number of population doublings that occur *in vivo* prior to surgical resection of the primary tumor mass. Since 10^3 injected Mel-STR cells are sufficient to form a primary Mel-STR tumor (data not shown) we can infer that the frequency of injected cells that survive is $> 10^{-3}$. It follows that $N_0 > 10^3$, and therefore $\alpha < \log_2 (10^7/10^3) = \log_2 (10^4) < 14$. This, in turn, implies that the total number of individual cellular divisions (a quantity distinct from population doublings) that elapse prior to surgical resection of the primary tumor is less than

$$[(N_0) + (2)(N_0) + (2^2)(N_0) + (2^3)(N_0) + \ldots + (2^{\alpha-1})(N_0)] = (2^\alpha - 1)(N_0)$$

It follows that the total number of conversions *in vivo* from a non-metastatic clone to a metastatic clone is at most $(2^\alpha - 1)(N_0)(p)$, where p is the probability that a non-metastatic cell becomes metastatic after a single division. Assuming that such a conversion event will occur with equal probability in any of the $(2^\alpha - 1)(N_0)$ cell divisions that occur *in vivo*, one can determine that the average number of cellular descendants derived from a newly formed metastatic cell is α. Thus, the total number of metastatic cells in the primary tumor mass at the moment of surgical resection is at most $(2^\alpha - 1)(N_0)(p)(\alpha)$.

The expected number of metastatic nodules in the lungs at the endpoint of the experiment can be calculated as:

(*number of metastasis-competent cells released into the circulation before resection*) x (*the probability that a metastasis-competent cell released into the circulation will ultimately form a visible nodule in the lung*)

The second quantity in the product above can be estimated to be less than one in 10^5 cells, since the injection of 10^5 Mel-STR cells directly into the murine tail-vein failed to yield

any visible lung metastases after a 2 month period (data not shown). The first quantity in the product above clearly depends on the number of tumor cells that are shed daily into the circulation. For a ≈1g tumor, this number has been previously estimated to be 10^6 cells per day [43]. Therefore,

(*10^6 cancer cells shed per day*) x (*18 days*) x

[$(2^{\alpha} -1)(N_0)(p)(\alpha)$ *metastatic cells in the tumor*] ÷ [N_f *total cancer cells in the tumor*]

is a conservative upper bound on the total number of metastatic cells released into the circulation prior to surgical resection of the primary tumor mass. This number is ≈$(2 \times 10^7)(p)(\alpha)$. As discussed above, it follows that

$$(10^{-5})(2 \times 10^7)(p)(\alpha) < (10^{-5})(2 \times 10^7)(p)(15) = 3000p$$

is an upper bound on the expected number of lung nodules at the endpoint of the experiment. Since greater than 30 metastatic nodules were observed in the mouse lungs at the endpoint of the tumor resection experiments, we have that

$$3000p > 30 \text{ or } p > 1/100$$

This frequency is significantly higher than known rates of genomic mutation.

Discussion

As a general rule, it is difficult to definitively eliminate the possibility that uncharacterized genetic lesions might be contributing to the phenotype of any given cancer cell line. This difficulty is compounded by the genomic instability that is a feature of malignant cancers. As a consequence, while the experiments in this chapter provide strong evidence to the contrary, it is impossible to completely rule out the possibility that factors beyond the introduced genes are facilitating Mel-STR melanoma metastasis

formation. Nonetheless, the Southern blot clonal analyses, comparative genomic hybridization studies, and tumor resection experiments together provide strong evidence against the notion that additional rare genetic lesions *in vivo* are required prior to metastasis formation by Mel-STR tumors. Indeed, the surgical resection experiment indicated that the Mel-STR tumors have already seeded metastatic cells into the lungs of the animals by 18 days post-injection.

Based on the results of these experiments, it was possible to estimate a conservative lower bound on the frequency with which metastasis-enabling alterations must be occurring *in vivo* if the Mel-STR cells must acquire the ability to metastasize subsequent to their introduction *in vivo*. This frequency, ~1/100, is several orders of magnitude more frequent than the estimated frequencies per cell generation of gene mutation (see Materials and Methods for mathematical justification). Thus, the experiments described in this chapter suggest that it is unlikely that additional genetic alterations beyond those initially introduced during the transformation protocol were required *in vivo* to enable the injected Mel-STR cells to metastasize.

While the experiments in this chapter are conducted using a single model of tumor metastasis, they have relevance for our understanding of the general mechanisms by which tumors acquire metastatic competence. A current issue in the field is the question of whether tumors acquire metastatic competence via the same Darwinian evolutionary process that characterizes the manner in which tumors acquire other phenotypic traits. The unexpected finding that gene expression profiles of early-stage tumors are effective predictors of the likelihood of ultimate prognosis suggests that metastatic competence is a trait that is determined far before the process of metastasis is

physically manifested. The results of this chapter lend support to this hypothesis, suggesting that it is plausible in the case of melanoma. More generally, these observations support the notion that the originating cell type of a cancer, which may differ even for cancers arising within a single tissue, can play a significant role in dictating the clinical course of the disease.

Some general considerations regarding cancer metastasis

The requirement for accumulated genetic lesions underlies the gradual development of adult cancers, many of which arise over a span of decades. This multifactorial genetic requirement is reflected in the extensive genomic instability of cancer cells, the latter of which is a conserved feature of adult malignancies and represents one common mechanism by which individual cancer cells sustain multiple genomic aberrations. The functional contribution of particular genetic lesions to cancer pathogenesis has been established, in many cases, by associating their presence with specific cancer phenotypes using *in vitro* and *in vivo* tumor models.

In addition to acquired genomic instability, a second mechanism by which cancer cells sustain multiple genomic lesions is through repeated cycles of mutation and subsequent clonal selection, resulting in the sequential fixation of mutations in the bulk tumor cell population. According to this Darwinian-like model, tumors evolve towards greater malignancy over time as a result of the expansion of individual cell clones that have sustained novel genetic lesions that confer a selection advantage within the primary tumor microenvironment. The Darwinian paradigm provides a compelling rationale for the presence of many of the genetic lesions commonly observed in human tumors. Examples of the selective advantage that specific lesions provide include: Bcl-2 over-

expression or p53 loss confer resistance to apoptosis, pRb loss confers resistance to growth-inhibitory signals, and amplification or gain-of-function mutations of Ras proteins confer the ability to proliferate in the absence of appropriate mitogenic signals.

The development of distant metastases is the final step in the progression of many adult malignancies. Given its success in conceptually unifying the mechanisms by which tumors successively acquire the phenotypic alterations that characterize their progression, the Darwinian model has naturally been extended to encompass the ultimate phenotype of cancer metastasis. However, the molecular basis of metastasis remains poorly understood, and that the experimental basis for such an extension is quite sparse. Indeed, several conceptual problems and (more recently) observational inconsistencies plague the Darwinian paradigm as it relates to the acquisition of metastatic competence by tumors (van, V et al. 2002; Minn et al. 2005a; Minn et al. 2005b; Kang et al. 2003).

Theoretical difficulties in extending the Darwinian model to cancer metastasis

The ability to proliferate in the absence of mitogenic signals, resist apoptotic stimuli, and induce angiogenesis each confers a patent selective advantage to cancer cells within a primary tumor microenvironment. In contrast, it is much less apparent how sequential cycles of selective pressure for metastatic ability to secondary organ sites (required under the Darwinian framework) would sensibly operate within the primary tumor microenvironment. An alternative to the Darwinian model would be the simultaneous stochastic acquisition of the molecular alterations required for metastatic dissemination within a single cancer cell. However, metastasis to secondary organ sites is a physically highly complex process, and this has resulted in the assumption that numerous genetic lesions are required within individual cancer cells prior to their

successful metastasis. In this case, the probability that the requisite lesions would occur by chance within a single cancer cell genome is negligibly small. Thus, while it is difficult to imagine why metastatic competence would be advantageous within the primary tumor microenvironment, it would appear inevitable that selection must be operating in some form to promote sequential rounds of clonal expansion, without which it would be very unlikely that a sufficient number of lesions would accumulate within a single cancer cell.

Several scenarios offer resolutions to this conceptual quandary:

(i) Some traits that are advantageous to cancer cells within the primary tumor microenvironment also contribute to metastatic competence. Resistance to apoptosis, for example, may be dually advantageous for cancer cells—for survival within the primary tumor microenvironment and also for survival in the circulation or at secondary organ sites (prior to adaptation or colonization), thereby contributing to metastatic competence.

(ii) Selective pressure within the primary tumor microenvironment for phenotype X results in the clonal expansion of cancer cells harboring a genetic lesion that also confers a second phenotype Y, the latter of which contributes to metastatic competence. Thus, cancer cells may acquire a particular phenotype that is advantageous within the primary tumor microenvironment through one of several possible genetic lesions, some of which unwittingly also confer additional phenotypes that facilitate cancer cell metastasis.

The possibilities delineated above (which are not mutually exclusive) describe how metastatic phenotypes may hitchhike along with phenotypes beneficial within the primary tumor microenvironment. Either scenario would resolve the *conceptual* difficulties inherent in extending a quasi-evolutionary model of tumor progression to include metastasis. However, recent unanticipated observations with tumor specimens obtained from cancer patients call into question the applicability of the Darwinian framework to

the acquisition of metastatic competence. In particular, classifiers based on mRNA expression profile have demonstrated that the transcriptional state of relatively early-stage primary tumors is predictive of the ultimate clinical prognosis of patients (VAN2002). This surprising finding appears to be fundamentally inconsistent with the stochastic nature of metastasis implied by the Darwinian model. Indeed, if it is the case that metastatic competence results from selection operating on cancer cell clones that have sustained random genomic alterations, then it ought not to be predictable whether any given early-stage tumor will ultimately metastasize. Under the Darwinian scheme, it appears inescapable that the ultimate acquisition of metastatic competence depends on the unknowable nature of future lesions that are randomly sustained by the cells of a tumor. The apparent incompatibility of the Darwinian scheme with the existence of a "poor-prognosis" microarray signature remains unresolved by (i) and (ii) above. Understanding the ability of early-stage tumor mRNA expression signatures to predict metastatic recurrence has important implications both for our conceptualization of metastasis and for the management of patient treatment. It remains to be determined whether these observations can be reconciled with the Darwinian mutation/selection model of cancer metastasis.

The influence of cell type of origin on metastatic proclivity

For many years, oncologists have been aware that certain kinds of cancers afford a poorer clinical prognosis relative to other types of cancers. For instance, melanomas are notorious for occasionally progressing to invasive and highly metastatic states, whereas basal-cell carcinomas of the skin rarely metastasize. Empirical observations such as these indicate that the cell type from which a particular cancer arises plays a

significant role in determining the likelihood that a given tumor will eventually metastasize, independently of genetic variation among individuals. Why is this? As tumors become more aggressive they tend towards greater and greater de-differentiation. In fact, the most aggressive tumors can be de-differentiated to a point where it is difficult or impossible to determine their tissue of origin based solely on histological examination (7% of all cancers are diagnosed as having an unknown primary origin). How is it, then, that malignant cancer cells retain a memory of the cell type from which they originated during later stages of tumor progression, a time at which they are often highly de-differentiated?

There are two conceptually disparate (but not mutually exclusive) models that could serve to explain the influence of cell type of origin on the natural history and progression of cancer:

(iii) The cell type of origin influences metastatic competence by impacting the nature of the genetic lesions that are selected for due to their ability to confer an advantage within the primary tumor microenvironment to a cell that has acquired them. A consequence of this would be that cancers, even at an early stage of development, would have different mutational spectra depending on their cell type of origin. This model proposes these differences in mutational spectra would be responsible for differences in metastatic propensities (perhaps due to mechanisms (i) or (ii) described in the previous subsection).

(iv) The expression, at various stages of tumor progression, of particular proteins that can influence eventual metastatic competence is in part dependent on the initial differentiation state of a cell prior to neoplastic conversion. Otherwise stated, the initial or acquired differentiation state of cell, possibly in conjunction with its mutational spectrum, provides an independent contribution to the eventual expression of metastasis-relevant proteins.

While both of these mechanisms are theoretically plausible, it may be that one is the predominant system utilized by autochthonous human cancers. Do differences in acquired or selected mutational spectra underlie cell type of origin-specific differences in metastatic propensity? Or is it the case that transcriptional and epigenetic differences present prior to or early during neoplastic transformation directly contribute to cell type of origin-specific variances in metastatic ability? The current experimental data are insufficient to establish or exclude the relevance of either of these mechanisms to human cancer. On the one hand, it is apparent from various genomic profiling studies that certain types of cancers are more prone to possess particular genetic lesions, such as N-ras mutations or PTEN deletions, providing support for model (iii). Experimental evidence in support of model (iv) is provided by the experiments in this thesis.

As discussed below, a resolution of these issues ultimately informs the interpretation of recent tumor microarray data and therefore also our understanding of cancer metastasis in general.

The relevance of cell type of origin the interpretation of recent tumor microarray data

Classifiers based on microarray profiles are readily able to distinguish between different types of cancers, and in some cases afford a finer distinction between cancer subtypes than is achievable using visual pathological examination alone (Sorlie et al. 2001). In fact, one can imagine a situation where the bioinformaticist is supplied with a set of 100 microarray profiles comprising 50 basal cell carcinomas and 50 melanomas of the skin, all derived from early stage tumors. One can further envision that the bioinformaticist is given these 100 profiles in a blinded fashion in the absence of any information about the pathological classification of the tumor samples from which they

derive, being supplied information only about the clinical outcome of the patient with respect to metastatic recurrence. Upon analyzing the data, the bioinformaticist will readily distinguish two subclasses based on expression profile similarity, and will be in a position to note that one profile subclass (corresponding to melanomas) affords a significantly poorer prognosis than the other profile subclass (corresponding to basal cell carcinomas). In effect, the bioinformaticist will have constructed classifiers based on microarray profiles of early-stage tumors that can predict the likelihood of eventual metastatic recurrence, and will have done so without *a priori* knowledge of the intrinsic subclasses into which the tumors segregate.

There is a formal analogy between the situation just described and the ability of microarray profile data from relatively early-stage tumors of the same tissue type to predict eventual metastatic outcome. As such, it is plausible that the ability of microarray-based classifiers to discriminate between good and poor-prognosis tumors is a consequence of the finer resolution afforded by mRNA expression profiles in distinguishing different tumor subtypes. Stated otherwise, it may be that tumors are classified as identical based on visual pathological examination alone, when in fact they harbor subclasses (distinguishable using mRNA expression profile data) that originate from different cell types and therefore exhibit distinct clinical outcomes. If this is indeed the case, then the microarray analyses would be identifying differences in the cell type of origin, which would in turn underlie differences in both the microarray profiles and metastatic proclivity. Assuming this scenario, the possibilities (iii) and (iv) delineated above would have the following respective correlates:

(v) Two early-stage tumors that appear phenotypically similar may in fact harbor very different sets of genetic lesions. One set of tumors might possess lesions that are permissive of future metastasis-enabling lesions. A second set of early-stage tumors might possess lesions which, for any number of reasons, are not permissive for additional metastasis-enabling mutations. Microarray analyses may be able to distinguish between these two types of tumors, which, despite phenotypic similarity, sustain very different genetic alterations and represent different tumor subclasses.

(vi) Specific proteins that can contribute at some point to metastatic competence may be expressed intensely in some tumors and not in others, depending on the cell type from which the cancer originated. The expression of these proteins may not be sufficient to confer metastatic competence, but may collaborate with other proteins to program metastatic ability, perhaps at later stages of tumor progression. Microarray analyses would be able to distinguish between these two subclasses of tumors.

In the next chapter, I provide evidence to support model (vi) above in the case of melanoma.

Materials and Methods

Southern blot analysis

Fresh tumor tissue or metastatic nodules were microdissected from organs of individual metastasis-laden mice at necropsy under a dissection microscope (see Figure 6, Chapter 2). Tissue fragments were minced and digested for 3 hours with agitation at 37°C, in culture medium (Dulbecco's Modified Eagle Medium containing with 10% fetal bovine serum) supplemented with collagenase (1 mg/ml; Boehringer Mannheim), hyaluronidase (125 U/ml; Sigma) and HEPES buffer (10 mM; Gibco). At one hour intervals, the tissue fragment suspensions were passed through a 16 gauge needle to facilitate tissue dispersion. After the incubation period, the cell suspensions were filtered through a nylon mesh to remove and cellular debris and tissue clumps. Dissociated cells were plated in Mel-STR medium and subjected to puromycin drug selection (1 ug/ml) for one week, resulting in pure populations of melanoma cells. Genomic DNA was isolated from the nodule-derived tumor cell populations and purified by phenol/chloroform extraction. 15μg of DNA was digested with BamHI, and Southern blotting performed as described (Kuperwasser et al. 2000a) In the case of the lung of mouse #305, gDNA from the entire metastasis-burdened organ was isolated as described above (in the absence of microdissection and intervening culture), and 30ug loaded for blotting. As a probe template, an 800bp EcoRI fragment from pWZL-GFP was used to synthesize ^{32}P-labeled probe using the Rediprime II kit as directed in the manufacturer's supplied protocol (Amersham).

Array CGH

Whole genome CGH array comprised of 1860 PAC and BAC clones were prepared as described (Snijders et al. 2003). Labeling of melanoma genomic DNA, array CGH hybridization and image processing were performed as previously described (Snijders et al. 2003) with slight modification. Briefly, 500 ng each of cell line and normal female genomic DNA were fragmented by DPNII digestion, labeled by random priming (Bioprime Labeling System, Invitrogen, Carlsbad, CA) with CY3- and CY5-dUTP (Amersham, Piscataway, NJ) respectively, co-precipitated with 50 μg of human cot-1 DNA (Life Technologies) and resuspended in 60 μl hybridization buffer (50% formamide, 10% dextran sulfate, 2X SSC, 4% SDS, 200μg yeast tRNA). This mixture was denatured at 75°C for 10 min followed by incubations at 37°C for 60 min. Just prior to hybridization, array slides were UV cross-linked. A rubber cement dam was placed around each array, hybridization mix was added and the slide was placed in a plastic slide holder, prewarmed to 37°C, containing 200 μl of wash buffer (50% formamide, 2X SSC) to prevent evaporation. Hybridization was carried out at 37°C for 48-72 hours on a gently rocking platform. Following hybridization, slides were immersed for 15 min at 48°C in wash buffer, followed by washes at 48°C in 2X SSC, 0.1% SDS for 30 min, and PN buffer (0.1 M sodium phosphate buffer, 0.1% NP40, pH 8.0) at room temperature for 10 min. Slides were then rinsed in 2X SSC and mounted with 4', 6-diamidino-2-pheylindole (DAPI, 0.5 μM) in 90% glycerol, 10% PBS for imaging using a 16-bit CCD camera. The CY3, CY5 and DAPI images were segmented and analyzed to determine CY3/CY5 ratios for each array element using custom software as described (Jain et al. 2002). Data are displayed as log2(CY3/CY5 intensity ratios) from pter to qter with chromosome 1 on the left and chromosomes 22 and X on the right based on the position

of the BAC on the July, 2003 freeze of the UC Santa Cruz genome sequence assembly (http://genome.ucsc.edu).

In vivo tumor resection experiments

For tumor resection experiments, subcutaneous primary tumors were permitted to grow for 18 or 28 days in male NOD-SCID animals. Mice were anesthetized using avertin (0.4-0.7 mg/g body wgt) and the tumors excised under a dissection microscope using DeWecker microdissecting spring scissors and a hand held cautery unit. Mice were monitored daily thereafter until the endpoint of the experiment.

Chapter 4

Melanoma and the Neural Crest[10]

[10] The work in this chapter has appeared in a published manuscript (Piyush B. Gupta, Charlotte Kuperwasser, Jean-Philippe Brunet, Sridhar Ramaswamy, Wen-Lin Kuo, Joe W. Gray, Stephen P. Naber, Robert A. Weinberg. **The melanocyte differentiation program predisposes to metastasis following neoplastic transformation.** *Nature Genetics.* (2005) Oct;37(10):1047-54). Part of the work in this chapter was performed in collaboration with other investigators, as detailed in footnote 10 of this chapter.

Introduction

The results of the previous two chapters provided a strong indication that intrinsic factors associated with the melanocyte differentiation program provide a significant contribution to melanoma's metastatic ability. Since epidermal melanocytes are derived from the uniquely migratory neural crest cell population, an attractive hypothesis is that embryonic motility programs are reactivated during melanoma progression, contributing to this cancer's metastatic ability (Tucker 2004a). For this to be plausible, it is necessary to postulate that a molecular memory of their neural crest origin is retained in differentiated melanocytes, albeit in a latent form that is not readily apparent from their phenotype.

There are indirect observations in the literature that suggest that there is indeed such a memory and that embryonic factors might be re-expressed in melanocytes upon their progression to melanoma. When screened for cytolytic activity against a panel of 23 neuroectodermal tumor cell lines, cytotoxic T cells derived from tumor infiltrating lymphocytes that recognize melanoma antigens were observed to cross-react with 3 Ewing's sarcoma cell lines but not any of the other histological subtypes of neuroectodermal tumors (which included retinoblastoma, neuroblastoma, neuroepithelioma, astrocytoma, and neuroglioma) (Shamamian et al. 1994a). Given the common neural crest cell origin of Ewing's sarcoma and melanoma, it would seem that tumor antigens recognized by tumor infiltrating lymphocytes can include those that are expressed during embryogenesis (Shamamian et al. 1994b). As another example, the Pax3 transcription factor, which is expressed in neural crest cells, is also expressed in Ewing's sarcomas, melanomas, and rhabdomyosarcomas (Shaw et al. 1987), all of which

have a neural crest cell origin. This protein has further been shown to contribute functionally to the resistance of melanoma cells to apoptosis.

In addition to these melanoma-centric observations, independent experimental observations suggest that cancer cell invasiveness in general may utilize molecular mechanisms that are also used by neural crest cells to migrate. In support of this notion, neural crest cell transcription factors of the Snail superfamily are associated with the invasiveness and loss of E-cadherin expression in various types of carcinomas (Uchikado et al. 2005; Elloul et al. 2005; Blanco et al. 2002; Palmer et al. 2004; Takeno et al. 2004; Miyoshi et al. 2005).

The experiments described in this chapter examine the connection between molecular factors governing neural crest cell migration and melanoma metastasis.

Expression of neural crest cell genes in culture melanocyte cell lines

Markers that are used to identify neural crest cells in developmental studies include Slug, HNK1, Pax3, Phox2a, Phox2b, Ret, p75 NTR, Endothelin receptor type B, 5-Ht2 type B receptor, MASH1, and Sox10. Of these, Slug is induced the earliest, and is expressed both in premigratory and migratory neural crest cells. In contrast, all of the other markers indicated are expressed exclusively on migratory neural crest cells. As such, Slug is widely considered to be the most reliable marker for the neural crest. Indeed, Slug is functionally important for both the initial specification and also the subsequent migration of neural crest cells (Tucker 2004b).

A complication arises when considering the role of Slug in relation to the neural crest in higher vertebrates, particularly mammals. This is due to studies in mouse

embryos, which indicate that expression of the closely related transcription factor, Snail, substitutes for Slug expression in the neural crest of this evolutionary lineage. Snail, the founding member of a zinc finger transcription factor family that includes Slug and Escargot, has activities that overlap significantly with Slug, yielding a significant degree of functional redundancy. On the basis of these observations in mice, it was extrapolated that Snail might be the superfamily member that has relevance for neural crest cells in other mammals, including humans. Therefore, we also examine Snail expression in the experiments below.

The results above indicated that the differentiation program of melanocytes could cooperate with oncogenic lesions to uniquely predispose their transformed counterparts to forming tumors that metastasize, when compared to fibroblasts and epithelial cells transformed with identical genes. Since the process of cancer cell invasion bears numerous cellular and molecular similarities to neural crest cell migration in the developing embryo, and given the known derivation of dermal melanocytes from the neural crest, I hypothesized that elements of the motility-associated molecular program mediating neural crest cell migration may contribute to melanoma's metastasis.

To determine if the Mel-STR or Mel-STM melanoma cells and their precursor cell lines expressed any neural crest cell markers, I used RT-PCR to measure Slug, Pax3, and Snail expression in the various human melanocyte cell lines that were generated as described in Chapter 2. I observed that both Slug and Pax3 were highly overexpressed in both the Ras- and TPR-met- transformed melanoma cells (Corsetti et al. 2000), relative to the human breast cancer cell line MCF7-Ras. In contrast, the Snail gene, which is highly homologous to Slug, was not overexpressed in the melanoma cell lines. Interestingly,

Slug expression was also observed in non-tumorigenic, immortalized melanocytes. This suggested that the expression of Slug was not a consequence of neoplastic transformation, and that rather Slug was expressed in immortalized cells of the melanocyte lineage. However, Slug protein was not detected using Western blotting in cultured primary melanocytes, despite there being a high level of *Slug* mRNA present in the cells (data not shown). Since primary melanocytes in culture exhibit a complex dendritic morphology, one plausible explanation for this apparent discrepancy is that the standard protein extraction protocol was insufficient to dissociate Slug protein from its normal subcellular compartment, which may be membrane-associated.

Expression of an embryonic motility network in human melanocytic nevi[11]

To determine if Slug is expressed in pre-neoplastic human melanocytes *in situ*, the expression of Slug was examined in pre-malignant precursors of melanomas, i.e., benign melanocytic nevi. Nevus biopsies were taken from human patients, pathologically classified as being histologically benign, and mRNA expression profiles were collected using Affymetrix expression microarrays (Bedrosian et al. 2000). It was observed that benign nevi from human patients expressed Slug mRNA. Moreover, expression of the Slug transcript in these samples correlated strongly and significantly ($p < 0.01$) with other genes known to be expressed in neural crest cells (Table 2). In these computational analyses, rank-based correlation coefficients were used together with p-values calculated using non-parametric permutation statistics. The use of these methods

[11] The work in this section was performed in collaboration with Jean-Philippe Brunet and Sridhar Ramaswamy when they were at the Cancer Genomics Group of the Broad Institute of MIT/Harvard. The microarray data on human nevi was obtained from an ongoing project at the Broad Institute and I am grateful to Todd Golub for sharing the unpublished data for this study. The computational analyses were performed by Jean-Phillipe Brunet.

minimizes assumptions regarding the nature of the underlying gene expression distribution. Importantly, these computational analyses were performed with no human intervention and were therefore not biased, providing strong evidence that the observed expression of Slug was not spurious and in fact was an accurate reflection of melanocyte biology.

Genes of the Snail-superfamily have previously been implicated in both promoting cancer cell invasiveness (Hajra et al. 2002) and governing neural crest cell migration (LaBonne and Bronner-Fraser 2000). Remarkably, several of the genes whose expression pattern correlated with that of Slug have been reported to be essential for

Figure 11 **a**, mRNA expression levels as determined by microarray analysis. Transcript levels of SLUGH, CD44, EDNRB and ERBB3 were correlated in 9 human nevus samples. **b**, Reference statistics for CD44 (*35*). 1000 correlation coefficients were obtained by randomly permuting the SLUGH expression profile template. Shown is a histogram plot of correlations corresponding to the rank of CD44 in the SLUGH neighborhood list. The correlation coefficient of CD44 with the non-permuted SLUGH template is indicated by a red arrow (0.958). There are only 4 permuted correlations larger than this value, resulting in strong statistical significance (p=0.004).

(a)

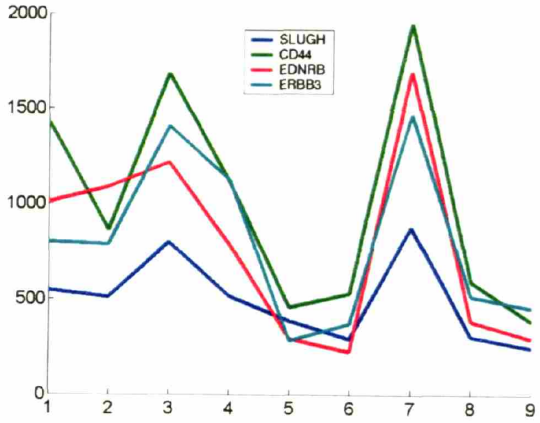
SLUGH
CD44
EDNRB
ERBB3
2000
1500
1000
500
0
1
2
3
4
5
6
7
8
9

(b)

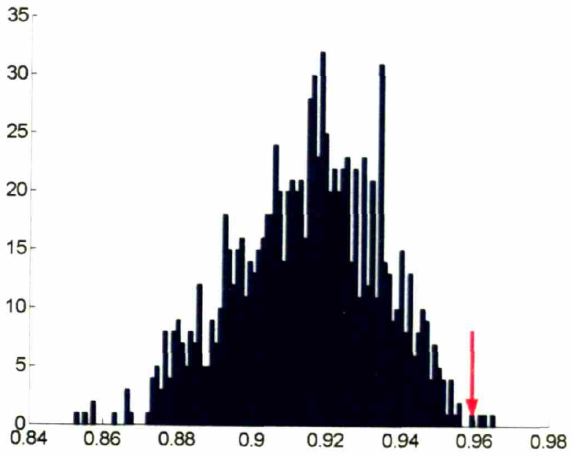
35
30
25
20
15
10
5
0
0.84
0.86
0.88
0.9
0.92
0.94
0.96
0.98

Table 2

Genes significantly correlated with SLUGH in a dataset of 9 nevus samples

Probe	Name
213139_at	slug homolog, zinc finger protein (chicken)
200984_s_at	CD59 antigen p18-20 (antigen identified by monoclonal antibodies 16.3A5, EJ16, EJ30, EL32 and G344)
211971_s_at	leucine-rich PPR-motif containing
222171_s_at	PBX/knotted 1 homeobox 2
204671_s_at	ankyrin repeat domain 6
213122_at	KIAA1750 protein
221524_s_at	Rag D protein
201735_s_at	chloride channel 3
204489_s_at	CD44 antigen (homing function and Indian blood group system)
210357_s_at	hypothetical protein
207040_s_at	suppression of tumorigenicity 13 (colon carcinoma) (Hsp70 interacting protein)
201178_at	F-box only protein 7
204271_s_at	endothelin receptor type B
212018_s_at	DKFZP564M182 protein
200811_at	cold inducible RNA binding protein
202454_s_at	v-erb-b2 erythroblastic leukemia viral oncogene homolog 3 (avian)
208717_at	oxidase (cytochrome c) assembly 1-like
31835_at	histidine-rich glycoprotein
206701_x_at	endothelin receptor type B
200005_at	eukaryotic translation initiation factor 3, subunit 7 (zeta, 66/67kD)
208319_s_at	RNA binding motif protein 3
213446_s_at	IQ motif containing GTPase activating protein 1
217354_s_at	calcium channel, voltage-dependent, gamma subunit 2
217530_at	
63305_at	PBX/knotted 1 homeobox 2
212361_s_at	ATPase, Ca++ transporting, cardiac muscle, slow twitch 2
213817_at	
219578_s_at	cytoplasmic polyadenylation element binding protein
201635_s_at	fragile X mental retardation, autosomal homolog 1
205535_s_at	BH-protocadherin (brain-heart)
215945_s_at	tripartite motif-containing 2
213854_at	synaptogyrin 1

202475_at	
201734_at	chloride channel 3
200972_at	tetraspan 3
213725_x_at	
209185_s_at	insulin receptor substrate 2
210470_x_at	non-POU-domain-containing, octamer-binding
209118_s_at	tubulin, alpha 3
218561_s_at	CGI-203 protein
214046_at	
207236_at	zinc finger protein 345
206913_at	bile acid Coenzyme A: amino acid N-acyltransferase (glycine N-choloyltransferase)
202412_s_at	ubiquitin specific protease 1
208931_s_at	interleukin enhancer binding factor 3, 90kD
201982_s_at	pregnancy-associated plasma protein A
203417_at	microfibrillar-associated protein 2
58780_s_at	hypothetical protein FLJ10357
203657_s_at	cathepsin F
217886_at	epidermal growth factor receptor pathway substrate 15
202993_at	ilvB (bacterial acetolactate synthase)-like
201031_s_at	heterogeneous nuclear ribonucleoprotein H1 (H)
205337_at	
212261_at	trinucleotide repeat containing 15
206645_s_at	nuclear receptor subfamily 0, group B, member 1
201416_at	SRY (sex determining region Y)-box 4
209789_at	coronin, actin binding protein, 2B
220474_at	solute carrier family 25 (mitochondrial oxodicarboxylate carrier), member 21
207323_s_at	myelin basic protein
204490_s_at	CD44 antigen (homing function and Indian blood group system)
215266_at	hypothetical protein DKFZp434N074
AFFX-BioB-5_at	
202975_s_at	KIAA0878 protein
213564_x_at	lactate dehydrogenase B
220193_at	hypothetical protein FLJ22938
212746_s_at	KIAA0470 gene product
204653_at	transcription factor AP-2 alpha (activating enhancer binding protein 2 alpha)
91920_at	chondroitin sulfate proteoglycan BEHAB/brevican
203587_at	ADP-ribosylation factor 4-like
211728_s_at	hyaluronoglucosaminidase 3
212070_at	G protein-coupled receptor 56

Figure 12 Suppression of Slug expression inhibits melanoma metastasis *in vivo*. **a**, Western blot analysis of Slug protein expression. Slug protein levels were examined in melanocyte cell lines engineered with LT (SVV), LT, hTERT & HGF (STH), LT, hTERT & TPR-Met (STM), LT, hTERT & RasV12 (STR), or LT, hTERT, RasV12 & GFP (STR-GFP), and in transformed kidney cells (293T). **b,** Quantitative RT-PCR performed on immortalized and transformed melanocyte populations stably expressing either siSlug (siSlug1, siSlug2, siSlug3) or control (siGFP2) siRNAs. Data were normalized to GAPDH expression and plotted as a percentage relative to Slug transcript levels in siGFP2-expressing cells. **c**, *In vivo* tumor growth curves of Mel-STR, MEC-STR, and BJ-STR cells stably expressing either siSlug3 or control (siGFP2, siLuc) siRNA contructs. **d**, Quantification of lung metastasis burden in siSlug3- or control siRNA (siGFP2, siLuc)- Mel-STR melanoma lines. Random lung sections were stained with a human-specific vimentin antibody and the area of brown color corresponding to stained Mel-STR cells was quantified using NIH Image software (Cifone and Fidler 1980).

(a)

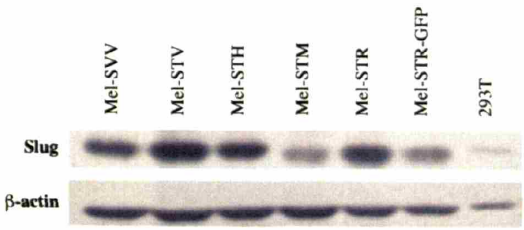
Mel-SVV
Mel-STV
Mel-STH
Mel-STM
Mel-STR
Mel-STR-GFP
293T
Slug
β-actin

(b)

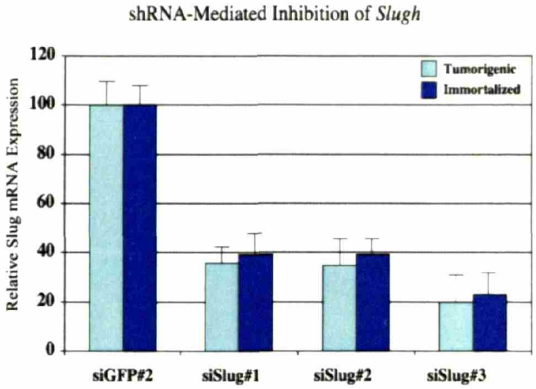
shRNA-Mediated Inhibition of *Slugh*
Relative Slug mRNA Expression
120
100
80
60
40
20
0
Tumorigenic
Immortalized
siGFP#2
siSlug#1
siSlug#2
siSlug#3

(c)

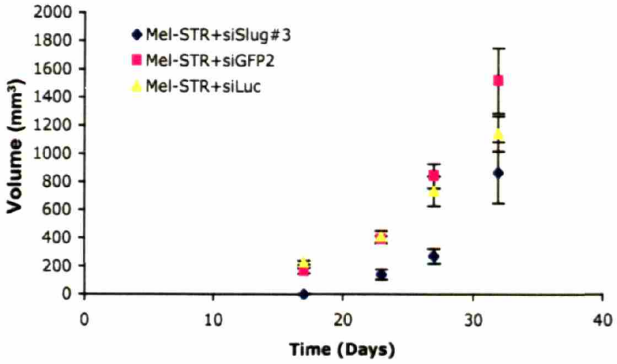
Volume (mm³)
2000
1800
1600
1400
1200
1000
800
600
400
200
0
Mel-STR+siSlug#3
Mel-STR+siGFP2
Mel-STR+siLuc
0
10
20
30
40
Time (Days)

(d)

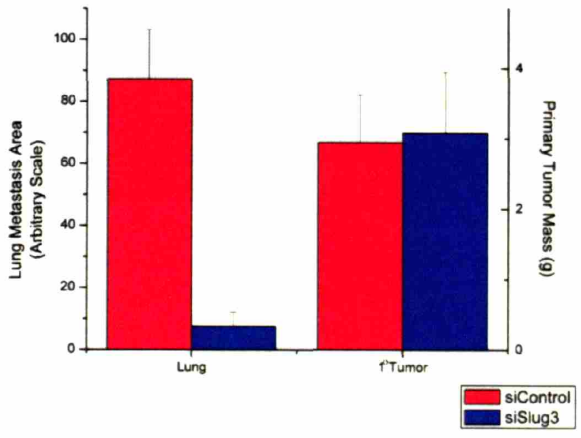
Lung Metastasis Area
(Arbitrary Scale)
100
80
60
40
20
0
Primary Tumor Mass (g)
4
2
0
Lung
f°Tumor
siControl
siSlug3

Figure 13 Mel-STR lung metastases express melanoma markers. H&E (**a**,**b**), MART-1 (**c**,**d**), pan-cytokeratin (**e**,**f**), and vimentin (**g**,**h**) stained sections of Mel-STR metastases encapsulating the lung vasculature. 10x (**a**,**c**,**e**,**g**) and 20x (**b**,**d**,**f**,**h**) magnifications are shown. Arrows in **f** indicate positively stained murine airway epithelium. M, metastasis.

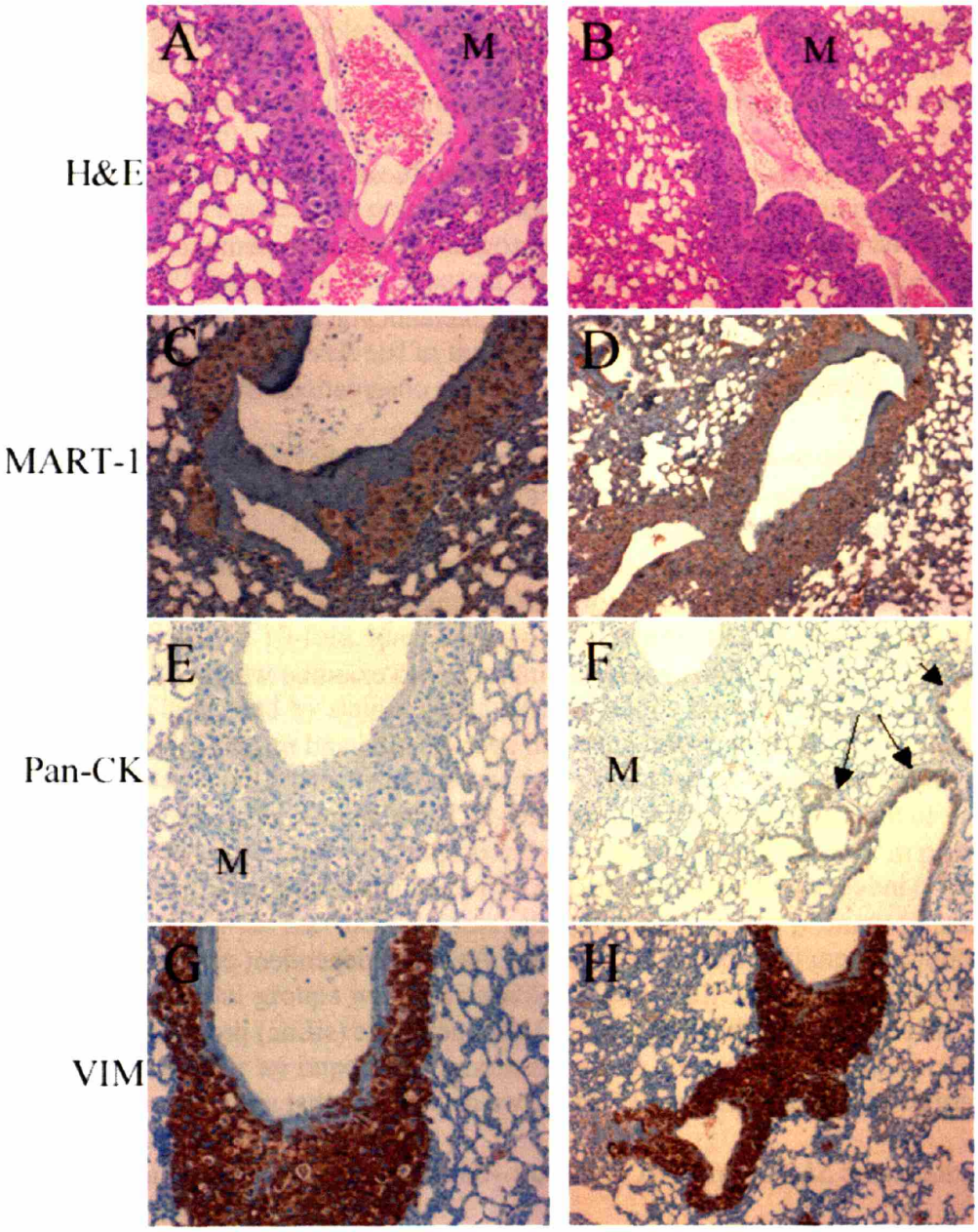
A
M
B
M
H&E
C
D
MART-1
E
M
F
M
Pan-CK
G
H
VIM

neural crest cell and/or melanoblast migrations during development (Figure 11, Table 2). These genes, in addition to Slug itself, include the Endothelin Receptor B (EDNRB)(Pla and Larue 2003), ErbB3, and CD44. Taken together, these findings indicated that components of an embryonic differentiation program involved in neural crest cell motility and migration were expressed in benign melanocytic lesions prior to neoplastic transformation. A question that followed from these observations is whether any of these genes might also contribute to the invasive and metastatic behavior of melanoma cells following melanocyte transformation.

Slug is Essential for Mel-STR Melanoma Metastasis *in vivo*

We utilized retrovirus siRNA-mediated inhibition to examine whether the expression of Slug, a master regulator of neural crest cell specification and migration, was in fact contributing to the metastatic ability of the Mel-STR melanoma cells. Accordingly, we designed three independent retrovirus siRNAs directed against *SLUGH* (siSlug1-3) and stably introduced them into the Mel-STR cells. As two independent controls, we also introduced siRNAs against the GFP (siGfp2) and luciferase (siLuc) proteins into the same cell population. Using quantitative RT-PCR, we determined that siSlug1 and siSlug2 reduced endogenous *SLUGH* mRNA levels by ~66%, whereas siSlug3 reduced endogenous mRNA levels by 80% (Figure 12). Essentially identical levels of relative *SLUGH* mRNA transcript reduction for each siRNA were observed when these same vectors were introduced into the Mel-STV cells (Figure 12)[12].

[12] Since transcription factors are frequently expressed at very low endogenous levels, the detection of Slug protein (see Figure 12) was only possible using a highly sensitive but non-linear signal-amplification protocol (ECL-Femto kit, Pierce). As a consequence, it was not feasible to quantitatively evaluate Slug protein loss due to siRNA-mediated

To test whether a reduction in Slug levels affected melanoma growth or progression, we introduced the Mel-STR+siSlug3 cells, as well as two control lines (Mel-STR +siGfp2 or +siLuc), subcutaneously into immunodeficient mice. *SLUGH* inhibition resulted in a slight decrease in primary tumor growth rates when compared to the control melanoma lines (Figure 12). No apparent differences were observed in the histologies of the primary tumors that developed in the Mel-STR+siSlug3 line versus control lines (data not shown).

In contrast, there was a marked reduction in the incidence of metastasis in the Slug-inhibited cells. Metastatic lung tumor burden in the Mel-STR+siSlug3 tumors was reduced by more than 10-fold when compared to control siGfp2 or siLuc tumors (Figure 12). This was evaluated by staining lung tissue sections for the Mel-STR-specific marker human vimentin, and subsequently quantifying the stained area in random fields with NIH Image software (Figure 13). Importantly, to control for differences in primary tumor growth rates, mice were sacrificed at times such that the average primary tumor burden in the two experimental groups was comparable (Figure 12). These results provide strong indication that Slug is an important component of the metastatic program in the Mel-STR melanoma cells.

Discussion

The siRNA-mediated inhibition experiments in this chapter indicate that the transcription factor Slug provides a strong contribution to the metastatic ability of the Mel-STR melanoma cells. Interestingly, Slug is expressed in both cultured melanocytes

---

repression using Western blotting. It is for this reason that quantitative RT-PCR was used instead to quantitatively determine mRNA inhibition, since this is established method is highly accurate and valid across a wide range of mRNA expression levels.

and melanocytes *in situ* prior to their transformation. Therefore, the expression of Slug is not dependent on the ability of the introduced genetic elements to convert melanocytes to a neoplastic state, and rather appears to be a biological property of the melanocyte cell lineage. Lending support to this notion is the finding that Slug expression in adult melanocytes correlates with the expression of other genes involved in neural crest cell migration. Moreover, this supports the idea that melanocytes within adult tissue retain molecular components of the neural crest cell signaling circuitry (Bronner-Fraser 1993). These observations suggest that this pre-existing neural crest circuitry, of which Slug is one component, can affect the metastatic behavior of melanoma cells following melanocyte transformation. This notion contrasts with the standard paradigm for how tumors acquire metastatic competence, where it is assumed that the potential for metastasis is acquired late during tumor progression and that factors present early in tumor progression play little role if any in enabling metastasis at a later stage of progression.

Materials and Methods

Retrovirus vectors and infections

Retroviral constructs for human HGF and mutant c-Met receptor (TPR-met) were generated by cloning the full-length cDNA of human HGF or TPR-met (kindly provided by G. Vande Woude) into the pBabe-puro vector system (Morgenstern and Land 1990). Other pBABE-based vectors included LTg-zeo (Elenbaas et al. 2001a), hTERT-hygro (Counter et al. 1998), and RasV12-puro (S. Lowe). PWZL-based vectors (Morgenstern and Land 1990) used were RasV12-blast (subcloned from pBABE-RasV12-puro using BamHI/SalI sites) and GFP-blast (gift from A. Orimo). For siRNA-mediated inhibition, three different siRNA sequences against human Slug (5'-AACTGGACACACATACAGTG-3', 5'-GAGGAAAGACTACAGTCCAAG-3', 5'-CAGACCCATTCTGATGTAAAG-3') were cloned into the pLKO lentiviral vector system (kindly provided by S.A.Stewart and W.C.Hahn). SiRNA sequences against GFP and luciferase were described (Counter et al. 1998).

Amphotropic retroviruses were created by transient cotransfection of DNA into 293T cells. 6cm plates were cotransfected with 1 μg of appropriate packaging plasmid (pCL-10A1 (Imgenex) for moloney-based infections and DHR8.1:VSVG (9:1) for lentiviral infections) and 1 μg of carrier vector using FuGene 6 (Roche). Viral supernatants were harvested at 48 hrs post-transfection, passed through a 0.4μm filter, and supplemented with 8 μg/ml polybrene (Sigma) prior to infection.

RT-PCR

Total RNA was isolated from tumor tissues or cell lines using TRIZOL reagent (Invitrogen), following manufacturer's protocols. Quantitative real time RT-PCR

analysis was performed using the iCycler apparatus (Bio-Rad) and SYBR Green PCR Core Reagents System (Perkin-Elmer Applied Biosystems). Results were evaluated using the iCycler IQ Real Time Detection System Software (Bio-Rad). Data were normalized relative to GAPDH expression. Primers used were 5'-ATTCGGGAAAGGTGAAGAGG-3' and 5'-CAGCTGTTCTGCTGTGAAGG-3' (*Pax3*), 5'-ATTCGGACCCACACATTACC-3' and 5'-GGTTTTGGAGCAGTTTTTGC-3' (*Slugh*), 5'-CTCTTTCCTCGTCAGGAAGC-3' and 5'-GGACAGAGTCCCAGATGAGC-3' (*Snail*), 5'-GCTTCCAGACTGTGGACTCG-3' and 5'-CCGTACTGTCCGGAAGACAT-3' (*ErbB3*), 5'-GACCCCTTCATTGACCTCAAC-3' and 5'-CTTCTCCATGGTGGTGAAGA-3' (*GAPDH).*

Quantification of lung metastasis

Entire lungs were removed from mice bearing subcutaneous melanomas and fixed in 10% neutral-buffered formalin for at least 12 hours. Immunohistochemistry was performed on lung tissues with a mouse monoclonal human-specific vimentin antibody, which specifically stains the human melanoma cells (see Figure 13). The area of melanoma burden was quantified using NIH Image software in at least 2 separate hotspot fields per lung, with at least 10 lungs per cell line. Software procedures were detailed previously (Petersen et al. 1996).

Animals and surgery

Athymic nude mice were purchased from Taconic Laboratories (NCR nude, nu/nu). NOD/SCID mice were bred and maintained in-house. All mice were housed in a

specific pathogen-free facility and were administered autoclaved food and water *ad libum*. For *in vivo* tumor experiments, 10^6 cancer cells were resuspended in 200ul of medium and injected subcutaneously into 10-12wk old male NOD/SCID mice or 8wk old irradiated athymic nude mice. Nude mice received 400 rad of γ-radiation using a dual ^{137}Cesium source one day prior to injection. Mice were monitored bi-weekly and tumor diameters were measured using precision calipers. For *in vivo* metastasis experiments, primary tumors were permitted to grow for ~7 weeks or until they reached a diameter of 2cm. For tumor resection experiments, primary tumors were permitted to grow for 18 or 28 days, at which point mice were anesthetized using avertin (0.4-0.7 mg/g body wgt) and the tumors excised under a dissection microscope using DeWecker microdissecting spring scissors and a hand held cautery unit. Mice were monitored daily thereafter until the endpoint of the experiment.

Immunohistochemistry

Immunohistochemistry was performed on formalin-fixed, paraffin-embedded tissues. Five micron sections were de-paraffinized, rehydrated through a graded alcohol series and subjected to antigen retrieval procedures for immunohistochemistry, as described previously(Kuperwasser et al. 2000b). Sections were incubated in mouse monoclonal antibodies against MART-1 (Ventana), pan-cytokeratin (Ventana), human E-cadherin (1:50 Santa Cruz), human β-catenin (1:50, Santa Cruz) or Large T antigen (Pab101, Santa Cruz 1:50). Immunocomplexes were visualized using the ABC peroxidase method (Vector Laboratories, Burlingame, CA). Sections were counterstained with hematoxylin.

RNA extraction and microarray hybridization

Benign nevi were surgically isolated from normal human patients and flash frozen. mRNA was isolated using CsCl gradient centrifugation, fluorescently labeled and subsequently hybridized on an Affymetrix U133A array (22283 genes), following the manufacturer's protocol.

Neighborhood analysis

Neighborhood analysis of SLUGH was performed in a dataset that consists of 9 nevi samples. Genes significantly correlated in their expression pattern with SLUGH were selected by non-parametric permutation testing, using a previously described procedure (Golub et al. 1999). First, all 22283 genes were ranked according to their correlation coefficients with respect to the SLUGH expression profile. 1000 random permutations of the SLUGH profile were then generated, and for each permutation the 22283 genes were re-ranked according to correlation with the shuffled SLUGH profile. A histogram of the distribution of correlation coefficients among 1000 permutations for the CD44 gene is shown in Figure 11. For any gene with a given rank in the original SLUGH correlation list, one determines how many of the 1000 permuted correlation coefficients corresponding to the same rank (but not necessarily the same gene) are greater than or equal to the original, non-permuted correlation coefficient. A p-value can then be assigned by dividing this quantity by the total number of permutations. This procedure for SLUGH in the 9 nevus samples dataset yielded 235 genes with $p<0.05$, of which 31 had $p<0.01$. Supplementary Table 1 online lists all 235 genes with their correlations and corresponding p-values.

Western blotting

Western blotting was performed using standard protocols. Primary antibodies used were against Large T antigen (Pab101, Santa Cruz), Ras (C-20; Santa Cruz), Slug (G-18; Santa Cruz), and ß-actin (Abcam). Goat anti-mouse (115-035-146) and goat anti-rabbit (111-035-144) HRP-conjugated secondary antibodies were purchased from Jackson Immunoresearch.

Chapter 5

Conclusion

Conclusion

While a fundamental feature of human melanoma is its tendency to metastasize to numerous organs throughout the body, very few animal models recapitulate this essential aspect of the disease. In the work described, it is demonstrated that human dermal melanocytes, transformed by the introduction of the SV40ER, hTERT, and RasG12V genes, form primary tumors that are invasive and highly metastatic to secondary sites in the body. Moreover, the anatomical sites of metastasis exhibited by the melanoma cells created in this manner are analogous to those observed in human patients. To our knowledge, this is the first human melanoma model that exhibits multi-organ metastases from a single subcutaneous site with high penetrance.

The introduction of an identical set of genes into human epithelial and fibroblast cell types results in localized tumor formation in the absence of metastasis. Importantly, implementation of an isogenic transformation protocol controls for the possibility that oncogene-specific differences are responsible for the various cancer phenotypes observed upon experimental conversion of primary human epithelial, fibroblast, and melanocyte cell types to a neoplastic state. These results therefore indicate that the rapid progression of human melanomas to a metastatic state can be attributed in part to lineage-specific factors associated with the melanocyte differentiation program.

In support of the notion that normal melanocytes prior to transformation express a differentiation program that harbors factors capable of promoting migratory behaviors, is a commonly observed histologic occurrence in human lymph nodes termed nevus cell aggregates [29-31]. These are characterized by clusters of histologically normal

melanocytes detected within the capsule of lymph nodes, particularly those from the axillary, cervical, and inguinal regions. This unique clinical observation, made in the absence of any malignant histology, suggests that dermal melanocytes indeed possess latent migratory abilities.

The present results validate a previously untested speculation made some years ago (9) that the particularly aggressive nature of melanomas is ascribable to the derivation of dermal melanocytes from the embryonic neural crest. By controlling for oncogene-specific differences, our experiments demonstrate that the differentiation program of normal melanocytes can collaborate with oncogenic lesions to predispose their transformed derivatives to forming invasive and metastatic tumors. This notion is supported by analysis of microarray data from benign human nevus tissues, which reveal co-regulated expression of genes known to be important for neural crest cell migrations during development, prior to neoplastic transformation of melanocytes. Moreover, one of these genes, encoding the neural crest cell transcription factor Slug, plays an important functional role in the metastatic spread of the Mel-STR melanoma cells. An interesting question not answered by this work is whether other genes that were identified that correlate with Slug expression in human nevi, which are known to be involved in neural crest cell migration, also contribute to melanoma's metastatic ability.

It is quite possible that melanocytes within human skin are not all identical with respect to their epigenetic or differentiation state. As such, it is formally possible that one or another of the melanocyte subtypes might represent the originating cell type of the majority of melanomas observed in human patients. At the very least, in accordance with the primary observation described in this thesis, the phenotype of any given melanoma

tumor may well depend on the identity of the melanocyte cellular subtype from which it originated. Thus, while the transformation of a bulk isolated primary melanocyte cell population in culture offers certain experimental advantages, it should be noted that it also carries with it the danger of transforming a cellular subtype that is not representative of the cell type from which the human disease originates.

The present results do not address whether Slug expression is sufficient to enable melanoma metastasis. The multi-step nature of metastasis makes it unlikely that a single factor can orchestrate this complex process. Moreover, the fact that Slug is expressed in benign melanocytic lesions implies that acquisition of its expression following transformation is not a pathogenetic event enabling metastasis. Nevertheless, the preexisting expression of Slug in benign precursor lesions may reduce the number of additional rate-limiting alterations required to enable metastasis following melanocyte transformation, when compared to cancers arising from other cell types. These experiments indicate that lineage-specific factors associated with melanocyte differentiation can significantly impact the tumorigenic and metastatic phenotype observed following neoplastic transformation.

Reference List

Ackermann J, Frutschi M, Kaloulis K, McKee T, Trumpp A and Beermann F. (2005a). *Cancer Res,* **65,** 4005-4011.

Ackermann J, Frutschi M, Kaloulis K, McKee T, Trumpp A and Beermann F. (2005b). *Cancer Res,* **65,** 4005-4011.

Bardeesy N, Bastian BC, Hezel A, Pinkel D, DePinho RA and Chin L. (2001b). *Mol Cell Biol,* **21,** 2144-2153.

Bardeesy N, Bastian BC, Hezel A, Pinkel D, DePinho RA and Chin L. (2001a). *Mol Cell Biol,* **21,** 2144-2153.

Bedrosian I, Faries MB, Guerry Dt, Elenitsas R, Schuchter L, Mick R, Spitz FR, Bucky LP, Alavi A, Elder DE, Fraker DL and Czerniecki BJ. (2000). *Ann Surg Oncol,* **7,** 262-7.

Blanco MJ, Moreno-Bueno G, Sarrio D, Locascio A, Cano A, Palacios J and Nieto MA. (2002). *Oncogene,* **21,** 3241-3246.

Boehm JS, Hession MT, Bulmer SE and Hahn WC. (2005). *Mol Cell Biol,* **25,** 6464-6474.

Boissy RE. (2003). *Exp Dermatol,* **12 Suppl 2,** 5-12.

Bond JA, Oddweig NG, Rowson J, Ivan M, White D and Wynford-Thomas D. (1996). *Int J Cancer,* **67,** 563-572.

Bronner-Fraser M. (1993). *Trends Cell Biol,* **3,** 392-7.

Burstyn-Cohen T, Stanleigh J, Sela-Donenfeld D and Kalcheim C. (2004). *Development,* **131,** 5327-5339.

Cameron MD, Schmidt EE, Kerkvliet N, Nadkarni KV, Morris VL, Groom AC, Chambers AF and MacDonald IC. (2000). *Cancer Res,* **60,** 2541-2546.

Chedekel MR and Zeise L. (1988). *Lipids,* **23,** 587-591.

Chin L. (2003). *Nat Rev Cancer,* **3,** 559-70.

Chin L, Pomerantz J, Polsky D, Jacobson M, Cohen C, Cordon-Cardo C, Horner JW and DePinho RA. (1997). *Genes Dev,* **11,** 2822-2834.

Chin L, Tam A, Pomerantz J, Wong M, Holash J, Bardeesy N, Shen Q, O'Hagan R, Pantginis J, Zhou H, Horner JW2, Cordon-Cardo C, Yancopoulos GD and DePinho RA. (1999). *Nature,* **400,** 468-72.

Christiansen JH, Coles EG and Wilkinson DG. (2000a). *Curr Opin Cell Biol,* **12,** 719-724.

Christiansen JH, Coles EG and Wilkinson DG. (2000b). *Curr Opin Cell Biol,* **12,** 719-724.

Cifone MA and Fidler IJ. (1980). *Proc Natl Acad Sci U S A,* **77,** 1039-43.

Cohen C, Zavala-Pompa A, Sequeira JH, Shoji M, Sexton DG, Cotsonis G, Cerimele F, Govindarajan B, Macaron N and Arbiser JL. (2002). *Clin Cancer Res,* **8,** 3728-3733.

Corsetti RL, Allen HM and Wanebo HJ. (2000). *Ann Surg Oncol,* **7,** 456-60.

Counter CM, Hahn WC, Wei W, Caddle SD, Beijersbergen RL, Lansdorp PM, Sedivy JM and Weinberg RA. (1998). *Proc Natl Acad Sci U S A,* **95,** 14723-8.

Cruz J, Reis-Filho JS, Silva P and Lopes JM. (2003). *Oncology,* **65,** 72-82.

De CJ, Araya C, Marchant L, Riaz CF and Mayor R. (2005). *Development,* **132,** 2587-2597.

Demunter A, Libbrecht L, Degreef H, De Wolf-Peeters C and van den Oord JJ. (2002a). *Mod Pathol,* **15,** 454-461.

Demunter A, Libbrecht L, Degreef H, De Wolf-Peeters C and van den Oord JJ. (2002b). *Mod Pathol,* **15,** 454-461.

Diamandopoulos GT, Miller MH, McLane MF and Evans PG. (1976). *Cancer Res,* **36,** 3171-3177.

Dupin E and Le Douarin NM. (2003). *Oncogene,* **22,** 3016-3023.

Elenbaas B, Spirio L, Koerner F, Fleming MD, Zimonjic DB, Donaher JL, Popescu NC, Hahn WC and Weinberg RA. (2001b). *Genes Dev,* **15,** 50-65.

Elenbaas B, Spirio L, Koerner F, Fleming MD, Zimonjic DB, Donaher JL, Popescu NC, Hahn WC and Weinberg RA. (2001a). *Genes Dev,* **15,** 50-65.

Elloul S, Elstrand MB, Nesland JM, Trope CG, Kvalheim G, Goldberg I, Reich R and Davidson B. (2005). *Cancer,* **103,** 1631-1643.

Elsayed AM, Albahra M, Nzeako UC and Sobin LH. (1996). *Am J Gastroenterol,* **91,** 1001-6.

Giordano S, Bardelli A, Zhen Z, Menard S, Ponzetto C and Comoglio PM. (1997). *Proc Natl Acad Sci U S A,* **94,** 13868-72.

Giordano S, Ponzetto C, Di Renzo MF, Cooper CS and Comoglio PM. (1989). *Nature,* **339,** 155-6.

Golub TR, Slonim DK, Tamayo P, Huard C, Gaasenbeek M, Mesirov JP, Coller H, Loh ML, Downing JR, Caligiuri MA, Bloomfield CD and Lander ES. (1999). *Science,* **286,** 531-7.

Gorden A, Osman I, Gai W, He D, Huang W, Davidson A, Houghton AN, Busam K and Polsky D. (2003). *Cancer Res,* **63,** 3955-3957.

Goydos JS, Mann B, Kim HJ, Gabriel EM, Alsina J, Germino FJ, Shih W and Gorski DH. (2005). *J Am Coll Surg,* **200,** 362-370.

Hahn WC, Counter CM, Lundberg AS, Beijersbergen RL, Brooks MW and Weinberg RA. (1999a). *Nature,* **400,** 464-8.

Hahn WC, Counter CM, Lundberg AS, Beijersbergen RL, Brooks MW and Weinberg RA. (1999b). *Nature,* **400,** 464-468.

Hajra KM, Chen DY and Fearon ER. (2002). *Cancer Res,* **62,** 1613-8.

Jain AN, Tokuyasu TA, Snijders AM, Segraves R, Albertson DG and Pinkel D. (2002). *Genome Res,* **12,** 325-32.

Jouneau A, Yu YQ, Pasdar M and Larue L. (2000). *Pigment Cell Res,* **13,** 260-272.

Kageshita T, Hamby CV, Ishihara T, Matsumoto K, Saida T and Ono T. (2001). *Br J Dermatol,* **145,** 210-216.

Kang Y, Siegel PM, Shu W, Drobnjak M, Kakonen SM, Cordon-Cardo C, Guise TA and Massague J. (2003). *Cancer Cell,* **3,** 537-549.

Kanitakis J. (2002). *Eur J Dermatol,* **12,** 390-399.

Kumar R, Angelini S, Snellman E and Hemminki K. (2004). *J Invest Dermatol,* **122,** 342-348.

Kuperwasser C, Hurlbut GD, Kittrell FS, Dickinson ES, Laucirica R, Medina D, Naber SP and Jerry DJ. (2000a). *Am J Pathol,* **157,** 2151-9.

Kuperwasser C, Pinkas J, Hurlbut GD, Naber SP and Jerry DJ. (2000b). *Cancer Res,* **60,** 2723-9.

LaBonne C and Bronner-Fraser M. (2000). *Dev Biol,* **221,** 195-205.

Li G, Schaider H, Satyamoorthy K, Hanakawa Y, Hashimoto K and Herlyn M. (2001). *Oncogene,* **20,** 8125-35.

Lundberg AS, Randell SH, Stewart SA, Elenbaas B, Hartwell KA, Brooks MW, Fleming MD, Olsen JC, Miller SW, Weinberg RA and Hahn WC. (2002). *Oncogene,* **21,** 4577-4586.

Minn AJ, Gupta GP, Siegel PM, Bos PD, Shu W, Giri DD, Viale A, Olshen AB, Gerald WL and Massague J. (2005a). *Nature,* **436,** 518-524.

Minn AJ, Kang Y, Serganova I, Gupta GP, Giri DD, Doubrovin M, Ponomarev V, Gerald WL, Blasberg R and Massague J. (2005b). *J Clin Invest,* **115,** 44-55.

Miyoshi A, Kitajima Y, Kido S, Shimonishi T, Matsuyama S, Kitahara K and Miyazaki K. (2005). *Br J Cancer,* **92,** 252-258.

Morgenstern JP and Land H. (1990). *Nucleic Acids Res,* **18,** 3587-96.

Natali PG, Nicotra MR, Di Renzo MF, Prat M, Bigotti A, Cavaliere R and Comoglio PM. (1993). *Br J Cancer,* **68,** 746-50.

Omholt K, Karsberg S, Platz A, Kanter L, Ringborg U and Hansson J. (2002). *Clin Cancer Res,* **8,** 3468-3474.

Omholt K, Platz A, Kanter L, Ringborg U and Hansson J. (2003a). *Clin Cancer Res,* **9,** 6483-6488.

Omholt K, Platz A, Kanter L, Ringborg U and Hansson J. (2003b). *Clin Cancer Res,* **9,** 6483-6488.

Palmer HG, Larriba MJ, Garcia JM, Ordonez-Moran P, Pena C, Peiro S, Puig I, Rodriguez R, de la FR, Bernad A, Pollan M, Bonilla F, Gamallo C, de Herreros AG and Munoz A. (2004). *Nat Med,* **10,** 917-919.

Papp T, Schipper H, Kumar K, Schiffmann D and Zimmermann R. (2005). *Melanoma Res,* **15,** 401-407.

Petersen SL, Gardner E, Adelman J and McCrone S. (1996). *Endocrinology,* **137,** 234-9.

Phillips DL, Benner KG, Keeffe EB and Traweek ST. (1987). *J Clin Gastroenterol,* **9,** 563-7.

Pla P and Larue L. (2003). *Int J Dev Biol,* **47,** 315-325.

Pollock PM, Stark MS, Palmer JM, Walters MK, Aitken JF, Martin NG and Hayward NK. (2001a). *Genes Chromosomes Cancer,* **32,** 89-94.

Pollock PM, Welch J and Hayward NK. (2001b). *Cancer Res,* **61,** 1154-1161.

Prince S, Illing N and Kidson SH. (2001). *Cell Biol Int,* **25,** 91-102.

Reifenberger J, Knobbe CB, Sterzinger AA, Blaschke B, Schulte KW, Ruzicka T and Reifenberger G. (2004). *Int J Cancer,* **109,** 377-384.

Rimm DL, Caca K, Hu G, Harrison FB and Fearon ER. (1999). *Am J Pathol,* **154,** 325-329.

Rubinfeld B, Albert I, Porfiri E, Munemitsu S and Polakis P. (1997). *Cancer Res,* **57,** 4624-4630.

Shamamian P, Mancini M, Kawakami Y, Restifo NP, Rosenberg SA and Topalian SL. (1994a). *Cancer Immunol Immunother,* **39,** 73-83.

Shamamian P, Mancini M, Kawakami Y, Restifo NP, Rosenberg SA and Topalian SL. (1994b). *Cancer Immunol Immunother,* **39,** 73-83.

Shaw HM, McCarthy WH, McCarthy SW and Milton GW. (1987). *Arch Surg,* **122,** 1147-50.

Shinozaki M, Fujimoto A, Morton DL and Hoon DS. (2004). *Clin Cancer Res,* **10,** 1753-1757.

Si SP, Tsou HC, Lee X and Peacocke M. (1993). *J Invest Dermatol,* **101,** 383-386.

Snijders AM, Fridlyand J, Mans DA, Segraves R, Jain AN, Pinkel D and Albertson DG. (2003). *Oncogene,* **22,** 4370-9.

Sorlie T, Perou CM, Tibshirani R, Aas T, Geisler S, Johnsen H, Hastie T, Eisen MB, van de RM, Jeffrey SS, Thorsen T, Quist H, Matese JC, Brown PO, Botstein D, Eystein LP and Borresen-Dale AL. (2001). *Proc Natl Acad Sci U S A,* **98,** 10869-10874.

Takeno S, Noguchi T, Fumoto S, Kimura Y, Shibata T and Kawahara K. (2004). *Am J Clin Pathol,* **122,** 78-84.

Tietze MK and Chin L. (2000). *Mol Med Today,* **6,** 408-10.

Tolleson WH, Doss JC, Latendresse J, Warbritton AR, Melchior WB, Jr., Chin L, Dubielzig RR and Albert DM. (2005). *Arch Ophthalmol,* **123,** 1088-1094.

Tucker RP. (2004b). *Int J Biochem Cell Biol,* **36,** 173-177.

Tucker RP. (2004a). *Int J Biochem Cell Biol,* **36,** 173-177.

Uchikado Y, Natsugoe S, Okumura H, Setoyama T, Matsumoto M, Ishigami S and Aikou T. (2005). *Clin Cancer Res,* **11,** 1174-1180.

van ', V, Burgering BM, Versteeg R, Boot AJ, Ruiter DJ, Osanto S, Schrier PI and Bos JL. (1989). *Mol Cell Biol,* **9,** 3114-3116.

van ', V, Dai H, van d, V, He YD, Hart AA, Mao M, Peterse HL, van der KK, Marton MJ, Witteveen AT, Schreiber GJ, Kerkhoven RM, Roberts C, Linsley PS, Bernards R and Friend SH. (2002). *Nature,* **415,** 530-536.

Weeraratna AT, Jiang Y, Hostetter G, Rosenblatt K, Duray P, Bittner M and Trent JM. (2002). *Cancer Cell,* **1,** 279-288.

Yazdi AS, Palmedo G, Flaig MJ, Puchta U, Reckwerth A, Rutten A, Mentzel T, Hugel H, Hantschke M, Schmid-Wendtner MH, Kutzner H and Sander CA. (2003a). *J Invest Dermatol,* **121,** 1160-1162.

Yazdi AS, Palmedo G, Flaig MJ, Puchta U, Reckwerth A, Rutten A, Mentzel T, Hugel H, Hantschke M, Schmid-Wendtner MH, Kutzner H and Sander CA. (2003b). *J Invest Dermatol,* **121,** 1160-1162.

Appendix I

Estrogen Promotes the Growth of Estrogen Receptor-Negative Cancers[1]

[1] This work has been submitted for publication. The experiments described were initiated prior to my involvement in the project by Charlotte Kuperwasser (Tufts-NEMC). The data contained in Figure 1 of the manuscript therefore represents her own independent contribution. The data depicted in Figures 2-4 are the outcome of experiments designed and conducted with the active participation of both Dr. Kuperwasser and myself.

Estrogen promotes the growth of estrogen receptor-negative cancers

Piyush B. Gupta[1,2], David Proia[3], Janusz Weremowicz [3], Stephen P. Naber [4], Robert A. Weinberg[1,2] Charlotte Kuperwasser[3,5#]

[1] Department of Biology, Massachusetts Institute of Technology, Cambridge, MA 02142.

[2] Whitehead Institute for Biomedical Research, Nine Cambridge Center, Cambridge, MA 02142.

[3] Department of Anatomy & Cellular Biology, Tufts University School of Medicine, 136 Harrison Ave, Boston, MA 02111.

[4] Department of Pathology, Tufts-New England Medical Center,, Boston, MA 02111.

[5] Department of Radiation Oncology, Tufts-New England Medical Center, Molecular Oncology Research Institute, Boston, MA 02111.

To whom correspondence may be addressed:
Charlotte Kuperwasser
Tufts University School of Medicine
750 Washington Street, box 5609
Boston, MA 02111
Phone: (617) 636-2364
Fax: (617) 636-6127
Email: Charlotte.Kuperwasser@tufts.edu

Keywords: parturition, breast cancer, angiogenesis, EPC, stroma, systemic, estrogen, bone marrow

Abstract

Epidemiologic studies have revealed that, while one full-term pregnancy reduces the lifetime risk of developing breast cancer by 50%, there is a significant increase in age-adjusted risk in the 1-5 years immediately following parturition. The mechanisms responsible for this short-term increase in cancer incidence are not known, in part due to the lack of appropriate animal models to study this phenomenon. We have developed a novel human xenograft model of pregnancy-dependent breast tumorigenesis. Using this model, we identify systemic physiological changes following parturition that promote the formation and expansion of estrogen receptor (ER)-negative breast cancers at both orthotopic and heterotopic sites of growth. Use of pharmacological inhibitors reveals that estrogens are important mediators of the observed cancer growth following parturition, despite the absence of ER expression by cancer cells. We show that estrogens are able to promote the growth of ER-negative cancers by systemically enhancing neo-angiogenesis. The systemic enhancement of neo-angiogenesis is accompanied by an increase in the recruitment of cells from the peripheral circulation into the growing tumor mass, including myofibroblasts and endothelial progenitor cells. These results reveal a novel mechanism by which estrogens promote the growth of ER-negative cancers and indicate that the estrogen inhibitors may be useful in the treatment of ER-negative cancers in women.

Introduction

The etiology of breast cancer is complex, with numerous factors contributing to the lifetime risk of developing the disease. These factors include inherited genes, an

early age of menarche a late onset of menopause, and parity[1] (*1-3*). In particular, one full-term pregnancy reduces the lifetime risk of developing breast cancer by 50% (*4-7*). Despite the long-term protective benefit conferred by parity on breast cancer risk, uniparous and biparous women actually have a significant increase in age-adjusted breast cancer incidence within the first 5 years following parturition[2] (*4-12*). While a hormonal etiology is suspected, the mechanism(s) underlying this dual effect of parity on breast cancer risk remain unclear.

The roles that hormones plays in regulating post-natal mammary gland development are well understood (*13-16*). The mammary gland undergoes significant post-pubertal development during pregnancy, at which time the systemic hormones estrogen and progesterone drive further epithelial proliferation, side-branching and differentiation (*17, 18*). Following parturition, prolactin and oxytocin promote milk production and secretion until the cessation of nursing, at which point a period of mammary gland involution ensues, characterized by extensive apoptosis and stromal remodeling (*19-22*).

The changes occurring locally within the breast microenvironment during the period following parturition are accompanied by major systemic changes in physiology and circulating hormone levels. For instance, following lactation there is a rapid and sharp decline in levels of milk-producing factors, including prolactin, insulin-like growth factor-1, and glucocorticoids (*23, 24*). Additionally, once nursing ceases, circulating levels of estrogen and progesterone progressively increase until the re-initiation of the

---

1 pregnancy

2 childbirth

menstrual cycle. The influence of these and other systemic changes in physiology on breast cancer risk following parturition has remained essentially unexplored.

While the full repertoire of hormonal changes following parturition remains incompletely uncharacterized, it is widely presumed that the increased risk of developing breast cancer following pregnancy is due to the ability of pregnancy-associated hormones to promote the further proliferation of an initiated target cell population. However, the majority of breast cancers that develop during this time lack appreciable expression of either the estrogen or progesterone receptors (*25, 26*). In contrast, ~60% of the breast cancers that are not associated with pregnancy are ER/PR-positive. This important observation suggests that if hormones are involved in promoting breast cancer following pregnancy, they may not be doing so through direct binding to hormone receptor molecules expressed by breast epithelial cells.

In this paper, we investigate the hypothesis that steroid hormones promote the outgrowth of ER/PR-negative cancers by influencing host cell types distinct from the breast epithelium itself. We utilize a novel xenograft mouse model of parturition-induced breast carcinoma formation in which the tumors that arise following pregnancy are negative for the expression of hormone receptors, recapitulating the clinical situation described above. Despite lacking estrogen receptor expression, we show that the tumors that arise following pregnancy in this model require circulating estrogens for their formation. Moreover, we demonstrate that increasing the levels of circulating estrogens is sufficient to promote the formation and progression of ER-negative cancers via a systemic increase in host angiogenicity.

Materials and Methods

Cells, Tissue culture and Plasmids

Human breast epithelial cell lines were generated through the introduction of the SV40 large T antigen, hTERT and RasV12 as previously described (*27*). Cells were grown in DMEM:F12 (1:1) supplemented with 5% calf serum, insulin (10ug/ml), EGF(10ng/ml), hydrocortisone (1ug/ml). Two versions of these cells, termed pHMLER and hHMLER , differ in their levels of H-Ras protein expression (*27*). PC-3 human prostate cancer cells were purchased from ATCC (http://www.atcc.org/) and grown following the supplier's protocol.

In vivo tumorigenesis and angiogenesis experiments

All *in vivo* studies were carried out using immunocompromised NOD/SCID female mice maintained in a specific pathogen-free animal facility (Jackson Labs stock number: 001303). Unlike athymic nude mice, female NOD/SCID mice are fertile and exhibit normal mammary gland development. Involution studies were performed by breeding 2 female mice per one male animal and separating the females after the mice tested positive for vaginal plugs. Following parturition, females were allowed to nurse for 10 days with an equal number of pups per female to permit adequate and uniform lactation for all females. On day 10 or 11 of lactation, all pups were removed from nursing mothers to induce synchronous mammary gland involution. Experiments were initiated 24 hours after pup removal.

For tumorigenicity assays, $1x10^6$ breast epithelial cells were resuspended in ECM (Matrigel), diluted 1:3 with culture medium, and injected either subcutaneously

(s.c.) or into the 4th inguinal mammary glands of involuting or age-matched nulliparous female mice.

For hormone studies, slow-release pellets (Innovative Research of America) of 17ß-estradiol (1.7mg/pellet, 0.72mg/pellet, or 0.1mg/pellet), tamoxifen (25mg/pellet), and RU486l (50mg/pellet), or placebo pellets were introduced subcutaneously at the same time that cells were implanted into mice. All hormone pellets were 60-day slow release with biodegradable carrier-binders. Estrogen pellets of mass 0.1mg, 0.72mg, and 1.7mg resulted in circulating plasma levels of 50-75pg/ml, 300-400pg/ml, and >900pg/ml, respectively. Tamoxifen and RU486 pellets resulted in circulating drug levels of 3ug/ml and 2ug/ml, respectively. Letrozole was kindly provided by Dr. Dean Evans (Novartis Pharma, Basel Switzerland). Mice received daily s.c. injection of letrozole 10μg in 100ul of 0.3% hydroxyl propyl cellulose (in phosphate buffered saline). Control mice received 100ul injections of vehicle.

For angiogenesis studies, 8-week-old female NOD/SCID mice received a 250ul injection of diluted ECM containing 50ng/ml of basic fibroblasts growth factor (bFGF) (Sigma). Mice either received an estrogen pellet (1.7mg/pellet) or placebo pellet at the same time of injection. After 7 days, mice were sacrificed and the ECM plugs, along with blood, bone marrow, mammary glands, and uteri were isolated.

Bone Marrow Transplantation

C57/BL6-GFP transgenic mice were crossed onto a Rag-1^{null} background to generate Rag-1^{null}/GFP transgenic mice. 8- to 10-week old female mice were sacrificed and femur, tibia, and humerus bones were flushed with PBS to harvest bone marrow. Cells were washed and 10 x 10^6 bone marrow cells were injected into lethally irradiated

(3.81Gy gamma radiation from a Cesium source) NOD/SCID mice by retro-orbital plexus administration. Mice were utilized for experiments 4-6 weeks following bone marrow reconstitution.

Peripheral blood was collected from mice 4 weeks following bone marrow transplantation and was treated with red blood cell lysis buffer (Sigma) following the manufacturer's protocol. The resulting single cell suspensions were subjected to FACS analysis. A total of $1x10^5$ viable cells, determined by propidium iodide exclusion, were analyzed for each sample.

Histology and Immunostaining

For histological analysis, tumor tissue was removed from animals and immediately fixed in 10% buffered formalin, followed by paraffin embedding. Five micron sections were deparaffinized, rehydrated and subjected to either trichrome staining (to visualize collagen) or hemotoxylin and eosin staining. Immunohistochemistry (IHC) was performed following deparaffinization and antigen retrieval. Immunocomplexes were visualized by the ABC method (Vector Laboratories). Sections were counterstained with either hematoxylin or methyl green. Immunofluorescence was performed on 5 um frozen sections of tissues that were fixed in 4% para-formaldehyde, saturated with 20% sucrose, and embedded in OCT. Immunocomplexes were visualized with fluorescent avidin conjugated secondary antibodies (Vector Laboratories). Cell nuclei were visualized by DAPI staining.

Tissue sections were incubated with mouse monoclonal, rat or rabbit polyclonal antibodies against SV40 large T antigen (Santa Cruz Pab101), α-smooth muscle actin (NCL-SMA, Novacastra), von Willebrand Factor (DAKO), estrogen receptor (ERα:

DAKO, ERβ: Santa Cruz Biotechnology), GFP (Abcam), CD34 (Santa Cruz Biotechnology), CD31 (BD Biosciences), and human Flt-1 (Santa Cruz Biotechnology).

Angiogenesis Quantification

Paraffin sections of ECM plugs and tumor tissues were subjected to anti-von Willebrand Factor immunohistochemistry to visualize endothelial cells. Using the methodology described in (*28*) (*29*), a 49-point Chalkley eyepiece graticule was used to quantify the mean cross-sectional vessel area per section. Mean cross-sectional vessel boundary length was quantified using a Merz straight line interrupted graticule employed over the same regions (*28*) (*29*). For all measurements, at least 3-4 hotspot fields in at least 4 independent samples were evaluated.

Western Blot Analysis

Total protein was extracted from cell lines and tumor tissues using an extraction buffer of 50mM Tris, 100mM NaCl, 5mM EDTA, 1%NP40 detergent in the presence of protease inhibitors (Roche). Tissues were minced and then homogenized in 5 volumes of this extraction buffer. All tissue debris was removed by centrifugation and 50ug of total protein was analyzed by SDS-PAGE analysis. Blots were probe with antibodies against human ERα (Santa Cruz), ERβ (Santa Cruz), and β-actin (Abcam).

Results

Parturition enhances tumor growth, stromalization and angiogenesis in the mammary gland

Based on the epidemiology described above, we hypothesized that the altered hormonal milieu following pregnancy and parturition promotes the growth of breast

carcinomas. To examine this notion experimentally, we introduced pHMLER (*27*) breast cancer cells either into mice following parturition or into age-matched nulliparous mice, and monitored the animals for subsequent tumor growth. In order to effectively control for daily fluctuations in physiology following parturition, we synchronized the physiological states of the mice by inducing simultaneous mammary gland involution (see Materials and Methods). While pHMLER mammary tumors formed with high penetrance in both nulliparous mice and mice injected following parturition, tumors that formed in the latter cohort developed with a significantly shorter latency, arising 2-4 weeks prior to their counterparts in nulliparous hosts (Figure 1). In addition, although the orthotopic site of introduction precluded accurate measurements of growth kinetics *in vivo*, tumors harvested from mice injected following parturition were, at the endpoint of the experiment, four times as large as their counterparts in nulliparous mice (2021mg vs. 525mg; Figure 1).

Given these findings with breast carcinoma cells, we considered whether the host environment following parturition might also promote the outgrowth of initiated but weakly tumorigenic breast epithelial cells. We therefore utilized the weakly tumorigenic hHMLER cells (*27, 30*), which survive at the site of implantation, but rarely progress to form tumors (<5% penetrance within 12 wks) when injected either subcutaneously or into the mammary glands of mice. When introduced into the mammary glands of nulliparous mice, the hHMLER cells, as expected, did not form tumors yet remained viable at the site of injection, forming benign epithelial structures (Figure 1). In contrast, hHMLER cells injected into involuting mammary glands formed palpable mammary tumors within 8 weeks in a significant fraction of mice (Figure 1). These tumors were capable of growing

to a large size, indicating that the maintenance of hHMLER tumors, once formed in post-parturition animals, was not dependent upon continued mammary gland involution (data not shown).

Interestingly, hHMLER and pHMLER tumors that developed in mice injected following parturition exhibited striking histological differences compared to tumors arising in nulliparous hosts. While pHMLER mammary tumors that formed in nulliparous mice were poorly differentiated carcinomas with keratinized regions of metaplasia and minimal stromal involvement as previously described (26), those that arose in mice following parturition were significantly more differentiated and incorporated a large proportion of stromal cells within the tumor tissue (Figure 1). Tumors arising from hHMLER cells injected into involuting mammary glands similarly exhibited a highly stromalized histological phenotype (Figure 1). The abundance of stromal cells was confirmed by staining tumor sections for the SV40 Large T (LT) antigen, which is expressed in the introduced hHMLER or pHMLER cells; these revealed that host-derived stromal cells constituted as much as 50% of the tumor tissue in some areas (Figure 1). The enhanced stromal infiltration was accompanied by a significant increase in angiogenesis, as gauged by Chalkley counts and microvascular density measurements performed on pHMLER tumors arising either in mice following parturition or in nulliparous mice (Figure 1).

The histology of tumors arising in mice injected following parturition indicated a desmoplastic stromal response, which is often associated with the histology of aggressive clinical breast cancer samples (*31*). Desmoplasia is characterized by hyperactivation and proliferation in stromal regions surrounding malignant epithelial cells, with expression of

α-smooth muscle actin (αSMA) and secretion of large quantities of collagen and other factors by (myo)fibroblasts (*31*). In fact, mammary fibroblasts within the stroma of tumors arising in mice following parturition expressed significant levels of αSMA, confirming that the extensive stromal involvement included a desmoplastic response (Figure 1). Also in support of this notion, Mason's trichrome staining revealed large amounts of collagen deposition in these tumors (Figure 1). In contrast to these observations, little collagen deposition or αSMA expression was observed in pHMLER tumors arising in nulliparous mice (data not shown).

Taken together, these data indicated that the host environment following pregnancy and parturition enhanced tumor formation in the mammary gland by both overtly tumorigenic as well as initiated, non-tumorigenic breast epithelial cells. Moreover, tumor formation in hosts following parturition was accompanied by a significantly enhanced desmoplastic and angiogenic stromal response, relative to nulliparous hosts. Thus, an altered host physiology following parturition was capable of profoundly altering the growth and phenotype of carcinomatous and pre-malignant breast epithelial cells in the mammary gland.

Physiological alterations associated with parturition systemically promote breast tumor formation

Since post-partum hosts are characterized by physiological changes that occur both locally within the mammary gland as well as systemically, we reasoned that alterations of either type might be contributing to the enhanced tumor formation observed following parturition. To determine if systemic alterations following parturition were sufficient to enhance tumor formation, we performed experiments analogous to those

described above, doing so at subcutaneous sites of injection. For these and subsequent experiments, we utilized the hHMLER cells, whose weak tumorigenic ability served to magnify the tumor-enhancing effects associated with parturition in our experimental model system.

Remarkably, hHMLER cells introduced subcutaneously into mice following parturition frequently formed tumors, whereas the identical cells introduced subcutaneously into age-matched nulliparous mice failed to do so. This finding indicated that the tissue environment of the mammary gland was not required for the enhanced tumorigenesis observed following parturition and that systemic alterations in physiology occurring at this time were capable of promoting the observed tumor growth. Although the hHMLER cells were injected at a different anatomical site, the subcutaneous tumors that formed following parturition were well vascularized and stromalized, with histology quite similar to that exhibited by tumors growing at orthotopic sites. Upon histopathological examination these subcutaneous tumors were characterized as breast carcinomas bearing significant regions of desmoplastic stromal contribution, as gauged by Mason's trichrome and αSMA staining (Figure 1).

Estrogen systemically promotes the growth of ER-negative cancers

The systemic nature of the enhanced tumor growth in the experiments above suggested that circulating factors might be promoting the observed tumor formation following parturition. In fact, numerous experimental and clinical findings have implicated the female steroid hormones estrogen and progesterone in having pro-tumorigenic activities (*32-34*). To examine whether these hormones were playing a functional role in promoting tumor growth following parturition, we treated cohorts of

Figure 1. Human breast cancer growth is promoted following pregnancy in mice. **(A)** Histological and phenotypic analysis of tumors arising from pHMLER cells injected into the mammary glands of nulliparous or post-partum female NOD/SCID mice. H&E stained sections of pHMLER tumors (i,ii), LgT IHC (iii,iv) and von Willebrand factor IHC (v,vi) sections of tumors that developed eight weeks following injection. **(B)** Quantification of the tumor mass (blue) and stromal contribution (orange) within the tumors following pregnancy (i). Percent stroma was quantitated by counting LgT negative cells in tumor sections that developed in the mammary glands of nulliparous or post partum mice. Quantification of the microvasculature (ii) using Merz straight line interrupted (red) and chaukley counts (blue) on hotspot regions of vWF stained tumor sections from nulliparous or post partum mice. **(C)** Histological and phenotypic analysis of hHMLER cells injected into nulliparous or post-partum female NOD/SCID mice. H&E stained sections of hHMLER cells (i-iv) injected orthotopically (M.G) or subcutaneously (S.C) into nulliparous or post-partum mice. LgT IHC of tissues from hHMLER injections (v,vi) reveal benign cells or tumors that developed subcutaneously in nulliparous or post-partum mice, respectively. Characterization of desmoplastic stroma of hHMLER tumors by IHC for αSMA (vii) and Mason's Trichrome staining (viii). **(D)** Quantification of the tumor mass in the mammary glands (blue) or subcutaneously (orange) in nulliparous or post partum mice.

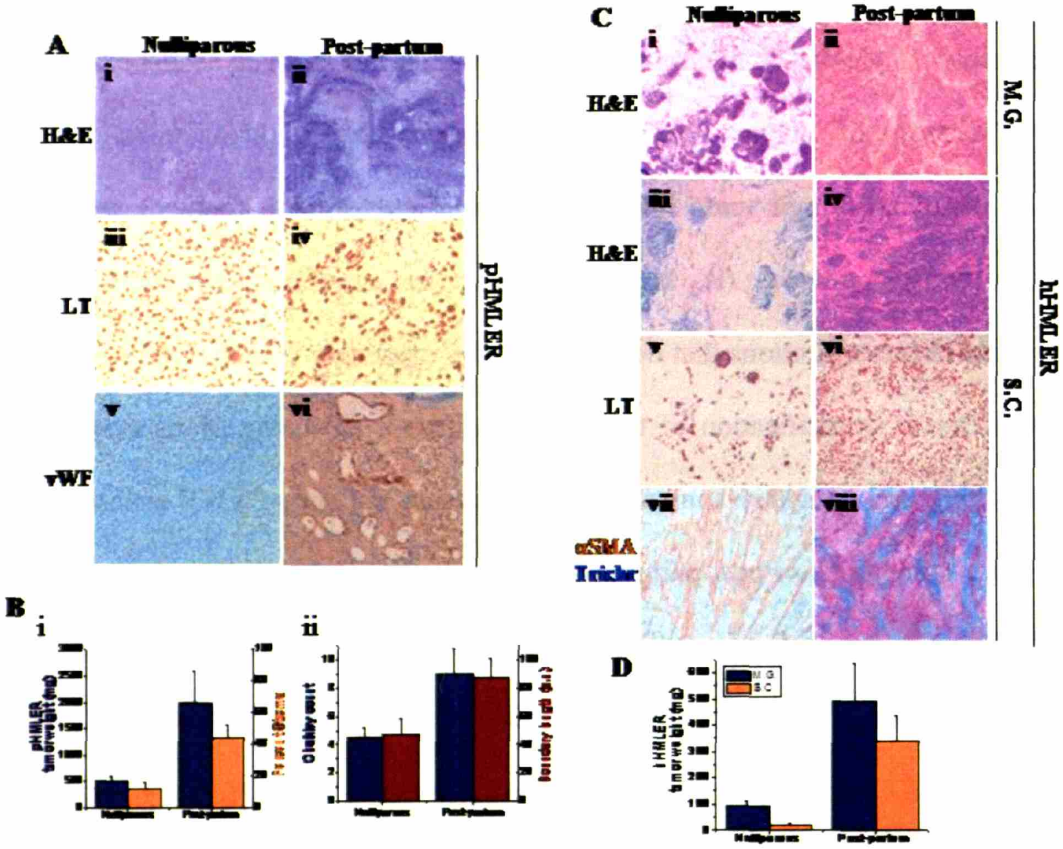
A
Nulliparous
Post-partum
H&E
LI
vWF
pHMLER
C
Nulliparous
Post-partum
H&E
H&E
LI
αSMA
Laminin
M.G.
S.C.
hHMLER
B
i
ii
D

mice that had been injected with hHMLER breast epithelial cells following parturition with pharmacological agents that inhibit the function of either estrogen or progesterone.

In vivo administration of the chemical compound letrozole, which prevents aromatase-dependent estrogen synthesis, inhibited hHMLER tumor formation in mice following parturition, compared to vehicle-treated control mice (Figure 2). In contrast, treatment with the selective estrogen receptor modulater (SERM), tamoxifen, failed to inhibit post-partum tumor formation. Treatment with the progesterone receptor-inhibitor RU486 also did not result in tumor inhibition, but rather appeared to enhance tumor formation following parturition compared to the placebo controls.

To determine if estrogen was sufficient to promote the growth of hHMLER cells in the absence of pregnancy, we implanted slow-release pellets of 17β-estradiol or placebo pellets into nulliparous mice immediately following subcutaneous hHMLER cell injection. Tumor formation occurred in the estrogen-treated animals in a dosage-dependent manner within six weeks (Figure 2); mice that received a high dose of estrogen (300-400pg/ml plasma) all developed tumors that progressed to a large size; at a lower dose of estrogen (50-75pg/ml plasma) about half of the animals developed tumors, exhibiting a penetrance similar to that observed for hHMLER tumors arising in mice following parturition. In contrast, placebo-treated mice failed to develop any palpable tumors.

Since extensive previous work (*32, 33, 35*) has established that estrogen has pro-tumorigenic activities, we were interested in further characterizing the mechanism by which estrogen was systemically promoting breast tumor growth in the experiments described above. Surprisingly, immunoblotting revealed that pHMLER and hHMLER

cells grown in culture do not express the estrogen (ER) or progesterone (PR) receptors and do not alter their growth *in vitro* in response to treatment with either estrogen or progesterone (data not shown). Likewise, ERα/β was not detectable in lysates from pHMLER tumors or in tumors that develop from hHMLER cells injected into either mice post-parturition or into estrogen-treated nulliparous mice (Figure 2).

The absence of ERα and ERβ expression in the hHMLER cells and tumors made it highly unlikely that the increased tumorigenesis in estrogen-treated mice was due to a direct influence of estrogen on the breast epithelial cells themselves. We speculated, rather, that estrogen was influencing host physiology in a manner that was conducive for breast tumor growth. To determine whether this effect of estrogen was restricted to breast tumor cells, we repeated the experiments above using an established human prostate cancer cell line (PC3) which is negative for ERα/β and androgen receptor expression (*36*). When PC3 cells were injected subcutaneously into estrogen-treated nulliparous mice, there was a marked increase in tumor growth and a reduction in tumor latency relative to placebo treated controls (Figure 2). In fact, all of the estrogen-treated mice developed palpable tumors within 2 weeks following injection, whereas the placebo-treated mice started developing palpable tumors at around 4 weeks post-injection.

Estrogen and parturition systemically induce angiogenesis independently of cancer growth

An extensive body of clinical and basic research has implicated estrogen in promoting angiogenesis through a variety of mechanisms that operate independently of cancer growth (*37-39*). These mechanisms, which are in effect during normal

Figure 2. Estrogen promotes tumor growth of ER-negative cells. (A) Estrogen is necessary to promote tumor growth following pregnancy. Quantification of the tumor mass that developed from hHMLER cells injected into mice following pregnancy treated with tamoxifen, RU486, letrozole or placebo. **(B)** Estrogen is sufficient to promote tumor growth of hHMLER cells. Tumor weight (i) of hHMLER cells that developed in nulliparous mice treated with low dose estrogen (blue) or high dose estrogen (orange). H&E stained sections (ii) of the injection plugs from placebo-treated mice and tumors that developed in estrogen-treated mice. **(C)** Breast epithelial cells do not express estrogen receptors. Western blot analysis (i) of ERα and ERβ expression in hHMLER and pHMLER cells grown *in vitro* or from protein lysates isolated from tumor tissues from nulliparous (pHMLERTu), estrogen-treated (hHMLERTu/E2) or post-partum mice (hHMLERPP). Positive controls for ERα and ERβ expression were MCF7 cells or breast reduction mammoplasty tissue, respectively. IHC analysis of ERα and ERβ expression in hHMLER tumor sections (ii). Human breast reduction mammoplasty tissue was stained as positive control of ER expression (inset). **(D)** Non-breast cancer growth is promoted by estrogen. Tumor growth curves (i) and tumor weight (ii) in mice injected with prostate cancer PC3 cells and treated with slow dose 17βestradiol or placebo pellets. **(E)** Increased tumor angiogenesis in estrogen-treated mice. IHC for von Willabrand factor in sections of hHMER (i,ii) or PC3 tumors (iii,iv) in mice treated with 17βestradiol. Quantification of the microvasculature (v) using Merz straight line interrupted (red) and chaukley counts (blue) on hotspot regions of vWF stained tumor sections from placebo or 17βestradiol treated mice.

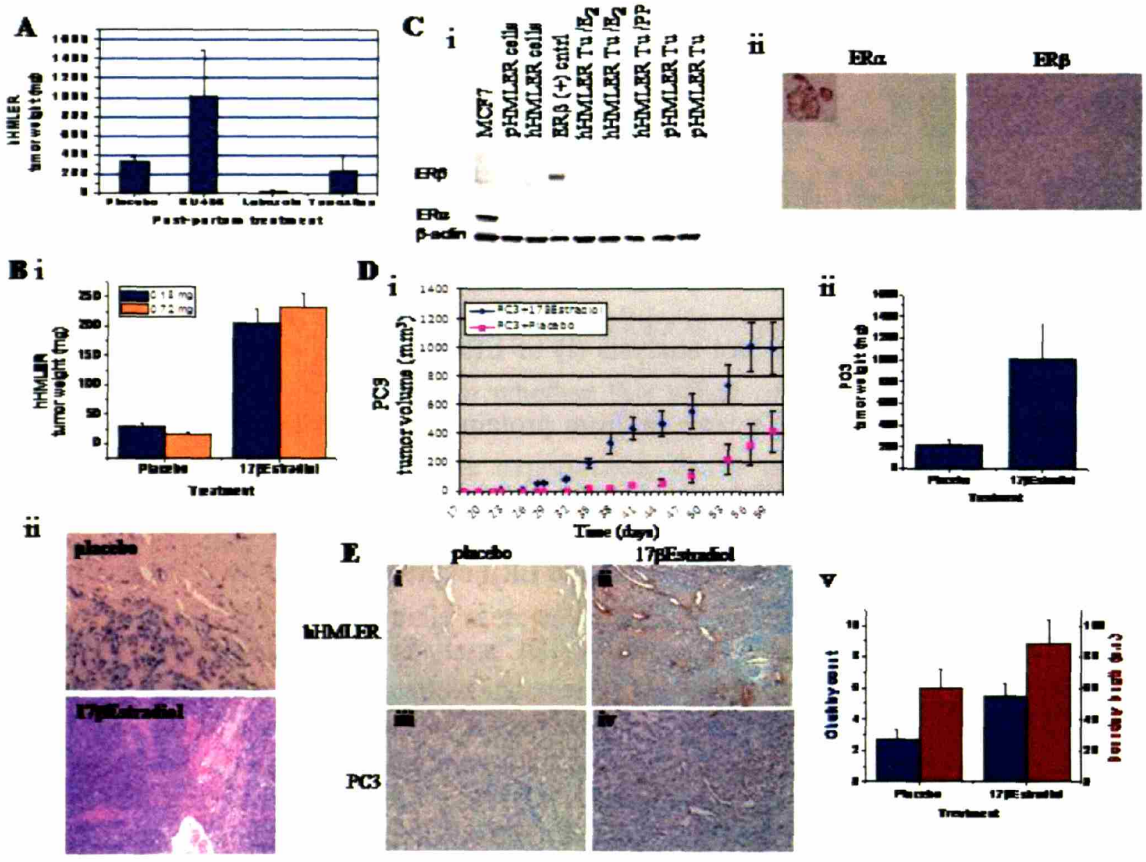
A
C
i
ii
ERα
ERβ
MCF7
pHMLER cells
hHMLER cells
ERβ (+) cntrl
hHMLER Tu /E2
hHMLER Tu /E2
hHMLER Tu /PP
pHMLER Tu
pHMLER Tu
ERβ
ERα
β-actin
B i
hHMLER tumor weight (mg)
Placebo
17βEstradiol
Treatment
ii
placebo
17βEstradiol
D
i
PC3 tumor volume (mm³)
PC3+17βEstradiol
PC3+Placebo
Time (days)
ii
PC3 tumor weight mg
Placebo
17βEstradiol
Treatment
E
placebo
17βEstradiol
hHMLER
PC3
v
Placebo
17βEstradiol
Treatment

homeostasis, include mitogenic stimulation of differentiated endothelia (which express the ER), mobilization of endothelial precursor cells (EPCs) into the peripheral circulation (*37*), and enhanced resistance of EPCs to apoptosis. The pro-angiogenic functions of estrogen are, in particular, believed to be required for normal reproductive physiology in women--serving to regulate uterine angiogenesis, which is an integral aspect of the follicular phase of the menstrual cycle (*38, 40, 41*). As mentioned above, examination of histological sections of pHMLER tumors had revealed that tumors arising in post-partum animals were significantly more vascularized than their counterparts arising in nulliparous mice (Figure 1). A marked increase in vascularization was also evident in PC3 tumors derived from 17β-estradiol-treated animals relative to placebo-treated animals (3.5-fold increase; Figure 3). Together, these findings supported the notion that estrogen could stimulate tumor angiogenesis via molecular pathways that did not require the expression of the ER in cancer epithelia. Since angiogenesis has been found to be a key rate-limiting step for hHMLER tumor formation (*30*), we wanted to explore the possibility that estrogen was exerting a pro-angiogenic effect which was responsible for systemically promoting hHMLER tumor formation.

While studies on estrogen's ability to stimulate tumor angiogenesis have focused on elucidating angiogenic factors whose expression is transcriptionally modulated in cancer epithelium in response to ER signaling (*42, 43*), this mechanism could not be responsible for the increased angiogenesis in response to estrogen of pHMLER and PC3 tumors, both of which are ER-negative. We hypothesized, instead, that circulating estrogen systemically promotes tumor formation and growth by ER-negative cancer cells by systemically enhancing neo-angiogenesis via its actions on non-carcinomatous cells of

host origin. To test this hypothesis, we determined whether an elevation in circulating estrogen is sufficient to increase angiogenesis systemically in the absence of cancer growth. Accordingly, we performed subcutaneous neo-angiogenesis assays in mice treated with slow-release pellets of either 17β-estradiol or carrier-compound placebo. To assay for neo-angiogenesis, we subcutaneously implanted extra-cellular matrix (ECM) plugs containing small amounts of the pro-angiogenic factor bFGF, and subsequently evaluated vascularization of the plugs upon harvest. Relative to placebo-treated control animals, ECM plugs derived from 17β-estradiol-treated mice displayed a significant increase in neo-angiogenesis, as gauged by Chalkley counts and microvascular density measurements performed on vWF-stained tissue sections (Figure 3). Histological examination of ECM plug sections from 17β-estradiol-treated animals revealed structures consistent with nascent vascular channel formation (arrows in Figure 3).

The experiments thus far indicated that estrogen mediates the enhanced tumorigenesis associated with parturition and is capable of systemically promoting angiogenesis independently of tumor growth. If estrogen's pro-angiogenic effects are causally responsible for the increased tumorigenesis associated with parturition, one would predict that angiogenesis is systemically enhanced in mice following parturition. To test this notion, we performed angiogenesis assays in post-partum and age-matched nulliparous mice. While minimal blood vessel formation was observed in ECM plugs carried by nulliparous mice, ECM plugs present in mice following parturition were significantly more vascularized, as assessed by microvascular density and Chalkley point counts (Figure 3). Indeed, the increased vascularization of ECM plugs derived from

Figure 3. Increased systemic angiogenesis and cell recruitment. **(A)** Characterization of ECM plugs following estrogen treatment. H&E (i,ii), Mason's Trichrome stained (Trichr) (iii,iv), and von Willabrand factor (vWF) immunostained sections of ECM plugs isolated from placebo or 17βEstradiol-treated mice. Evidence of early vascular channel formation (arrow) in plugs from estrogen-treated animals. **(B)** Quantification of cellularity and angiogenesis in ECM plugs. Microvasculature (i) was quantitated using Merz straight line interrupted (red) and chaukley counts (blue) on hotspot regions of vWF stained plugs from placebo or 17βEstradiol-treated mice. Cellularity (ii) was quantitated by counting the number of red nuclei from trichrome stained sections of ECM plugs from placebo or 17βEstradiol-treated mice. **(C)** Characterization of plugs following parturition. White light microscopy (i,ii) of ECM plugs isolated from nulliparous or post-partum mice. Large blood vessel recruitment is evident in plugs from post-partum mice. H&E stained sections (iii,iv) of ECM plugs from nulliparous and post-partum mice. Although similar numbers of vessels were observed in hot spot regions, blood vessels in the plugs from post-partum mice were significantly larger in size. **(D)** Quantification of cellularity and angiogenesis in plugs. Microvasculature (i) was quantitated using Merz straight line interrupted (red) and chaukley counts (blue) on hotspot regions of vWF stained Matrigel plugs from nulliparous or post-partum mice. Cellularity (ii) was quantitated by counting the number of red nuclei from trichrome stained sections of plugs.

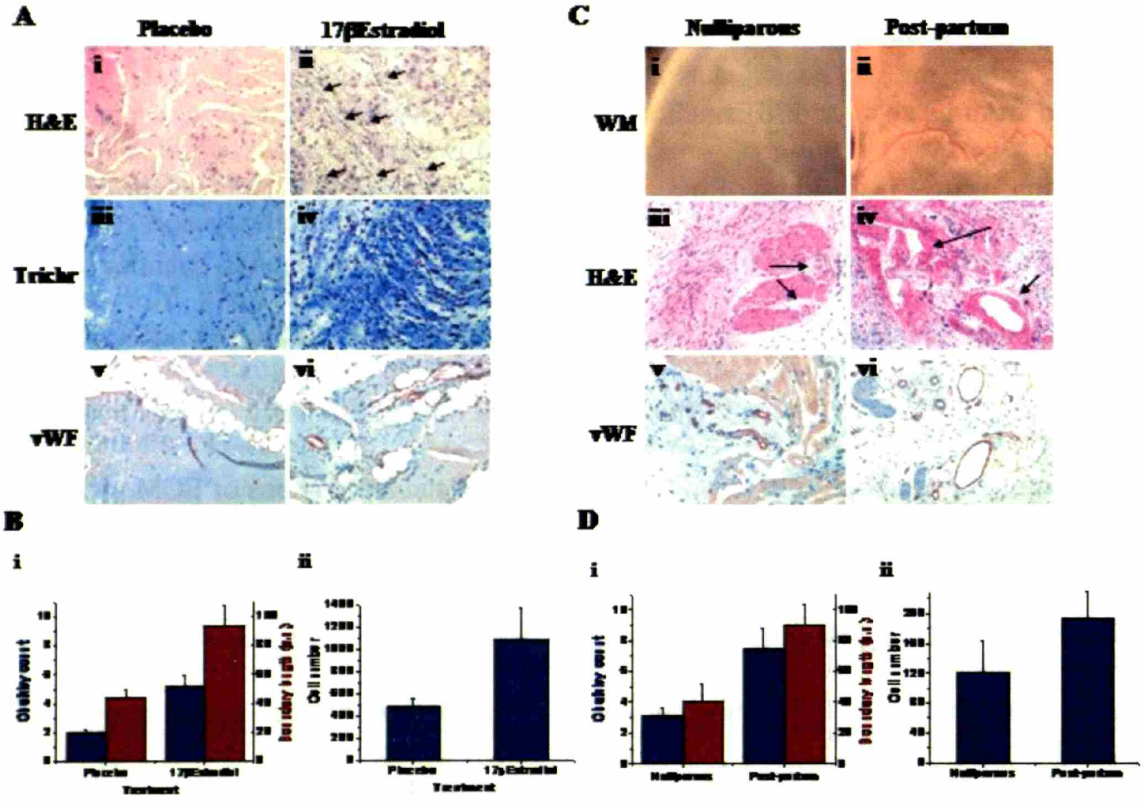
A
Placebo
17βEstradiol
H&E
Trichr
vWF
C
Nulliparous
Post-partum
WM
H&E
vWF
B
i
ii
Placebo
17βEstradiol
Treatment
D
i
ii
Nulliparous
Post-partum

post-partum animals was readily apparent upon gross examination under a dissection microscope (Figure 3).

Together, these experiments indicate that estrogen systemically stimulates normal and tumor angiogenesis through its actions on host cells distinct from the cancer epithelium. Moreover, they show that estrogen can exert these pro-angiogenic effects in the absence of any neoplastic growth.

Bone marrow-derived stromal cells are present in tumors in estrogen-treated mice

The above experiments revealed that tumors arising in either post-partum or estrogen-treated mice were significantly more stromalized and angiogenic than tumors arising in nulliparous animals. Previous reports have demonstrated that the enhanced repair of wounded vasculature in estrogen-treated animals is associated with endothelial precursor cell (EPC) mobilization and recruitment from the circulation in a nitric oxide synthase-dependent manner (*44*). Published work has also indicated that various stromal cell types in tumors, including EPCs and myofibroblasts, can be recruited from the peripheral circulation, deriving ultimately from the bone marrow. In light of these observations, we wanted to examine whether the tumor growth in estrogen-treated animals was accompanied by stromal cell recruitment from the peripheral circulation.

Accordingly, we repeated the experiments above in chimeric mice whose hematopoietic systems had been reconstituted with GFP-labeled donor bone marrow (Figure 4a). HMLER cells that had been labeled with red fluorescent protein (RFP) were injected subcutaneously into bone marrow-reconstituted mice that were concomitantly treated with estrogen. Following the harvest of tumors that developed in these animals, frozen tissue sections were microscopically examined for the presence of bone marrow-

derived cells. In fact, cursory examination of freshly isolated tumor tissue at low magnification using a fluorescence dissection microscope indicated the presence of significant numbers of RFP-labeled tumor cells and GFP-labeled bone marrow-derived cells (Figure 4D-i).

At high magnification, we observed a significant percentage of stromal cells within the tumor mass, recapitulating the observations with pHMLER tumors that had developed in post-partum animals. Remarkably, ~90% of the tumor-associated stromal cells were GFP-labeled, indicating that a significant portion of the stroma in these tumors was bone marrow-derived (Figure 4D). Since our previous experiments had indicated that tumors developing in post-partum mice exhibited a myofibroblastic stroma, we performed immunofluorescence for αSMA on these tumor sections. This analysis revealed a significant number of myofibroblasts within the tumor stroma. Moreover, there was an extensive overlap between αSMA(+) myofibroblasts and GFP-labeled cells, indicating that a large fraction of the tumor myofibroblasts were bone marrow-derived. (Figure 4D-iii).

To investigate whether endothelial cells were also recruited into these tumors from the circulation, we stained tumor sections for CD31. While a significant number of CD31-positive blood vessels were visualized in these tumors, co-localization with GFP was rarely observed. However, there was a significant peri-vascular association of GFP-labeled cells with CD31-positive vasculature (Figure 4D-iv), as has been previously described (*45, 46*). Staining for the murine EPC marker, CD34, indicating the occasional presence of EPCs within the tumor stroma, a significant fraction of which were GFP-labeled and therefore bone marrow-derived (Figure 4D-v).

These findings indicated that significant numbers of stromal cells in tumors arising in estrogen-treated animals were bone marrow-derived. To determine if the cellular recruitment occurred in the absence of tumor growth, we repeated the above analyses with estrogen-treated chimeric animals using subcutaneous ECM plugs. ECM plugs harvested one week following implantation contained significant numbers of GFP-positive bone marrow derived cells (Figure 4C). In contrast to our observations with HMLER tumors, we did not observe any αSMA-positive myofibroblasts within the ECM plugs. While we did not observe CD34(+) EPCs within the ECM plugs, there was a peri-vascular association of GFP-labeled bone marrow-derived cells with CD31(+) endothelium (Figure 4C-ii).

The presence of peri-vascular GFP-labeled cells in both ECM plugs and HMLER tumors is consistent with previous findings that this phenomenon is associated with normal blood vessel growth. In contrast, the absence of bone marrow-derived CD34 (+) cells and myofibroblasts in ECM plugs may be a consequence of several plausible mechanisms. It could be that the recruitment of EPCs and myofibroblasts from the circulation is dependent upon tumor growth. Alternatively, the nature of the recruited cells could be identical in both situations, and the cancer cells subsequently convert the recruited cells into an activated, myofibroblastic phenotype, as has been previously reported. In either scenario, it is likely that these variations reflect differences in the tissue microenvironment of a growing tumor compared to that of uninjured normal tissue. Together, these observations indicate that the estrogen-mediated stimulation of ER-negative tumor formation, growth and angiogenesis is accompanied by a significant recruitment of stromal cells from the bone marrow.

Figure 4. Bone marrow-derived cells are recruited to sites of angiogenesis and tumor stroma (A) Reconstitution of NOD/SCID blood with Rag/GFP bone marrow. A schematic representation of the bone marrow transplantation protocol and experimental design for detecting bone marrow cell recruitment to ECM plugs and tumors. **(B)** Representative FACS analysis of reconstitution efficiency in GFP BMT mice. GFP-positive (FL1-H) cells from blood isolated from reconstituted mice represent nearly all of the cells in the blood. **(C)** Bone marrow-derived cells in ECM plugs. DAPI-stained (i) frozen sections of plugs harvested from BMT transplanted, 17βEstradiol-treated mice. Significant numbers of cells seen in the plugs were GFP-positive recruited cells. CD31 IHC analysis (ii) of ECM plugs demonstrating CD31+ vessels (red) and single CD31-positive endothelial cells (red), which are not GFP+ bone marrow derived. Note that GFP-positive cells are often peri-vascular. **(D)** Bone marrow derived cells found in the tumor stroma of estrogen-treated mice. RFP-labeled HMLER cells were injected in to Rag/GFP BMT mice and treated with 17βEstradiol. A fluorescence dissection microscope was utilized to examine the cells within the tumor mass that were derived from the bone marrow (i). A large proportion of the tumor consisted of GFP-positive bone marrow-derived cells as evidence by gross dissection (i) and in DAPI-stained frozen sections (ii) of estrogen treated mice. IHC analysis on frozen sections of HMLER tumor tissue (iii-vi) demonstrates that the majority of the GFP-positive bone marrow-derived cells expression αSMA (iii, blue), whereas rare GFP-positive cells are CD31+ (iv) endothelial cells (blue).. (v) CD34+ EPCs (blue) were detected in the stroma of HMLER tumors, which were occasionally also positive for GFP. (vi) IHC for human Flt-1 (blue) in HMLER tumor tissue demonstrates the cancer cells (red) express Flt-1, which is essentially absent in the mouse GFP+ stromal cells. **(E)** Percentage matrix of double-positive staining. The entry in (row, column) = (i, j) is the percent of i-labeled cells that are also j-labeled. For example, for (i, j) = (SMA, GFP), the percent of SMA-labeled cells that are also GFP-labeled is 60. Note that this matrix is asymmetric. STRO, stroma; ND, not determined.

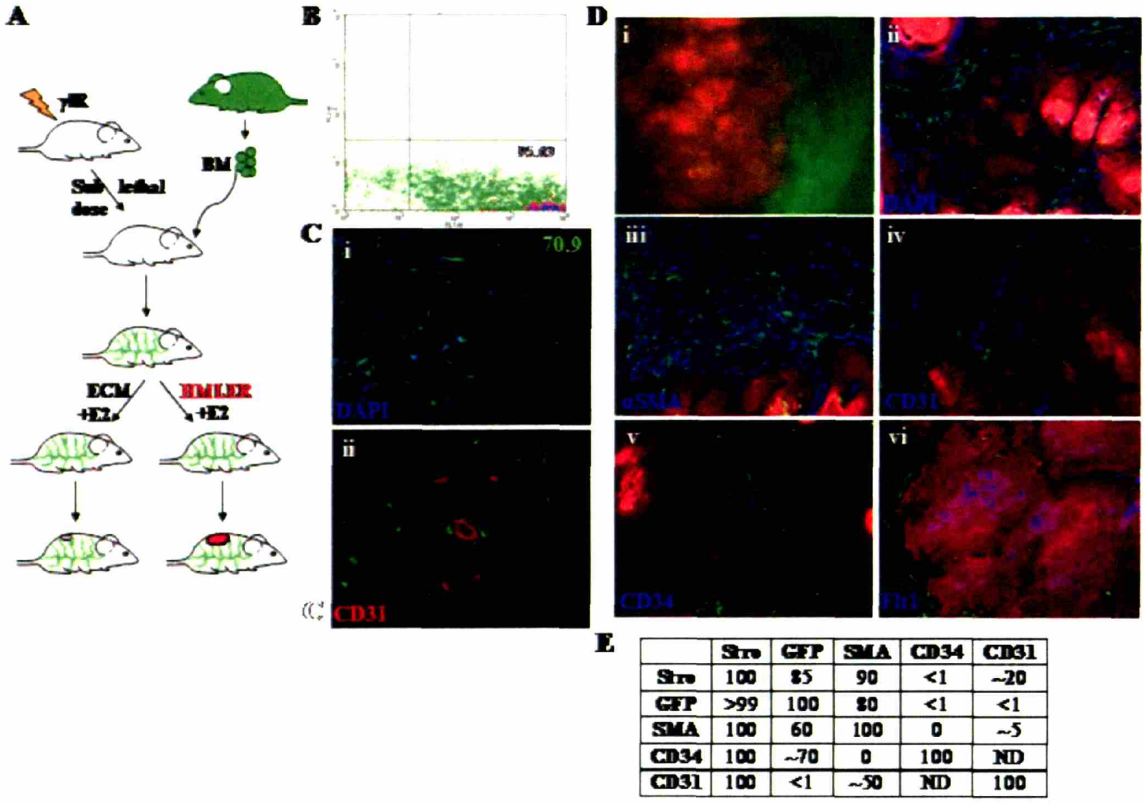

E

	Stro	GFP	SMA	CD34	CD31
Stro	100	85	90	<1	~20
GFP	>99	100	80	<1	<1
SMA	100	60	100	0	~5
CD34	100	~70	0	100	ND
CD31	100	<1	~50	ND	100

Figure 4

Discussion

There is an established epidemiologic connection between pregnancy and breast cancer incidence. However, animal models for investigating the mechanistic basis of this relationship have been lacking. In this paper, we describe a xenograft mouse model in which parturition systemically promotes tumor formation by initiated, pre-neoplastic breast epithelial cells. In accordance with the vast majority of tumors arising in women in the years following pregnancy (*25, 26, 47*), the tumors that arise following parturition in this model are also ER-negative.

While the tumors that arise in this model lack ER expression, their increased growth following parturition is strongly dependent upon estrogen signaling. Indeed, treatment with estrogens is sufficient to systemically enhance tumor formation concomitantly with increased tumor angiogenesis. The fact that estrogen's pro-tumorigenic influence is observed with ER-negative breast cancer cell lines as well as a prostate cancer cell line is compelling evidence that these effects occur via the influence of estrogens on host physiology, rather than by their action on the tumor cells themselves. Consistent with this view, both parturition and estrogen systemically enhanced angiogenesis in the absence of any neoplastic growth, indicating that these effects were not dependent on ER-signaling in tumor cells.

There are numerous reports in the literature implicating estrogens in promoting angiogenesis (*37*) in the absence of any neoplastic growth. Nevertheless, studies of estrogen's role in promoting the growth and vascularization of cancers in women have largely focused on the transcriptional effects of estrogen binding to its receptor in ER-

positive mammary and ovarian carcinomas. In this report, we describe a second important mechanism by which estrogens promote the growth of ER-negative cancers—namely, by systemically enhancing host angiogenesis. Taken together with the previous literature, this work suggests that anti-estrogenic therapy may be useful in the treatment of ER-negative cancers in women.

The lack of clinical responses of ER-negative tumors to tamoxifen therapy would seem to be at odds with this notion. However, tamoxifen is only a partial antagonist of ER's activities (*48*). Of particular relevance, previous reports have indicated that tamoxifen does not inhibit the pro-angiogenic effects of estrogen in the uterus (*49, 50*). Consistent with this observation, tamoxifen failed to attenuate the tumor formation observed following parturition in our model system, whereas letrozole succeeded in doing so. Thus, the signaling pathways by which estrogen promotes angiogenesis may be distinct from those inhibited by tamoxifen, and pharmacological agents that inhibits relevant endogenous estrogen signaling may elicit clinical responses in patients bearing ER-negative mammary carcinomas.

The present observations indicate that estrogen increases the systemic capacity for neo-angiogenesis, and that this mechanism is in part responsible for promoting tumorigenesis following pregnancy. An epidemiologic prediction of this work is that the known surge in breast cancer incidence among women following parturition may be accompanied by increases in the incidence during this period of other types of cancers that have remained latent due to inadequate angiogenesis.

Acknowledgements

We thank Tony Chavarria for technical assistance with animal experiments, and Phil Hinds, Antoine Karnoub, and Scott Dessain for critical reading of the manuscript. We are also grateful to Homayoun Vaziri and Scott Dessain for helpful advice and encouragement during the course of this work. This work was supported by grants from the Department of Defense BC033108 (P.B.G), the Breast Cancer Research Foundation (R.A.W), and the American Cancer Society RP85-128-18 (R.A.W.), the Jane Coffin Child Fellowship (C.K.), and Department of Defense BC03 (C.K.). R.A.W. is an American Cancer Society Research Professor and a Daniel K. Ludwig Foundation Research Professor.

References

1. J. L. Kelsey, M. D. Gammon, *Cancer Journal for Clinicians* 41, 146 (1991).
2. J. Harris, M. Lippman, U. Veronesi, W. Willett, *New England Journal of Medicine* 327, 390 (1992).
3. B. S. Hulka, *Genetics and Cancer Susceptibility* 159 (1996).
4. C. Hsieh *et al.*, *Eur. J. Cancer* 30A, 969 (1994).
5. D. T. Janerich, M. B. Hoff, *Am. J. Epidemiol.* 116, 737 (1982).
6. H. C. Moore, R. S. Foster, Jr., *Semin. Oncol.* 27, 646 (2000).
7. S. H. Olson, A. G. Zauber, J. Tang, S. Harlap, *Epidemiology* 9, 669 (1998).
8. M. Lambe *et al.*, *N. Engl. J. Med.* 331, 5 (1994).
9. J. R. Palmer, L. A. Wise, N. J. Horton, L. L. Adams-Campbell, L. Rosenberg, *J. Natl. Cancer Inst.* 95, 478 (2003).
10. J. Wohlfahrt, P. K. Andersen, H. T. Mouridsen, M. Melbye, *Am. J. Epidemiol.* 153, 1079 (2001).
11. J. Wohlfahrt, M. Melbye, *Epidemiology* 12, 68 (2001).
12. G. Albrektsen, I. Heuch, S. Hansen, G. Kvale, *Br. J. Cancer* 92, 167 (2005).
13. S. Z. Haslam, G. Shyamala, *Biochem. J.* 182, 127 (1979).
14. I. Lamote, E. Meyer, A. M. Massart-Leen, C. Burvenich, *Steroids* 69, 145 (2004).
15. Y. J. Topper, C. S. Freeman, *Physiological Reviews* 60, 1049 (1980).
16. J. L. Fendrick, A. M. Raafat, S. Z. Haslam, *Journal of Mammary Gland Biology and Neoplasia* 3, 7 (1998).
17. Z. Feng *et al.*, *The Journal of Cell Biology* 131, 1095 (1995).
18. C. S. Atwood *et al.*, *J Endocrinology* 167, 39 (2000).
19. R. Strange, F. Li, S. Saurer, A. Burkhardt, R. R. Friis, *Development* 115, 49 (1992).
20. L. Lund *et al.*, *Development* 122, 181 (1996).
21. P. A. Furth, *Journal of Mammary Gland Biology and Neoplasia* 4, 123 (1999).

22. V. Djonov, A. Andres, A. Ziemiecki, *Microsc. Res. Tech.* 52, 182 (2001).

23. I. Forsyth, *Journal of Mammary Gland Biology and Neoplasia* 2, 3 (1997).

24. G. Weiss, *J. Clin. Endocrinol. Metab* 85, 4421 (2000).

25. A. M. Ruder *et al.*, *Cancer* 64, 196 (1989).

26. N. G. Hildreth *et al.*, *J. Natl. Cancer Inst.* 70, 1027 (1983).

27. B. Elenbaas *et al.*, *Genes Dev.* 15, 50 (2001).

28. S. B. Fox *et al.*, *J. Pathol.* 177, 275 (1995).

29. H. Gundersen *et al.* APMIS 96, 379-394. 1988.

30. R. S. Watnick, Y. Cheng, A. Rangarajan, T. A. Ince, R. A. Weinberg, *Cancer Cell* 3, 219 (2003).

31. R. A. Walker, *Breast Cancer Res.* 3, 143 (2001).

32. L. A. Brinton, C. Schairer, *Epidemiologic Reviews* 15, 66 (1993).

33. H. Spencer Feigelson, B. E. Henderson, *Carcinogenesis* 17, 2279 (1996).

34. C. Schairer *et al.*, *JAMA* 283, 485 (2000).

35. M. C. Pike, D. V. Spicer, L. Dahmoush, M. F. Press, *Epidemiologic Reviews* 15, 17 (1993).

36. M. J. Linja, K. J. Savinainen, T. L. Tammela, J. J. Isola, T. Visakorpi, *Prostate* 55, 180 (2003).

37. D. W. Losordo, J. M. Isner, *Arterioscler. Thromb. Vasc. Biol.* 21, 6 (2001).

38. C. E. Gargett, P. A. Rogers, *Reproduction.* 121, 181 (2001).

39. D. E. Morales *et al.*, *Circulation* 91, 755 (1995).

40. U. A. Kayisli *et al.*, *J. Clin. Endocrinol. Metab* 89, 5794 (2004).

41. J. W. Maas *et al.*, *Hum. Reprod.* 16, 1557 (2001).

42. M. Elkin, A. Orgel, H. K. Kleinman, *J. Natl. Cancer Inst.* 96, 875 (2004).

43. H. Buteau-Lozano, M. Ancelin, B. Lardeux, J. Milanini, M. Perrot-Applanat, *Cancer Res.* 62, 4977 (2002).

44. K. Strehlow *et al.*, *Circulation* 107, 3059 (2003).

45. I. Rajantie *et al.*, *Blood* 104, 2084 (2004).

46. M. De Palma, M. A. Venneri, C. Roca, L. Naldini, *Nature Medicine* 9, 795 (2003).

47. J. L. Kelsey, M. D. Gammon, E. M. John, *Epidemiologic Reviews* 15, 36 (1993).

48. Y. Shang, M. Brown, *Science* 295, 2465 (2002).

49. S. Hague *et al.*, *Br. J. Cancer* 86, 761 (2002).

50. A. Gagliardi, D. C. Collins, *Cancer Res* 53, 533 (1993).

Appendix II

Breast Cancer-Associated Fibroblasts Contribute to Tumor Angiogenesis[1]

[1] This work has been published. (Orimo A, Gupta PB, Sgroi DC, Arenzana-Seisdedos F, Delaunay T, Naeem R, Carey VJ, Richardson AL, Weinberg RA. **Stromal fibroblasts present in invasive human breast carcinomas promote tumor growth and angiogenesis through elevated SDF-1/CXCL12 secretion.** *Cell.* (2005) May 6;121(3):335-48.). I was actively involved in the design and implementation of experiments relating to the effects of fibroblasts on endothelial precursor cell recruitment, both *in vitro* and *in vivo*. The remainder of the work represents Dr. Orimo's independent contribution.

Stromal fibroblasts present in invasive human breast carcinomas enhance tumor growth and increase angiogenesis through recruitment of endothelial progenitor cells

Akira Orimo[1], Piyush B. Gupta[1,2], Dennis C. Sgroi[4], Rizwan Naeem[6], Vincent J. Carey[5], Andrea L. Richardson[3], Robert A. Weinberg[1,2,7]

[1]Whitehead Institute for Biomedical Research, Cambridge, Massachusetts 02142, [2]Department of Biology, Massachusetts Institute of Technology, Cambridge, Massachusetts 02139, [3]Department of Pathology, the Brigham and Women's Hospital, Harvard Medical School, [4]Department of Pathology, Harvard Medical School, Molecular Pathology Research Unit, Massachusetts General Hospital, Massachusetts 02129 [5]Channing Laboratory, Harvard Medical School, Massachusetts 02115, [6]Texas Children's Cancer Center, Department of Pediatrics and Pathology Baylor College of Medicine, Houston, TX 77030

[7]Correspondence: weinberg@wi.mit.edu phone: 617-258-5159 Fax: 617-258-5213

Running title: Fibroblasts in a tumor mass enhance tumor growth

Keywords; stromal fibroblasts, tumor stroma, invasive human mammary carcinoma, angiogenesis, endothelial progenitor cells (EPCs), stromal cell-derived factor 1 (SDF-1)

Abstract/Summary

Fibroblasts very often constitute a majority of the stromal cells within a breast carcinoma mass. It is not well established whether these stromal fibroblasts play a supportive role in breast carcinoma progression. Here, we provide evidence that fibroblasts extracted from invasive human breast cancer masses enhance breast cancer growth to a significantly higher extent than do mammary stromal fibroblasts extracted from outside of the tumor masses. Surprisingly, these fibroblasts stably retain this tumor-enhancing ability without ongoing contact with nearby carcinoma cells. We also find that carcinomas developing in the presence of such fibroblasts are far more angiogenic through increased recruitment of endothelial progenitor cells (EPCs) into the tumor mass. This effect is mediated by the elevated release of stromal cell-derived factor 1 (SDF-1) from these fibroblasts. Our findings demonstrate that fibroblasts present within invasive mammary carcinomas maintain the ability to enhance tumor growth by promoting angiogenesis through recruitment of EPCs.

Introduction

Neoplastic epithelial cells co-exist in carcinomas with several distinct stromal cell types which together create the microenvironment of the cancer cells. The contribution of the stromal microenvironment to the development of a wide variety of tumors has been supported by extensive clinical evidence (Coussens and Werb, 2002; Jacobs et al., 1999) and by the use of many experimental mouse models of cancer pathogenesis (Barcellos-Hoff and Ravani, 2000; Elenbaas et al., 2001; Sieweke et al., 1990; Tuxhorn et al., 2002). The accumulated evidence indicates that tumor cells actively recruit stromal cells, such as inflammatory cells (Coussens et al., 2000; Lin et al., 2001), vascular cells (Hanahan and Folkman, 1996), and fibroblasts (Cunha et al., 2003; Olumi et al., 1999; Tlsty, 2001), into the tumor and that this recruitment is essential for the generation of a microenvironment that actively contributes to tumor growth.

In most invasive human breast cancers, the presence of large numbers of myofibroblasts is apparent in the stromal compartments of these tumors (Sappino et al., 1988) as well as in primary cultured fibroblasts explanted from tumors (Ronnov-Jessen et al., 1992). These myofibroblasts, which can be readily identified by their expression of α-smooth muscle actin, are presumed to derive directly from the differentiation of preexisting fibroblasts in the stroma (Ronnov-Jessen et al., 1995) as well as from bone marrow-derived progenitor cells (Ishii et al., 2003). Such myofibroblasts, sometimes termed "activated fibroblasts", are also known to be present in areas of inflammation and in tissues undergoing remodeling, such as the remodeling that occurs during wound healing (Serini and Gabbiani, 1999).

Various types of "reactive" or "desmoplastic" stroma generate granulation tissue, which is composed of these myofibroblasts as well as large amounts of accumulated extracellular matrix (Bissell and Radisky, 2001). Desmoplastic stroma is often found in commonly occurring epithelial malignancies, including those of the breast, prostate, colon, lung and uterus (Orimo et al., 2001). Further biochemical characterizations have revealed that such desmoplastic stroma can be induced in experimental models by platelet-derived growth factor (PDGF) (Shao et al., 2000; Skobe and Fusenig, 1998) and transforming growth factor-β (TGF-β) (Berking et al., 2001; Lohr et al., 2001). These

factors are released by carcinoma cells, indicating that much of the desmoplastic stroma is likely to be induced and maintained by heterotypic signals released by nearby epithelial cancer cells.

The precise functional contributions of fibroblasts within human breast carcinomas to carcinoma growth and progression remain poorly understood. The enhanced expression of several genes such as those encoding c-Met (Tokunou et al., 2001), Ki-67 (Hasebe et al., 2000), PAI-1 (Dublin et al., 2000), and osteonectin (Koukourakis et al., 2003) in the tumor stroma correlates with poor prognosis of human cancer patients. In addition, gene expression profiles derived from microdissected breast cancer stroma are distinct from those derived from the stroma of the normal mammary gland (Iacobuzio-Donahue et al., 2002). These findings indicate that fibroblasts in tumor masses possess biochemical characteristics distinct from those of normal fibroblasts in benign tissue *in vivo,* but shed little light on the specific physiologic contributions of these cells to tumor growth.

It is also unclear how the distinctive phenotype of these activated fibroblasts is maintained. Thus, expression of this phenotype may depend on continuous signals received from the carcinoma cells within a tumor. Alternatively, once these fibroblasts have acquired an activated or myofibroblast phenotype, this state may be maintained stably without a continued dependence on heterotypic signals received from the epithelial cancer cells. In this study we attempted to describe the distinct properties of fibroblasts isolated from within invasive human mammary carcinomas, and to uncover biological and molecular mechanisms that enable these cells to potentiate tumorigenesis.

Results

Isolation of pure populations of carcinoma-associated and counterpart fibroblasts from invasive human breast cancers

We hypothesized that fibroblasts present in invasive mammary carcinomas might affect the growth of carcinoma cells differently than would fibroblasts from normal mammary tissue. In order to test this hypothesis, we extracted carcinoma-associated fibroblast (CAF) population from six human breast cancer samples isolated from mastectomies. CAFs were isolated from within masses of invasive carcinoma, as determined by gross examination at the time of surgical excision and subsequent histological analysis.

In addition to the CAF populations, we isolated from each of the same six patients fibroblasts from non-cancerous breast stroma, residing no closer than 2 cm. to the outer margin of the tumor mass. We termed these fibroblasts "counterpart fibroblasts". As both CAF and counterpart fibroblast populations were isolated from each individual, we were able to use them as matched control pairs, thus avoiding bias in our experimental assays due to inter-individual differences. In addition, we extracted fibroblasts from the breast stroma of a sample obtained from a reduction mammoplasty, in which only normal mammary tissue was detectable. These primary cultured fibroblasts were isolated in the same way, by tissue dissociation followed by differential sedimentation, plating, and growth in high serum media, conditions which select for fibroblast growth. Each fibroblast was then expanded into two 15 cm petri dishes within 8-10 days after breast tissue dissociation. We used fibroblasts passaged for up to 5 population doublings (PDs) for subsequent experiments, in order to minimize clonal selection and culture stress which could occur during extended tissue culture.

We examined the purity of the respective fibroblast populations by immunohistochemistry using several positive and negative markers for fibroblasts. No cells in our isolated fibroblast populations displayed cytokeratin expression (Fig.1A-d, e) or CD31 expression, excluding the possibility of contamination by epithelial, endothelial or leukocytic cells. In contrast, the fibroblast populations strongly expressed vimentin (Fig.1A-a, b), fibronectin, prolyl 4-hydroxylase and fibroblast surface protein (data not shown), all of which are markers of the fibroblast lineage. These results, summarized in

Table 1, indicate that the isolated fibroblast populations were free from contamination by other cell types, including specifically normal or neoplastic epithelial cells.

CAFs are more competent to enhance tumor growth in a stroma-reconstructed human breast cancer xenograft model

In order to assess the contribution of various fibroblast populations to tumor growth *in vivo*, we developed a human tumor xenograft model that enabled us to specify the majority of cells constituting both the stromal and epithelial compartments of the engrafted tumors. We mixed CAFs, counterpart fibroblasts or normal fibroblasts in a 3:1 ratio with green fluorescent protein (GFP)-labeled MCF-7-ras human breast cancer cells and inoculated these cell mixtures subcutaneously into immunodeficient mice. These MCF-7-ras cells derive from MCF-7 human mammary carcinoma cells into which a mutant, activated *ras* oncogene had been introduced to enable these cells to proliferate in the absence of exogenous estrogen stimulation (Kasid et al., 1985).

We confirmed that the initially injected GFP-labeled MCF-7-ras cells, when co-mingled with the CAFs, contributed prominently to the resulting reconstructed tumors by demonstrating strong immunoreactivity against GFP in essentially all cancer cells within the tumors (Fig 1B-1, 2). We thereby addressed the possibility that contamination by parental breast cancer cells, originally present in the tissues from which the fibroblast populations were derived, was responsible for the observed tumors in our system.

In addition, we observed that the co-inoculated CAFs (Fig 1B-3) as well as counterpart and normal fibroblasts (data not shown) survive in large numbers in tumors together with the GFP-positive MCF-7-ras cells for periods of up to 9 weeks after injection, as determined by immunohistochemistry using antibodies specific for human vimentin. Thus, these xenograft tumors consist of an epithelial carcinoma compartment formed by the MCF-7-ras cells and a stromal compartment formed by the commingled human fibroblasts together with additional stromal cells contributed by the mouse host.

We compared the growth kinetics of the tumors formed by MCF-7-ras cells injected alone, to those formed by MCF-7-ras cells co-injected with CAFs, counterpart fibroblasts, or normal fibroblasts. We observed that the presence of any of these types of fibroblasts

stimulated tumor growth. However, CAFs were generally far more capable of stimulating tumor formation by the MCF-7-ras cells than were counterpart or normal fibroblasts. Tumors formed by MCF-7-ras cells co-injected with CAFs showed higher tumor volume (Fig.1C-1) and weight (Fig.1C-2) compared to tumors containing no fibroblasts, normal fibroblasts, or counterpart fibroblasts. In addition, these tumors containing CAFs also contained far more GFP-labeled carcinoma cells than did tumors without CAFs (Fig.1C-3). To further evaluate tumor growth, we determined the average slope of the tumor growth curves for each tumor type that indicates tumor growth rate (See Experimental Procedures).

To confirm our results, we repeated these initial experiments with five additional pairs of human breast carcinoma-associated and counterpart fibroblast populations isolated from five patients as well as with additional normal fibroblast populations. The weights and tumor growth rates of CAF-containing tumors were again compared to those of tumors containing matched patient-specific counterpart fibroblasts or normal fibroblasts. In summary, we observed that four out of six CAF populations were more competent in enhancing MCF-7-ras tumor growth than were normal mammary stromal fibroblasts (Table 2). And four out of six CAF populations were more competent in enhancing MCF-7-ras tumor growth when compared to patient-specific counterpart fibroblasts (Table 2). We concluded from these observations that during the course of tumor progression, stromal CAFs acquire a tumor-enhancing ability that enables them to enhance cancer cell growth in our *in vivo* assay system. These observations echo findings of others demonstrating that the stromal fibroblasts isolated from human prostate carcinomas have an increased ability to foster tumor formation when compared with normal prostatic fibroblasts (Olumi et al., 1999).

The stability with which the tumor-enhancing phenotype of the CAFs was retained remained to be addressed. Retention of the tumor-enhancing phenotype might require their ongoing contact with mammary carcinoma cells. Alternatively, once CAFs acquired such a unique phenotype, they might well retain this ability even in the absence of continuous contact with carcinoma cells.

Figure 1 Enhanced tumor growth kinetics of MCF-7-ras breast cancer cells co-mingled with CAFs in a stroma-reconstructed xenograft tumor model

A, Properties of primary fibroblasts explanted and cultured from human breast cancers (CAFs) (b, e) and patient-specific control counterpart fibroblasts (a, d) were explanted from cancer-containing mastectomies. Both types of fibroblast populations were positively immunostained by an anti-vimentin antibody (a, b), whereas they were negatively stained by an anti-cytokeratin antibody (d, e). In contrast, MCF-7-ras cells were positive for cytokeratin staining (f) and negative for vimentin staining (c). **B**, GFP-labeled MCF-7-ras cells and CAFs co-exist in xenograft tumors Sections of CAF-containing tumors at 60 days after injection were immunostained using an anti-GFP antibody (2) and by H&E (1). In serial sections (1 and 2), GFP-positive signals (brown color) are basically shown in all cancer cells. A different section (3) from a CAF-containing tumor was immunostained using both anti-GFP and anti-vimentin antibodies. GFP-positive signals (pink color) are shown in the GFP-labeled MCF-7-ras cells and vimentin-positive signals (brown color) are detected in CAFs. Sections were also stained with a hemotoxylin nuclear stain (blue color). The human-specific anti-vimentin antibody does not react with either mouse stromal cells or MCF-7-ras cells (data not shown). Scale bar, 100 μm **C**, CAFs stimulate MCF-7-ras breast cancer cell growth in nude mice. (1) Different fibroblasts co-mingled with GFP-labeled MCF-7-ras cells were subcutanously injected into nude mice. In addition, GFP-labeled MCF-7-ras cells were injected alone. CAF (n=10)-, counterpart (n=12)-, normal (n=12)- and non-fibroblast (n=10)- containing tumors were measured. Calculated tumor volumes are plotted. Error bars depict standard error of the mean. *: $p<0.05$ by Student's t-test (2) CAFs increase MCF-7-Ras tumor weight. Tumor weights were measured at 58-60 days after injection. (3) Increased numbers of GFP-labeled MCF-7-ras cells in CAF-containing tumors. Numbers of GFP-labeled MCF-ras cells in each tumor were counted by flow cytometry at 58-60 days after injection. D, CAFs stably retain a tumor-enhancing phenotype CAF1 cells were cultured for 10 population doublings (PDs) in order to examine the stability of their tumor-enhancing phenotype. CAF1 cells, passaged for 5 or 10 PDs, counterpart and normal fibroblasts, passaged for 5 PDs, were co-mingled with GFP-labeled MCF-7-ras cells. The cell mixtures were then subcutanously injected into nude mice. CAF (5PDs)(n=9)-, CAF (10PDs)(n=13)-, counterpart (n=12)-, normal (n=12)- and non-fibroblast (n=10)- containing tumors were measured and their calculated tumor volumes are plotted.

Fig. 1 (A)

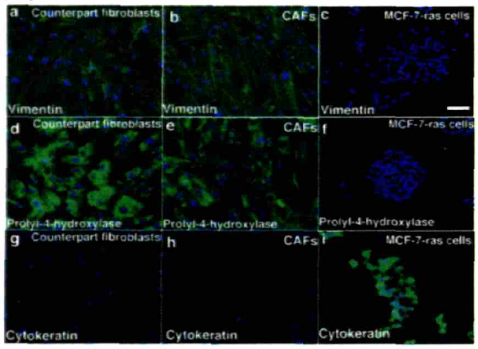

(B)-1

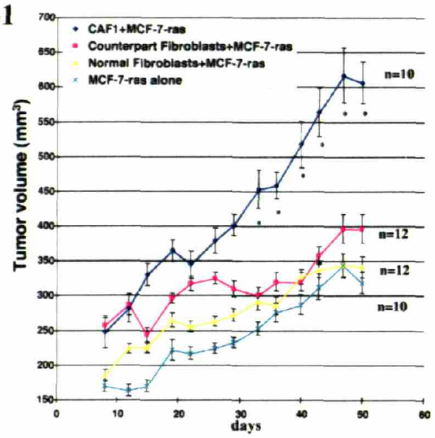

(B)-2

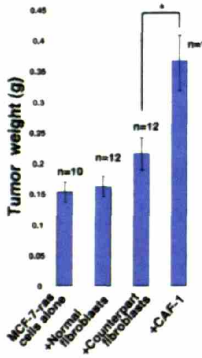

(B)-3

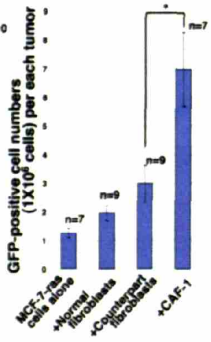

(C)

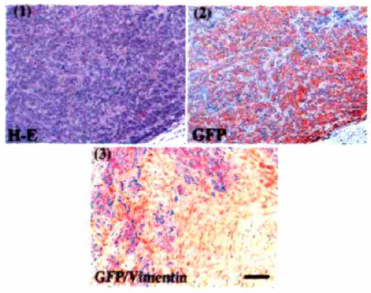

(D)

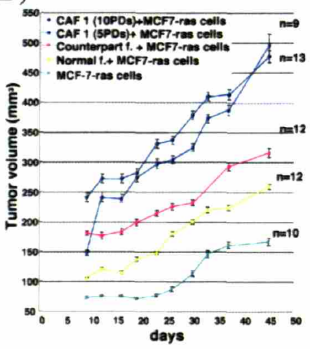

To address this issue, we passaged CAF1 cells for 5 additional PDs *in vitro* and assessed whether their ability to enhance tumor growth is still detectable. Indeed, as indicated in Figure 1D, the CAFs passaged for up to 10 PDs as pure cultures largely retained this phenotype, indicating that this phenotype can be maintained for some period of time, even in the absence of an ongoing stream of instructive signals received from closely apposed carcinoma cells.

CAFs retain α-smooth muscle actin expression in culture

The "activated" stromal fibroblasts that are responsible for the desmoplastic response seen in many human mammary carcinomas can be distinguished from other fibroblasts because of their expression of α-smooth muscle actin (SMA). We therefore examined whether such activated, α-SMA-expressing fibroblasts were present in the original patients' breast cancer tissues from which the various fibroblast populations were prepared and whether the phenotype of α-SMA expression was manifest in cultured, tumor-supporting CAFs that we had prepared from the various breast tumor samples. Extensive immunoreactivity with an anti-α-SMA antibody was seen in fibroblasts within breast cancer-associated stroma (Fig. 2A-f), while α-SMA staining in normal breast tissue (Fig. 2A-d) and tissue distal from the cancer mass (Fig. 2A-e) was confined to myoepithelial cells and blood vessel-associated pericytes.

In order to determine whether the increased α-SMA expression was retained in CAFs explanted in culture, we immunostained three sets of CAFs and counterpart fibroblasts as well as two independent normal fibroblast populations in culture. These analyses indicated that an increased proportion of α-SMA-positive cells existed in the CAF1 population passaged for 5, 7 or 9 PDs (Fig.2B-c), CAF2, and CAF3 (Fig. 2C) when compared to their cognate counterpart fibroblasts 1-3 (Fig. 2B-b, Fig. 2C). In addition, normal fibroblasts (Fig. 2B-a Fig. 2C) demonstrated a far lower percentage of α-SMA-positive cells in the population (0.6% positive cells per field). These observations indicate that the explanted CAFs retain the physiologically activated state that is associated specifically with the myofibroblast phenotype, and that they maintained this activation

phenotype even after being propagated for up to 9 PDs in culture in the absence of nearby breast cancer cells.

CAFs display traits of functionally activated fibroblasts

Fibroblasts are activated in certain pathological conditions, such as wound healing, injury, fibrosis, and neointima (Serini and Gabbiani, 1999). In order to address whether CAF populations are functionally activated in a similar way, we evaluated their characteristics with respect to cell proliferation, motility and tissue contraction. We found that the CAF1 cells proliferated faster in culture when compared to their cognate counterpart fibroblasts and to two independent normal fibroblast populations (Fig 3-A). In fact, 5 out of 6 CAF populations proliferate more rapidly when compared to their cognate counterpart fibroblasts and normal fibroblasts *in vitro* (data not shown). Additionally, the CAF1 cells were capable of sealing wound scratches made in confluent cell monolayers more rapidly than did control counterpart fibroblasts and normal fibroblasts, demonstrating an increased migratory ability (Fig 3-B).

Activated myofibroblasts have been shown to be capable of contracting a collagen gel, into which they have been placed, more strongly than do non-activated fibroblasts (Hinz et al., 2001). Accordingly, we tested whether the CAF1 cells had a greater potential to contract a collagen gel in a microtiter well using a collagen contraction assay. We observed that the CAF1 population contracted collagen gels to a much greater extent than did their counterpart fibroblasts and two independent normal fibroblast populations (Fig. 3C). Significantly, CAF1 populations passaged for 10.5 PDs *in vitro* in the absence of parental breast cancer cells contracted collagen gels to nearly the same extent as CAF1 cells passaged for 5 PDs (Fig. 3C), indicating the stability of expression of this particular activation phenotype. Ultimately, we observed a far stronger contractile ability in all 6 independently isolated CAF populations when compared to their cognate counterpart fibroblast populations and two independent normal fibroblast populations (data not shown). These results lent additional support to the idea that CAFs stably exhibit phenotypic alterations, characteristic of activated fibroblasts, that affect their function in these various biological assays.

Figure 2 CAFs inherit characteristics of "myofibroblasts" from parental human breast cancers

A. Cancer-associated stroma predominantly produces α-smooth muscle actin (SMA)

Parental human breast tissues from which CAFs, counterpart and normal fibroblasts have been extracted were immunostained by an anti-α-SMA antibody (d, e, f) and also stained with H&E (a, b, c). Normal breast (a, d), non-tumor stroma (b, e), dissected from the cancer patient, and tumor stroma (c, f) tissues are represented. Positive signals in myoepithelial cells are indicated by asterisks (d, e) and a representative weak signal in pericytes surrounding vasculature is indicated by an arrowhead (e) and strong signals in myofibroblasts are indicated by an arrow (f). Scale bar, 100 μm

B. Increased numbers of α-SMA-positive cells in CAF populations

Normal fibroblasts (a) extracted from the healthy tissue (Fig.2A-a), CAF1 (c, d) isolated from the breast cancer mass (Fig.2A-c), and counterpart fibroblast1 (b) that was present in non-cancer stroma (Fig.2A-b) were cultured in DMEM with 2% FCS on slide glasses. Immunofluorescence of these different fibroblasts was then carried out using an anti-α-SMA antibody. A staining by mouse IgG did not show any positive signals on CAF1 (d). Scale bar, 50 μm

C. Accelerated collagen gel contractile ability in CAF1 cells. $2X10^5$ fibroblasts, such as CAF1 (5 PDs), CAF1 (10.5 PDs), counterpart fibroblast1 (5 PDs), two independent normal fibroblast1, 2 (5 PDs), were seeded in 300 μl of collagen gels in 24 well plates. The diameter of 4-5 independent collagen gels for each fibroblast type was measured at the indicated times after release of the collagen gels from the edge of the well. The area (mm^2) was calculated.

Fig.2 (A)

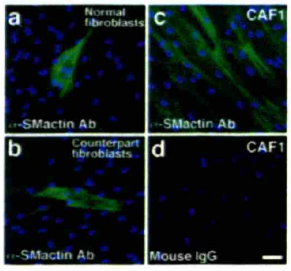
a
Normal fibroblasts
α-SMactin Ab
c
CAF1
α-SMactin Ab
b
Counterpart fibroblasts
α-SMactin Ab
d
CAF1
Mouse IgG

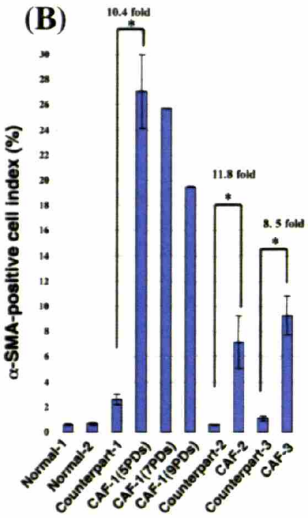
(B)
10.4 fold
11.8 fold
8. 5 fold
α-SMA-positive cell index (%)
Normal-1
Normal-2
Counterpart-1
CAF-1(5PDs)
CAF-1(7PDs)
CAF-1(9PDs)
Counterpart-2
CAF-2
Counterpart-3
CAF-3

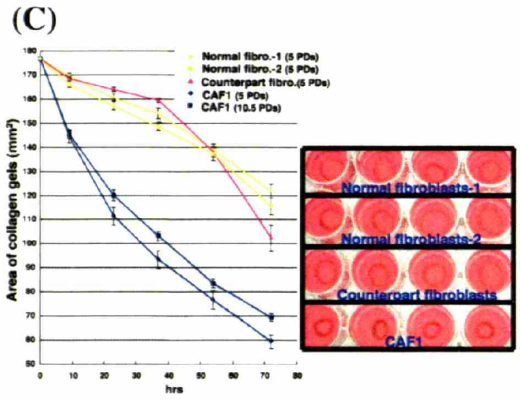
(C)
Normal fibro.-1 (5 PDs)
Normal fibro.-2 (5 PDs)
Counterpart fibro.(5 PDs)
CAF1 (5 PDs)
CAF1 (10.5 PDs)
Area of collagen gels (mm²)
hrs
Normal fibroblasts-1
Normal fibroblasts-2
Counterpart fibroblasts
CAF1

We reasoned that these activated properties of CAFs might be correlated to their tumor-enhancing ability *in vivo*. In order to address this possibility, we performed mixed effects model estimation (Pinheiro and Bates, 2000) to examine correlation between activated property of CAFs (evaluated by areas of contracted collagen gels calculated relative to measurements of their cognate counterpart fibroblasts), and growth rate (mm^3/day) of tumors formed by MCF-7-ras cells co-injected with CAFs. We noted that strongly activated CAFs show more increased tumor growth rate than do weakly activated CAFs ($p<0.001$) (Fig.3D).

CAFs enhance tumor angiogenesis

Cursory examinations of tumor sections stained with hematoxylin and eosin (H&E) indicated that MCF-7-ras tumors containing admixed CAFs were more vascularized than those tumors containing admixed counterpart fibroblasts. This led us to hypothesize that CAFs may assist in tumor angiogenesis *in vivo*, and motivated us to undertake a more detailed evaluation of the extent of vascularization in the various reconstructed tumors. We evaluated vascular formation on serial sections (taken at 2 mm intervals) from 6 independent CAF-, counterpart fibroblast-, normal fibroblast- and non-fibroblast-co-mingled xenograft tumors. Both Masson's trichrome stain (Fig. 4A-a) and anti-CD31 immunostaining (Fig. 4A-d) revealed extensive vascular formation in tumors containing CAFs. In contrast, capillaries in tumors containing counterpart (Fig. 4A-b, e) or normal fibroblasts (Fig. 4A-c, f) were less developed.

We also quantified the relative abilities of various fibroblast populations to promote tumor angiogenesis by assessing averaged micro-vascular density (Fig. 4-B-1) and Chalkley point counting (Fig. 4-B-2) per microscopic field. These metrics both indicated 4.7 and 7.6 fold increases, respectively, in the degree of vascularization in CAF-containing tumors. Taken together, these observations suggested that CAFs enhance tumor growth, at least in part, by promoting tumor angiogenesis and thus neovascularization.

Figure 3. CAFs potentiate tumor angiogenesis of the MCF-7-ras cells

A, Increased microvascular formation in the CAF-containing xenograft tumors. CAF1- (a, d), counterpart fibroblast1- (b, e), normal fibroblast- (c, f) or non-fibroblast-containing MCF-7-ras xenograft tumors were analyzed for the degree of angiogenesis at 55-58 days after injection. 30 serial sections (taken at 2 mm interval) from 6 independent tumors of each type were immunostained using an anti-CD31 antibody (d, e, f) and also by H&E (a, b, c). Scale bar, 100 μm **B**, Quantitative evaluation of the tumor vascular formation in xenograft tumors (1) Increased microvascular density in tumors co-mingled with CAFs . Microvascular density (the number of manually counted vessels per field) was assessed in the three most vascular areas according to the method previously described (Weidner et al., 1991), the three areas containing the maximum numbers of microvessels were identified by scanning the section at low power (X100). Individual microvessels were then counted at X400 magnification. (2) Increased Chalkley counting in tumors co-mingled with CAFs. Vascular volumetric evaluation in each tumor was performed. After counting each field for evaluation of microvascular density, a 49-point Chalkley point eyepiece graticule was employed over the same tumor region and the number of points at X400 magnification within areas of highlighted vessels were counted. **: $p<0.01$. **C**, CAFs stimulate mobilization and recruitment of EPC-enriched Sca1/CD31-double positive cells into tumor masses. (1) Increased recruitment of EPC-enriched cells into MCF-7-ras xenograft tumors co-mingled CAFs MCF-7-ras tumors co-mingled with CAF1 (n=8), counterpart fibroblast1 (n=7), normal fibroblasts (n=6), or non-fibroblast (n=6) were taken at 60-63 days after injection and they were dissociated into single cells. The cells were analyzed using both anti-Sca1 and anti-CD31 antibodies in order to evaluate numbers of EPC-enriched cells in the tumors. Both Sca1- and Sca1/CD31 double- positive cell ratios are significantly increased in CAF-containing tumors. *: $p<0.05$ (2) Sca1-positive cells co-localize with CD31-positive vascular vessels in MCF-7-ras tumors co-mingled CAFs. Frozen sections from the CAF-containing MCF-7-ras tumors were immunostained using both FITC-conjugated anti-Sca1 (a) and PE-conjugated anti-CD31 antibodies (b) and a merged view is shown in (c). Scale bar, 50 μm. (3) Increased mobilization of circulating EPC-enriched cells into peripheral blood of mice bearing CAF-containing tumors. Peripheral blood cells were taken from mice bearing tumors containing CAF (n=9), counterpart (n=10), normal (n=10), or non-fibroblast (n=9) at 60-63 days after injection. Ratios of EPC-enriched cells mobilized into the peripheral circulation were quantified using both anti-Sca1 and anti-CD31 antibodies. As a control, non-tumor bearing mice (n=12) were also examined. Both Sca1- and Sca1/CD31 double- positive cell populations are more increased in mice bearing CAF-containing tumors. *: $p<0.05$

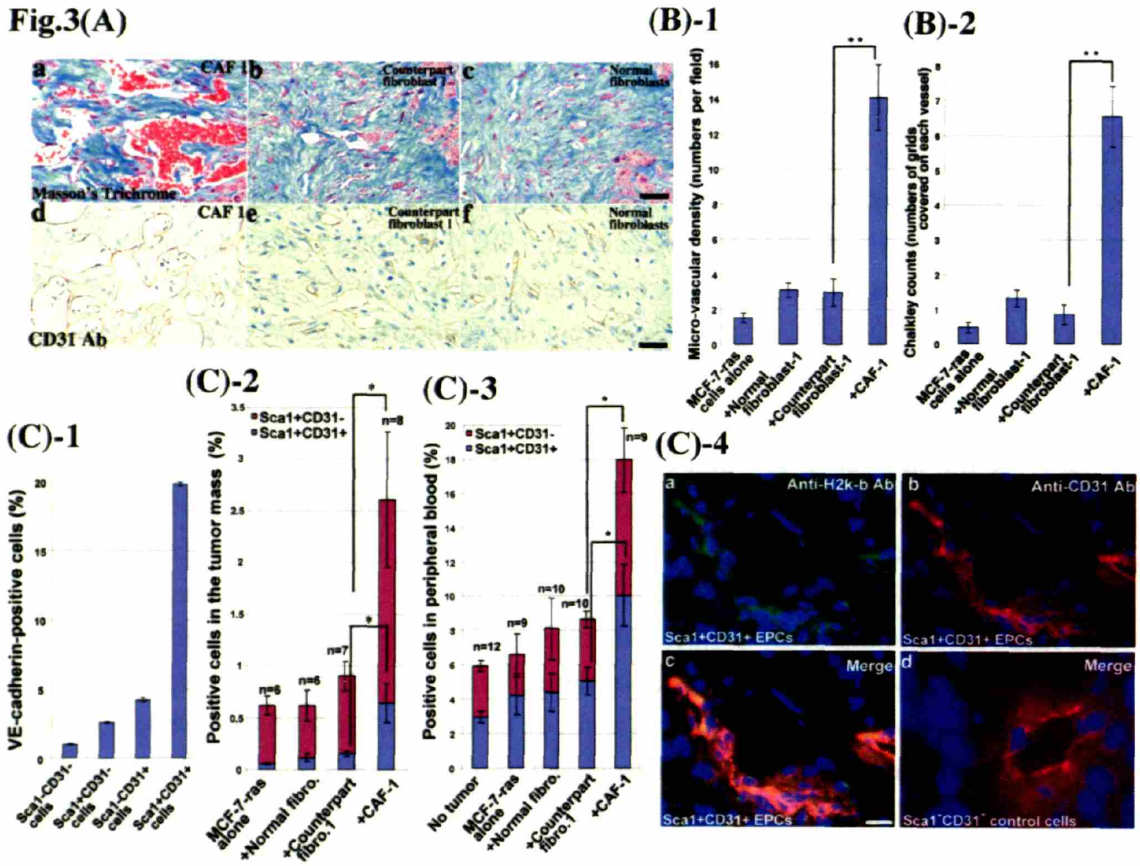
Fig.3(A)
(B)-1
(B)-2
(C)-1
(C)-2
(C)-3
(C)-4
a
CAF 1
b
Counterpart fibroblast 1
c
Normal fibroblasts
Masson's Trichrome
d
CAF 1
e
Counterpart fibroblast 1
f
Normal fibroblasts
CD31 Ab
Micro-vascular density (numbers per field)
Chalkley counts (numbers of grids covered on each vessel)
MCF-7-ras cells alone
+Normal fibroblast-1
+Counterpart fibroblast-1
+CAF-1
VE-cadherin-positive cells (%)
Sca1-CD31- cells
Sca1+CD31- cells
Sca1-CD31+ cells
Sca1+CD31+ cells
Positive cells in the tumor mass (%)
Sca1+CD31-
Sca1+CD31+
MCF-7-ras alone
+Normal fibro.
+Counterpart fibro.1
+CAF-1
Positive cells in peripheral blood (%)
No tumor
Anti-H2k-b Ab
Anti-CD31 Ab
Sca1+CD31+ EPCs
Merge
Sca1-CD31- control cells

CAFs induce mobilization and recruitment of endothelial progenitor cells

Tumor angiogenesis has previously been demonstrated to occur in part through the recruitment of circulating endothelial progenitor cells (EPCs) (Bertolini et al., 2003; Lyden et al., 2001). Accordingly, we were interested in examining whether the demonstrated ability of CAFs to promote tumor angiogenesis was associated with an increased ability of CAFs to recruit these EPCs into a tumor mass. Thus, we undertook to count the number of EPCs in MCF-7-ras tumors containing different fibroblast populations at 60-63 days after the initial subcutaneous injection of various cell populations. To do so, we dissociated cells from whole tumor masses and performed flow cytometry using anti-Sca1 and anti-CD31 antibodies, which are cell surface markers expressed by EPCs.

We found a far higher percentage of Sca1-positive hematopoietic progenitor (2.9 fold) and Sca1/CD31-double-positive EPC-enriched cells (4.2 fold) in CAF-containing tumors when compared to counterpart-, normal fibroblast-, non-fibroblast-containing tumors (Fig. 4C-1). As gauged by two-color immunofluorescence, the Sca1/CD31-double-positive cells were localized in tumor blood vessels (Fig. 4C-2). Additionally, we confirmed that these Sca1/CD31-double-positive cells, explanted from the tumor mass, are EPC-enriched cell populations that enable to form colonies that are positive for both acetylated LDL-uptake and *Ulex europaeus* agglutinin I (lectin) binding *in vitro* (Kalka et al., 2000) (data not shown).

Such EPCs are likely to arrive in tumors via the circulation, having been mobilized in the bone marrow and thereafter introduced into the peripheral circulation (Heissig et al., 2002). To examine this possibility, we evaluated the extent of EPC mobilization into the peripheral blood of mice harboring either CAF-, counterpart, or normal fibroblast-containing tumors. We observed a more increase in the proportion of Sca1- (2.1 fold) and Sca1/CD31-double-positive (2.0 fold) mononuclear cells in the circulation of mice bearing CAF-containing tumors when compared to those in mice bearing counterpart fibroblast-containing tumors (Fig. 4C-3), whereas we failed to observe a significant increase in mice bearing either counterpart-, normal fibroblast-, or non-fibroblast-containing tumors compared to those in non-tumor bearing mice.

On the basis of these observations, we concluded that the presence of admixed CAFs in these various subcutaneous tumors induced higher degrees of tumor vascularization, and that the increased angiogenesis correlated closely with increased levels of EPCs in the tumor masses as well as in peripheral blood. This makes it likely that one of the tumor-enhancing functions of CAFs derives from their ability to induce EPCs to enter into the circulation and enter into the tumor mass. We speculated, therefore, that mobilized circulating EPCs could serve as progenitors of the abundant vasculature observed in CAF-containing MCF-7-ras tumors. In addition, it would be addressed in future about biological contribution to angiogenesis of increased $Sca1^+$ progenitor cell fraction induced by CAFs in the tumor masses as well as in peripheral blood.

CAFs express high levels of stromal cell-derived factor 1 (SDF-1)

Several secreted factors, such as vascular endothelial growth factor (VEGF), stromal cell-derived factor 1 (SDF-1), soluble c-Kit ligand, and matrix metalloproteinase 9 (MMP9), have been implicated as possible regulators of EPC proliferation, mobilization, and migration (Heissig et al., 2002). In order to examine factors involved in EPC's regulation, we performed DNA microarray expression analysis on three sets of CAFs and patient-specific counterpart fibroblasts. This indicated elevated expression of SDF-1 in CAFs when compared to control counterpart fibroblasts (data not shown).

We therefore compared SDF-1 mRNA levels among three pairs of CAFs and cognate counterpart and normal fibroblasts by real time PCR (RT-PCR) and found a more increased expression of SDF-1 mRNA in CAF1 (5.0 fold), CAF2 (2.0 fold) and CAF3 (2.3 fold) cell populations when compared to their respective cognate counterpart fibroblasts (Fig 5A). In addition, higher levels of the SDF-1 protein in CAF1 (1.8 fold) and CAF3 (3.1 fold) were found by ELISA performed on medium conditioned by the various fibroblast populations (Fig 5B).

We subsequently performed immunohistochemistry using anti-SDF-1 (K15C) and anti-α-SMA antibodies on invasive human breast cancer and non-cancer stroma tissue sections. We found much higher expression of SDF-1 protein (Fig 5C-a) in a subset of the α-SMA-positive fibroblasts (Fig 5C-b) in tumor stroma, but failed to detect SDF-1

Fig. 4. CAFs produce increased SDF-1 at both mRNA and protein levels

A, Up-regulated SDF-1 mRNA expression in primary cultured CAFs. $2X10^6$ CAF1-3 and their counterpart fibroblast1-3 and normal fibroblasts were cultured in DMEM with 2% FCS for 2 days. SDF-1 mRNA level in each fibroblast was quantified by real time PCR. These data were then normalized by expression level of β2-microglobin gene as an internal control for each sample. Error bars represent standard error of the mean by three independent experiments. *: $p<0.05$; **: $p<0.01$

B, Increased secretion of SDF-1 from primary cultured CAFs. $2X10^6$ CAF1, 3, cognate fibroblast1, 3 and two independent normal fibroblast populations were cultured in DMEM with 2% FCS for 2 days. And SDF-1 concentration in conditioned medium of cultured fibroblasts was measured by ELISA. Error bars represent standard error of the mean by three independent experiments. *: $p<0.05$; **: $p<0.01$

C, Increased SDF-1 protein expression on α-SMA-positive myofibroblasts present within invasive human breast carcinoma. The parental invasive human breast cancer from which CAFs have been extracted was immunostained by anti-SDF-1 (a) and anti-α-SMA (b) antibodies. A subset of α-SMA-positive myofibroblasts (b) (indicated by arrows) in the tumor stroma are positively stained for SDF-1 (a) (indicated by arrows) whereas fibroblasts in non-tumor associated stroma (c) are negative for SDF-1 (indicated by arrowheads) as well as α-SMA (data not shown). Benign epithelial cells (c) in non-tumor stroma are also positively stained, consistent with previous literature (Pablos, et al. 1999). Scale bar, 100 μm

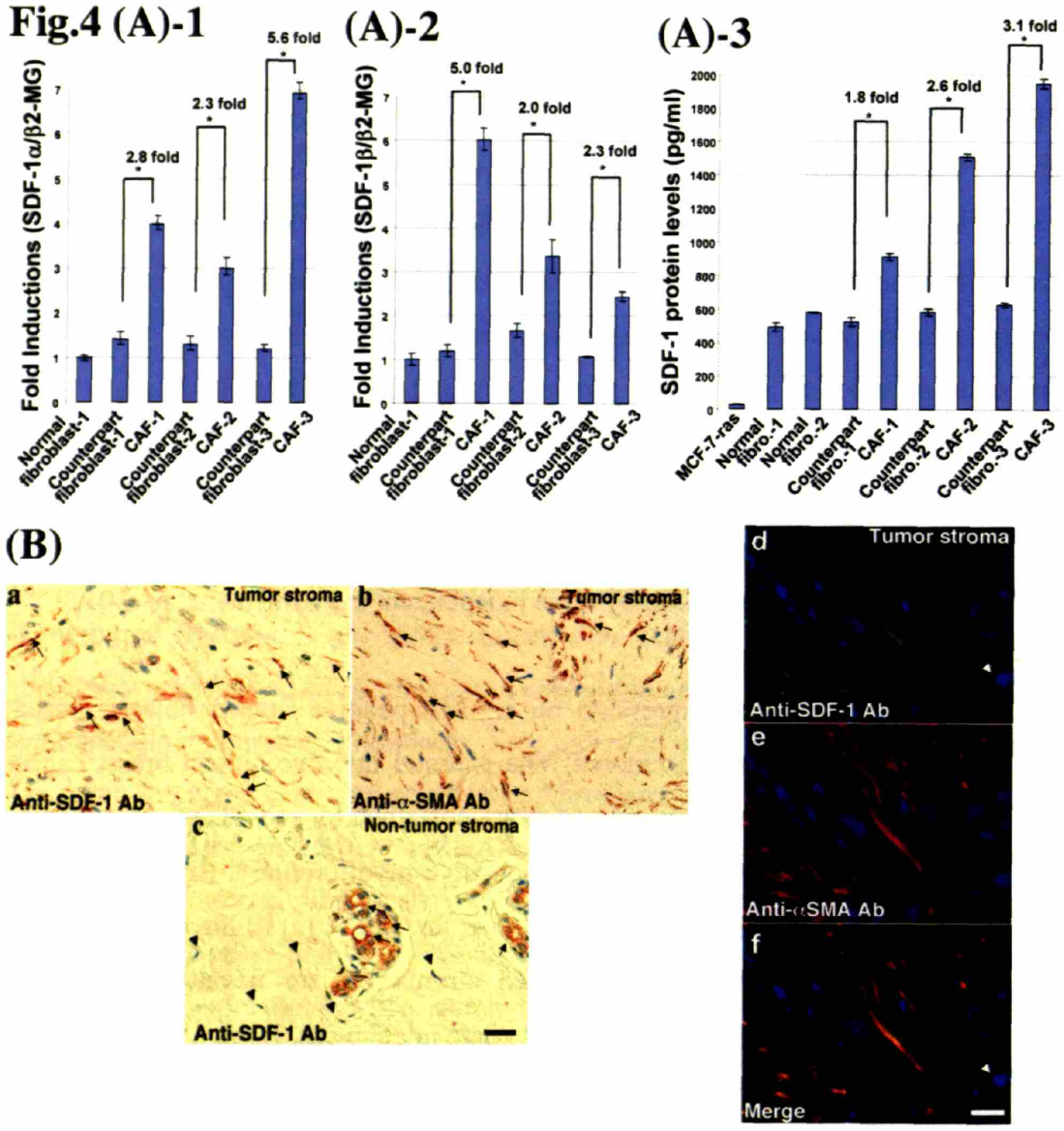
Fig.4 (A)-1
Fold Inductions (SDF-1α/β2-MG)
2.8 fold
2.3 fold
5.6 fold
Normal fibroblast-1
Counterpart fibroblast-1
CAF-1
Counterpart fibroblast-2
CAF-2
Counterpart fibroblast-3
CAF-3
(A)-2
Fold Inductions (SDF-1β/β2-MG)
5.0 fold
2.0 fold
2.3 fold
(A)-3
SDF-1 protein levels (pg/ml)
1.8 fold
2.6 fold
3.1 fold
MCF-7-ras
Normal fibro.-1
Normal fibro.-2
Counterpart fibro.-1
Counterpart fibro.-2
Counterpart fibro.-3
(B)
a
Tumor stroma
Anti-SDF-1 Ab
b
Tumor stroma
Anti-α-SMA Ab
c
Non-tumor stroma
Anti-SDF-1 Ab
d
Tumor stroma
Anti-SDF-1 Ab
e
Anti-αSMA Ab
f
Merge

expression on fibroblasts in non-cancer stroma (Fig 5C-c). We also observed expression of SDF-1 on normal epithelial (Fig 5C-c) and endothelial cells (data not shown), as has been previously reported (Pablos et al., 1999).

SDF-1 released by CAFs mediates the chemotaxis and recruitment of EPCs

We wished to test whether SDF-1 released from CAFs might indeed play a functional role in stimulating EPC recruitment. To this end, we developed an *in vitro* transwell chemotaxis assay. Sorted GFP-labeled bone marrow fractions were seeded into the upper wells of chambers, while lower wells of these chambers contained confluent layers of various fibroblast populations. As an EPC-enriched fraction, we used Sca-1/CD31-double-positive cells, which we confirmed are capable of forming colonies that take up Dil-labeled-acetylated-LDL and bind FITC-conjugated *Ulex europaeus agglutinin* I (lectin) *in vitro* (data not shown).

GFP-positive cells that migrated into the lower well were counted under a microscope at 18h after initial co-culture. We found a 3.3-fold increase in the chemotaxis index of the EPC-enriched fraction when cocultured with CAFs in the lower well (Fig 6A-a, Fig 6 B-1), when compared with coculture with counterpart (Fig 6A-b, Fig 6B-1) or normal mammary stromal fibroblasts (Fig 6A-c, Fig 6B-1). Significantly, treatment with an anti-SDF-1 neutralizing antibody (10 or 20 μg/ml) demonstrated a dose-dependent inhibition of the chemotaxis toward CAFs whereas a control mouse IgG failed to show this effect (Fig 6B-1). Moreover, chemotaxis toward counterpart or normal fibroblasts was not affected by the anti-SDF-1 neutralizing antibody (20 μg/ml). Interestingly, we found that the Sca-1/CD31-depleted fraction of the bone marrow cells showed a lower degree of chemotaxis that was largely SDF-1-independent and unaffected by the type of fibroblasts cultured in the lower well (Fig 6B-1).

The significantly lower SDF-1-dependent migration of bone marrow cells depleted of the EPC-enriched cells led us to hypothesize that differences in the expression of CXCR4, the cognate receptor of SDF-1, might be responsible for the markedly different responses of the various marrow populations. We therefore compared the levels of CXCR4 expression among the Sca-1/CD31-double-positive, bone marrow depleted of these

Fig. 5. SDF-1 mediates the increased migration of EPC-enriched cells toward CAFs
A, Increased migration of GFP-labeled Sca1/CD31-double positive cells towards CAFs *in vitro*. GFP-labeled Sca1/CD31 double-positive bone marrow cells were seeded in the upper well of a transwell apparatus harboring carcinoma-associated (a) -, their counterpart (b) -, normal (c) - or non-fibroblast (d) - containing lower chambers. GFP-positive cells that migrated into the lower wells are shown. Scale bar, 100 μm. **B**, Quantification of the increased migration of GFP-labeled Sca1/CD31-double positive cells toward CAFs *in vitro*. (1) GFP-labeled Sca1/CD31-double positive or -depleted fractions were seeded in the upper well and the co-culture assay was performed with lower wells containing CAF1, counterpart fibroblast 1, normal and non-fibroblast cell populations. An anti-SDF-1 neutralizing antibody (10 or 20 μg/ml) and control mouse IgG1 (20 μg/ml) was applied to the lower well one day prior to the co-culture. GFP-positive cells that migrated into the lower well were counted under a fluorescence microscope at 18 hrs after co-culture. All experiments were done using 4-5 independent wells from each fibroblast type. The chemotaxis index was calculated as the ratio of the number of cells that migrated toward a respective fibroblast population to that of the number of cells that migrated toward medium-only wells. Error bars represent standard error of the mean by three independent experiments. **: $p<0.01$. (2) Increased expression of CXCR4 in the EPC-enriched cell population. Bone marrow cells were incubated with anti-FITC-conjugated CXCR4, anti-PE-conjugated Sca1, and anti-APC-conjugated CD31 antibodies. CXCR4 positive cell populations were compared among Sca1/CD31-double positive, Sca1/CD31-depleted, and whole bone marrow cell fractions. **C**, The migrated Sca1/CD31-double positive cells form colonies positive for Dil-labeled acetylated-LDL uptake and FITC-conjugated *Ulex europaeus agglutinin* I (lectin) binding. After the transmigration assay (described above), Sca1/CD31-double positive cells were cultured for additional 5 weeks on top of the fibroblast monolayers. Colonies formed on a CAF1 monolayer are positive for FITC-conjugated *Ulex europaeus agglutinin* I (lectin) binding (a) and uptake of Dil-labeled-acetylated-LDL (b). (c) is a merged image of (a) and (b). (d) is a merged image of a colony formed on a counterpart fibroblast1 monolayer. Scale bar, 100 μm. **D**, Increased colony formation of EPC-enriched cells on CAFs. Identical numbers of Sca1/CD31-double positive cells were seeded on CAF1 or counterpart fibroblast1 monolayers. Double positive colonies for Dil-labeled acetylated-LDL uptake and FITC-conjugated *Ulex europaeus agglutinin* I (lectin) were counted under a fluorescence microscope at 5 weeks after coculture. **: $p<0.01$

Fig. 5(A)

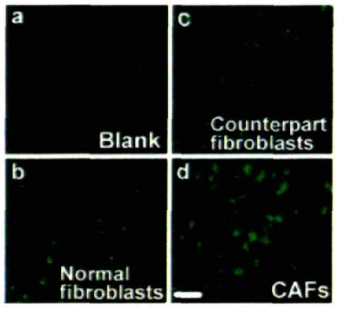
a
Blank
c
Counterpart fibroblasts
b
Normal fibroblasts
d
CAFs

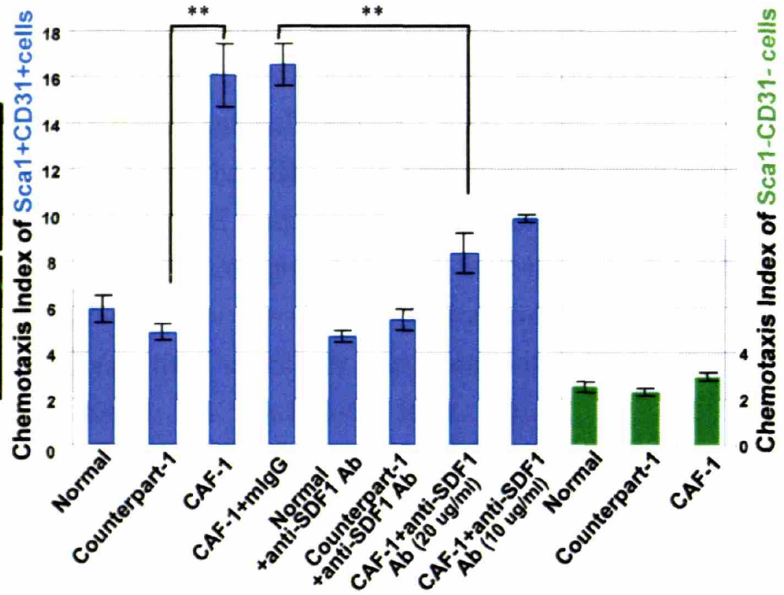
**
**
Chemotaxis Index of Sca1+CD31+cells
Chemotaxis Index of Sca1-CD31- cells
0
2
4
6
8
10
12
14
16
18
Normal
Counterpart-1
CAF-1
CAF-1+mIgG
Normal +anti-SDF1 Ab
Counterpart-1 +anti-SDF1 Ab
CAF-1+anti-SDF1 Ab (20 ug/ml)
CAF-1+anti-SDF1 Ab (10 ug/ml)
Normal
Counterpart-1
CAF-1

(B)

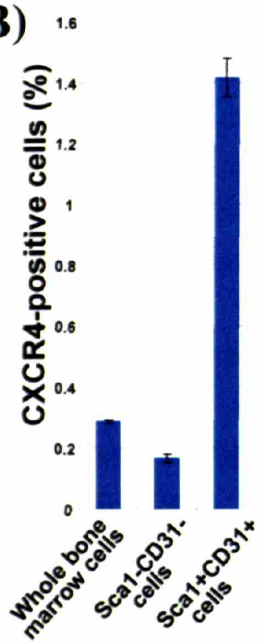
CXCR4-positive cells (%)
0
0.2
0.4
0.6
0.8
1
1.2
1.4
1.6
Whole bone marrow cells
Sca1-CD31- cells
Sca1+CD31+ cells

(C)

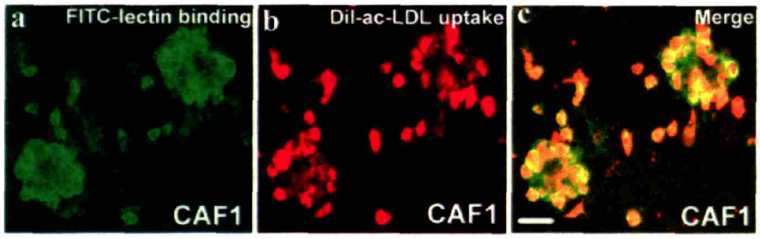
a
FITC-lectin binding
CAF1
b
DiI-ac-LDL uptake
CAF1
c
Merge
CAF1

double positive cells, and whole bone marrow fractions. Using flow cytometry, we found that the percentage of cells expressing CXCR4 was 8.6-fold higher in the Sca-1/CD31-double-positive fraction when compared to the Sca-1/CD31-depleted fraction (Fig. 6B-2). Thus, differences in CXCR4 expression may explain much of the observed differences in SDF-1-induced migration that distinguished the two bone marrow fractions used in our assay. Finally, as an additional control, we verified that the migrated Sca-1/CD31-double-positive cells in these chamber assays were EPCs, by demonstrating their ability to form colonies above the fibroblast monolayers that take up Dil-labeled-acetylated-LDL and bind FITC-conjugated *Ulex europaeus agglutinin* I (lectin) (Fig 6C).

CAFs stimulate EPCs' colonization *in vitro*

Upon long-term culture after our transwell chemotaxis migration assay, CAFs induced the appearance of an increased number of large EPC colonies (Fig 6C-a,b,c) when compared to the counterpart fibroblasts (Fig. 6C-d). We therefore proceeded to plate equal numbers of Sca1/CD31-double-positive cells on top of different fibroblast monolayers and subsequently counted the numbers of colonies double-positive for Dil-labeled acetylated-LDL uptake and FITC-conjugated *Ulex europaeus agglutinin* I (lectin) binding. We observed a significant increase (7.4 fold) in the number of double-positive colonies on top of the CAFs when compared to the counterpart fibroblasts (Fig 6D), indicating enhanced colonization of the recruited EPCs by CAFs.

Stromal SDF-1 enhances tumor growth by paracrine stimulation of tumor cells

Recent reports have indicated that SDF-1 boosts the proliferation of several cancer cell lines in culture, including breast carcinoma cells (Allinen et al., 2004; Hall and Korach, 2003). For this reason, we tested whether CAF-secreted SDF-1 could also directly stimulate MCF-7-ras cell proliferation. Thus, we first treated MCF-7-ras cells with recombinant SDF-1⟨ protein in culture. Indeed, SDF-1 (applied at 1, 10 or 100 ng/ml) stimulated MCF-7-ras cell proliferation in a dose-dependent manner, generating 1.2-, 1.37- or 1.5-fold increases in cell numbers, respectively, when compared to non-SDF-1-treated MCF-7-ras cells (Fig.6-B1). Moreover, an anti-CXCR4 neutralizing

antibody (20 μg/ml), which should block the ability of the CXCR4 receptor to bind its SDF-1 ligand, largely inhibited the SDF-1-induced proliferation (Fig. 6-B1), implicating CXCR4 displayed by the MCF-7-ras cells as the mediator of this proliferation effect.

We then determined whether direct paracrine stimulation of tumor cells by stromal SDF-1 occurs *in vivo*. Furthermore, we sought to confirm that SDF-1 acts through the CXCR4 on the tumor cells themselves in addition to other CXCR4-expressing cells such as EPCs. To do so, we constructed MCF-7-ras cells unable to respond to SDF-1 by introducing lentiviral vectors expressing CXCR4-siRNA into these cells. The resulting significant inhibition of CXCR4 receptor protein expression (by 73-78%) in the MCF-7-ras cells by either of two CXCR4-siRNA lentivirus vectors (Fig. 6B-2) completely abrogated the ability of SDF-1 to stimulate MCF-7-ras cancer cell proliferation (Fig. 6B-3). In contrast, a control GFP-siRNA construct failed to have this effect. Importantly, the loss of CXCR4 did not affect MCF-7-ras cell proliferation in the absence of SDF-1 (Fig 6-B3), indicating that the CXCR4-siRNA vectors did not retard MCF-7-ras cell proliferation through non-specific effects.

In addition, we generated normal human mammary stromal fibroblasts expressing retroviral SDF-1⟨- or control GFP-expression vectors. SDF-1 ⟨-expressing fibroblasts exhibited an 18-fold higher level of SDF-1 protein, as measured by ELISA, when compared to control GFP-expressing fibroblasts (Supplemental Fig. 3). We admixed MCF-7-ras cells carrying CXCR4- or GFP-siRNAs with SDF-1⟨- or control GFP-expressing fibroblasts before injecting them subcutaneously into nude mice. We found that MCF-7-ras tumors expressing either CXCR4-siRNA vector showed more attenuated tumor growth kinetics and significantly reduced tumor volume ($p<0.05$) in the presence of SDF-1⟨-expressing fibroblasts compared to MCF-7-ras tumors expressing a control GFP-siRNA vector (Fig.7-A). This observation demonstrates that stromal SDF-1 enhances tumor growth *in vivo* in part by direct paracrine stimulation through CXCR4 on MCF-7-ras breast cancer cells.

We also found that MCF-7-ras tumors carrying either CXCR4-siRNA vector admixed with control GFP-expressing fibroblasts grew more slowly and had a significantly decreased tumor volume ($p<0.05$) than did tumors arising from these same carcinoma

cells that had been commingled with SDF-1⟨-expressing fibroblasts (Fig. 7-A). This result shows that stromal SDF-1, as proposed above, also boosts tumorigenesis by affecting other CXCR4-expressing cells besides the MCF7-ras tumor cells; these other targets might include the EPCs studied in the earlier experiments. Together, these findings strongly suggest that CAF-secreted SDF-1 promotes carcinoma growth *in vivo* by direct paracrine stimulation through CXCR4 present on breast carcinoma cells in addition to its endocrine effects that allow EPC recruitment into tumors (Fig7-A, B).

Fig. 6. An anti-SDF-1 neutralizing antibody attenuated the increased growth of MCF-7-ras tumor developing in the presence of CAFs, decreased angiogenesis, and reduced recruitment of EPCs into tumors

A, Mice bearing MCF-7-ras tumors co-mixed with CAF1 cells or control counterpart fibroblasts were intraperitoneally treated with either anti-SDF-1 antibody or control mouse IgG twice a week for a period of 68 days after initial injection of the tumor cells. We examined tumor growth kinetics (1), tumor weight (2), angiogenesis (3) and the percentage of Sca1+CD31+ EPCs (4) within the tumor masses. *: $p<0.05$

B, (1) Recombinant SDF-1〈 protein was added to cultured MCF-7-ras cells in the presence of either control IgG or anti-CXCR4 neutralizing antibody (20 μg/ml). Total numbers of MCF-7-ras cells in each of 4 independent wells were counted at day 3 and 5. (2) Two independent CXCR4-siRNA or control GFP-siRNA lentivirus vectors were introduced into MCF-7-ras cells. CXCR4 protein expressed on the surface of MCF-7-ras cells was then analyzed using an anti-CXCR4 antibody by flow cytometry. (3)MCF-7-ras cells expressing various siRNAs or non-siRNA were cultured in the presence or absence of SDF-1 (100 ng/ml). Total cell numbers in each of 4 independent wells were counted at day 5.

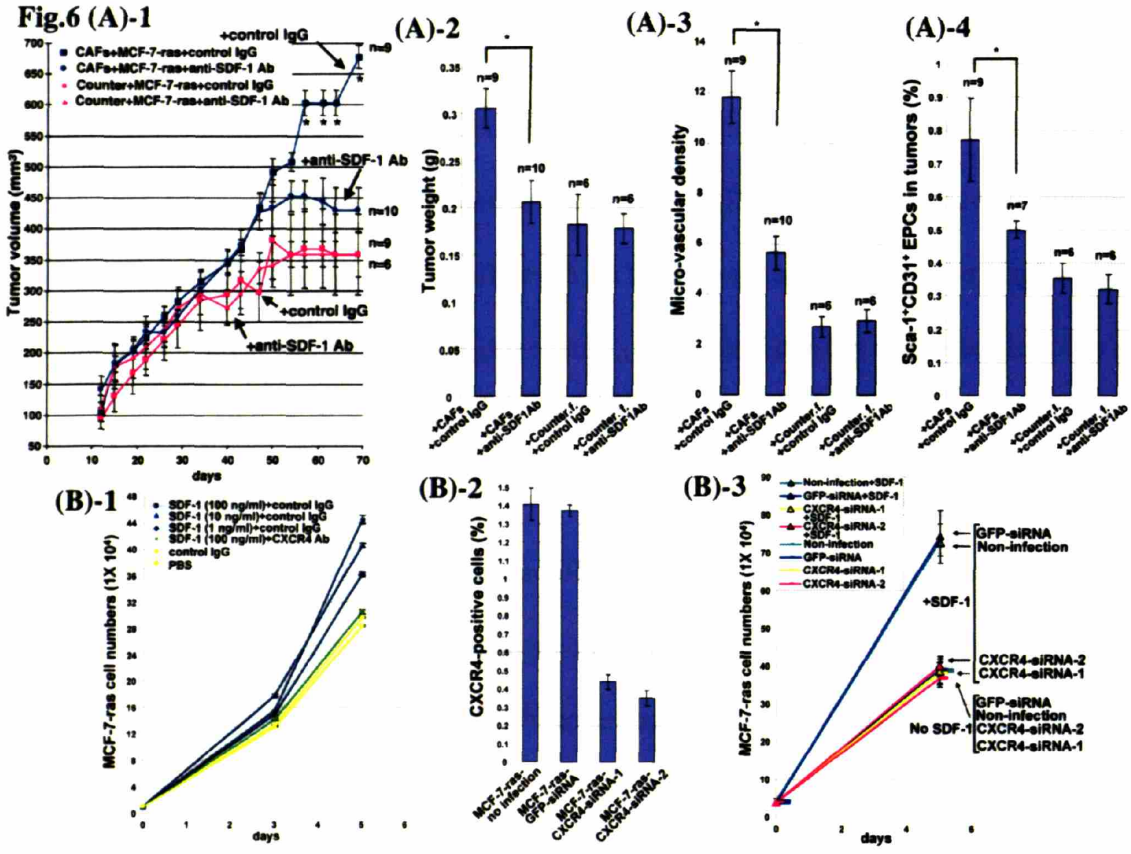
Fig.6 (A)-1
CAFs+MCF-7-ras+control IgG
CAFs+MCF-7-ras+anti-SDF-1 Ab
Counter+MCF-7-ras+control IgG
Counter+MCF-7-ras+anti-SDF-1 Ab
+control IgG
+anti-SDF-1 Ab
+control IgG
+anti-SDF-1 Ab
n=9
n=10
n=6
n=6
Tumor volume (mm³)
days
(A)-2
Tumor weight (g)
(A)-3
Micro-vascular density
(A)-4
Sca-1⁺CD31⁺ EPCs in tumors (%)
(B)-1
SDF-1 (100 ng/ml)+control IgG
SDF-1 (10 ng/ml)+control IgG
SDF-1 (1 ng/ml)+control IgG
SDF-1 (100 ng/ml)+CXCR4 Ab
control IgG
PBS
MCF-7-ras cell numbers (1X 10⁴)
days
(B)-2
CXCR4-positive cells (%)
MCF-7-ras-no infection
MCF-7-ras-GFP-siRNA
MCF-7-ras-CXCR4-siRNA-1
MCF-7-ras-CXCR4-siRNA-2
(B)-3
Non-infection+SDF-1
GFP-siRNA+SDF-1
CXCR4-siRNA-1 +SDF-1
CXCR4-siRNA-2 +SDF-1
Non-infection
GFP-siRNA
CXCR4-siRNA-1
CXCR4-siRNA-2
MCF-7-ras cell numbers (1X 10⁴)
GFP-siRNA
Non-infection
+SDF-1
CXCR4-siRNA-2
CXCR4-siRNA-1
GFP-siRNA
Non-infection
No SDF-1
CXCR4-siRNA-2
CXCR4-siRNA-1
days

Discussion

While the presence of fibroblasts in the stroma of invasive mammary carcinomas is well-documented, the specific contributions of these fibroblasts to tumor growth are unclear. We have shown here that fibroblasts present in invasive human mammary carcinoma masses are biologically very different from their counterparts located outside of the tumor masses in several important respects. (1) Fibroblasts extracted from within invasive human breast cancer masses are more competent than their counterparts to enhance tumor formation by co-mingled breast cancer cells. (2) They are a functionally activated fibroblast population exhibiting an increased percentage of α-smooth muscle actin (SMA) expression as well as increased proliferation, motility and tissue contraction. (3) When co-mingled with breast cancer cells, these fibroblasts give rise to highly vascularized tumors while normal stromal fibroblasts do not. (4) Fibroblasts present in invasive human breast cancers as well as fibroblasts explanted from the carcinoma masses produce increased level of SDF-1 in comparison to fibroblasts in normal breast tissue and extracted normal and counterpart fibroblasts. (5) These fibroblasts are more competent to recruit endothelial progenitor cells (EPCs) into the tumor mass, in part, through increased SDF-1 production, leading in turn to the enhanced tumor angiogenesis.

Importantly, both tumor-enhancing and activated properties found in these carcinoma-associated fibroblasts (CAFs) explanted from the cancer masses are likely to be maintained, at least, for up to 10 population doublings (PDs) in the absence of continuous interaction with epithelial cancer cells. These retained phenotypes may be a result of either genetic changes-deletions and/or mutations-or epigenetic changes affecting gene expression. A recent paper has documented a high frequency of somatic p53 and PTEN mutations in both stromal and epithelial regions microdissected from human breast cancer masses (Kurose et al., 2002). Although it is unclear precisely which stromal cell lineages carry the observed mutations, this report raises the possibility that the accumulation of genetic mutations may contribute to the CAFs' activated and tumor-enhancing phenotypes. We note, however, that the CAFs prepared by us show no anchorage-independent growth in culture, no tumorigenicity *in vivo*, and no detectable aneuploidy as determined by karyotype analysis (data not shown). Moreover, some of

them begin to senesce after 15 PDs in culture. These observations suggest that CAFs remain non-tumorigenic, even if they harbor mutations or epigenetic alterations of certain genes.

The Activated properties of CAFs are involved in enhancing tumor development

Activated myofibroblasts are often found in various injured organs as well as in tumor stroma (Serini and Gabbiani, 1999). These activated fibroblasts are likely to produce more abundant growth factors, cytokines and extracellular matrix which could mediate inflammation, angiogenesis, re-epithelialization, and tumor cell growth (Fukumura et al., 1998; Ronnov-Jessen et al., 1996). Thus, we wondered whether the activation of fibroblasts is related to their acquiring a tumor-enhancing ability. Our results show a significant correlation between the activated property of CAFs evaluated by collagen gel contraction *in vitro*, and their tumor-enhancing ability *in vivo*. This observation, made with 6 independent CAFs, suggests that factors involved in activation of fibroblasts might also govern fibroblasts' tumor-enhancing ability. It raises an interesting question whether myofibroblasts extracted from wounds or injuries could also enhance tumor growth using our experimental model.

In addition, it remains to be addressed how CAFs have acquired these unique phenotypes, either by evolving from normal preexisting stromal fibroblasts or by being recruited cells that had originally possessed the activated phenotypes. Preliminary evidence in favor of the first hypothesis comes from experiments in which we co-mingled puromycin-resistant normal human mammary stromal fibroblasts, carrying a telomerase catalytic subunit (hTERT)-GFP expression vector, with MCF-7-ras cells, and then incubated both cell types in immunodeficient mice for 3-4 months. Interestingly, the GFP-positive human fibroblasts extracted from the resulting tumors cultured under the puromycin treatment showed a far greater collagen contraction ability and increased α-SMA-positive cell population compared to those of the parental human fibroblasts that had not been incubated with any tumor cells (Orimo, et al., manuscript in preparation).

CAFs enhance tumor growth by increased angiogenesis through endothelial progenitor cells (EPCs)

We have observed that most of the CAF populations isolated from 6 independent human invasive breast cancers are more competent in assisting the growth of co-injected MCF-7-ras cancer cells than are co-introduced counterpart and normal fibroblasts. We initially considered two possible mechanisms as to how the CAFs stimulate tumor growth in our system: 1) CAFs directly stimulate MCF-7-ras cell growth through soluble or non-soluble factors that they release; or 2) CAFs indirectly stimulate tumor growth through promoting the generation of a cancer-prone microenvironment (e.g., recruitment of vascular cells or inflammatory cells).

We have observed that CAFs weakly stimulate MCF-7-ras cell growth in *in vitro* co-culture assays using adherent and non-adherent conditions with MCF-7-ras cells (data not shown). Consequently, we surmised that indirect mechanisms involving the generation of a more supportive microenvironment *in vivo* were more likely to explain the increased ability of CAFs to promote tumor formation. Consistent with this thinking, we have found that tumors arising from MCF-7-ras populations carrying co-mingled CAFs display a substantial increase in capillary density when compared to tumors co-mingled with counterpart or normal fibroblasts. We initially hypothesized that angiogenic factors up-regulated in CAFs might locally stimulate tumor angiogenesis. Supporting this idea, we observed a 1.8-2 fold increase in the level of VEGF-A and PDGF-A mRNAs in CAFs (data not shown), and a 3-5 fold increase in the level of SDF-1 mRNA in CAFs, all these being compared to the levels present in counterpart fibroblasts. However, CAFs were not functionally competent to stimulate cell proliferation and migration of human umbilical vein endothelial cells (HUVECs) under a variety of co-culture assay conditions (data not shown).

We therefore speculated that the CAFs might stimulate tumor angiogenesis systemically, either by affecting the mobilization of EPCs from the marrow into the peripheral circulation, or by efficiently recruiting already-circulating EPCs from the circulation into the tumor stroma, or through both mechanisms. In fact, both mechanisms appear to be operative here, as indicated by the increased numbers of EPCs in the

peripheral circulation and the substantially denser, tumor-associated vasculature induced by the CAFs. Importantly, while the CAFs may contribute in a major way to the recruitment of EPCs, presumably essential for angiogenesis and tumor growth (Lyden et al., 2001), the present research does not address how these cells, once ensconced within tumor masses, are induced to differentiate into endothelial cells capable of constructing the microvasculature.

CAFs induce SDF-1-dependent recruitment of EPCs

SDF-1 is more highly expressed in stromal fibroblasts present within invasive human breast cancers as well as in CAFs extracted from the carcinoma masses. Moreover, CAFs are more competent in attracting EPCs in a transwell assay, doing so in through signaling that can be substantially reduced by an anti-SDF-1 neutralizing antibody. These findings suggest that the release of SDF-1 by CAFs mediates the mobilization and recruitment of EPCs into the tumor stroma *in vivo*. Previous work (Heissig et al., 2002) regarding the role of SDF-1 in maintaining hematopoietic stem cell (HSC) homeostasis suggested to us that SDF-1 may also stimulate the mobilization of EPCs into the circulation of mice bearing CAF-co-mingled MCF-7-ras tumors. However, when we checked the plasma concentration of SDF-1 in mice bearing CAF-co-mingled MCF-7-ras tumors, we saw no significant increase in plasma SDF-1 levels when compared with those in mice bearing tumors with co-mingled counterpart or normal fibroblasts (data not shown). Therefore, we speculate that VEGF, released by CAFs, might be responsible for the increase in EPC mobilization, perhaps in collaboration with SDF-1, into the peripheral blood of CAF-co-mingled tumor-bearing mice. Alternatively, additional factors released into the circulation by CAFs may sensitize EPCs to become mobilized by SDF-1 at relatively low levels in the blood, indeed at levels not readily detectable by ELISA. Precedents for this idea can be found in the literature, as it has been reported that HGF, SCF and MMP9 produced during liver injury significantly up-regulate CXCR4 expression levels on human $CD34^+$ stem cells (Kollet et al., 2003).

Our proposed notion that CAF-derived SDF-1 contributes to the homing of EPCs into a tumor mass (Fig. 7) mirrors previous work showing that SDF-1 released from stromal

fibroblasts in an ischaemic cardiomyopathy model plays a key role in recruiting $CD34^+$ human progenitor cells and in subsequent tissue regeneration (Askari et al., 2003). Importantly, fibroblasts are known as "sentinel cells" that are promptly recruited into various damaged tissues including tumors (Silzle et al., 2004). Our work takes these ideas still further, demonstrating that carcinoma cells can utilize the normal host stromal response in order to maintain a tumor-prone microenvironment specifically through the recruitment of fibroblasts, the probable induction of their phenotypic conversion to CAFs, leading to the recruitment of EPCs into the tumor stroma (Fig. 7).

Importantly, endogenous CXCR4 expression on carcinoma cells is known to correlate with a poor prognosis for several types of carcinomas (Balkwill, 2004; Staller et al., 2003), although relatively little is known about the role of its ligand, SDF-1, in primary tumor growth. It is also known that CXCR4 ectopically expressed on carcinoma cells enhances primary tumor growth in a mouse xenograft model (Darash-Yahana et al., 2004), and that the knockdown of CXCR4 expression in breast carcinoma cells abrogates the tumor growth (Lapteva et al., 2004; Smith et al., 2004). Moreover, a small-molecule inhibitor of CXCR4 reduces primary brain tumor growth (Rubin et al., 2003). Thus, it is likely that SDF-1 secreted by stromal myofibroblasts significantly affects CXCR4-expressing human breast carcinomas through direct paracrine stimulation. Inhibition of the activated SDF-1/CXCR4 signal pathway in a primary tumor environment may therefore attenuate carcinoma growth in breast cancer patients.

Fig. 7 Schematic representation of tumor-enhancing stromal environment created by fibroblasts present in invasive human mammary carcinomas

Fibroblasts within mammary carcinomas derive from proximal fibroblasts in breast stroma (Ronnov-Jessen et al., 1995) as well as from distal bone marrow-derived progenitor cells (Ishii et al., 2003). Heterotypic interactions between breast cancer and stromal cells convert the recruited fibroblasts into activated myofibroblasts, which express higher levels of SDF-1. These activated fibroblasts induce mobilization, recruitment and colonization of EPCs derived from the bone marrow, resulting in increased angiogenesis and enhanced tumor growth. The elevated level of SDF-1 released by activated fibroblasts mediates these mobilization and recruitment of EPCs into the carcinoma mass. Importantly, these fibroblasts present in invasive human breast carcinomas retain an ability to continue to enhance tumor development even in absence of ongoing contact with nearby breast carcinoma cells.

Fig. 7-A

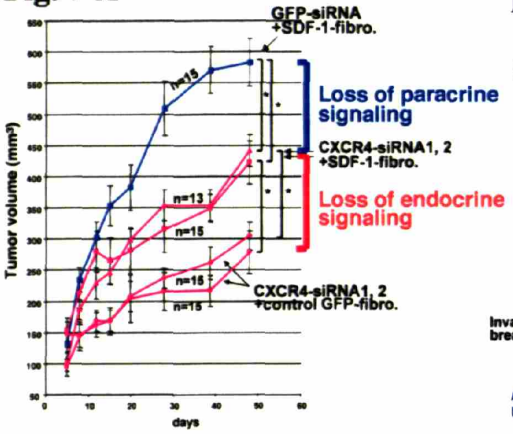
GFP-siRNA
+SDF-1-fibro.
Loss of paracrine signaling
CXCR4-siRNA1, 2
+SDF-1-fibro.
Loss of endocrine signaling
CXCR4-siRNA1, 2
+control GFP-fibro.
n=15
n=13
n=15
n=15
n=15
Tumor volume (mm³)
days

Fig.7-B

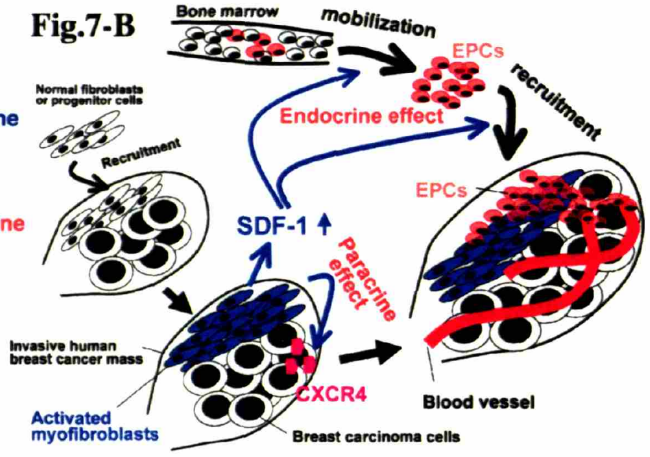
Bone marrow
mobilization
EPCs
recruitment
Normal fibroblasts
or progenitor cells
Recruitment
Endocrine effect
EPCs
SDF-1
Paracrine effect
Invasive human
breast cancer mass
CXCR4
Blood vessel
Activated
myofibroblasts
Breast carcinoma cells

Experimental Procedures

Isolation of human breast fibroblasts and cell culture

Breast tissues were obtained from six independent cases of sporadic invasive ductal breast carcinomas. Fibroblasts were isolated from cancer- and non-cancer-associated regions of whole breast tissues dissected from whole breast mastectomies. The cancer-associated regions were selected to be minimally necrotic regions of the tumor mass. Non-cancer associated stroma, which was isolated from tissue at least 2 cm. distal to the outer margin of the cancer mass, exhibited normal epithelial and stromal breast histology. Fibroblasts were explanted and cultured from cancer- and non-cancer-associated regions. Tissues were digested with collagenase type I (1 mg/ml; Boehringer Mannheim) and hyaluronidase (125 units/ml; Sigma) at 37°C with agitation for 12-18 hrs in Dulbecco's Modified Eagle's Medium (DMEM) with 10% fetal calf serum (FCS). The dissociated tissues were incubated without shaking for 5 min at room temperature, followed by the separation of stromal cell-enriched supernatant to a new tube. The stromal fraction was centrifuged at 250 X g for 5 min and the pellet was resuspended in DMEM with 10% FCS and the cells were cultured on tissue culture plates. Each fibroblast was then expanded into two 15 cm petri dishes within 8-10 days after breast tissue dissociation and stored as cells passaged for 3 population doublings (PDs). MCF-7-ras cells (Kasid et al., 1985) were cultured in DMEM with 10% FCS.

Immunofluorescence of the human fibroblasts and breast cancer tissues

Primary cultured fibroblasts were plated on multiwell coverslides and grown in DMEM with 2 % or 10% FCS. Cells and frozen breast cancer sections were fixed in freshly prepared 4% paraformaldehyde-PBS for 10 min at room temperature (RT) and incubated in primary antibody at 4°C overnight and in secondary antibody for 2 hrs at RT. After antibody incubations and washes, samples were embedded in 25% glycerol with 4', 6' diamino-2-phenylindole (DAPI, Sigma). Images of labeled cells were taken using a mercury laser-equipped inverted epifluorescence microscope (Zeiss). Pictures were captured using an 8-bit source image with a CCD camera.

Primary antibodies used for staining included anti-pan-cytokeratin (Sigma), anti-human vimentin (V9; Novocastra Laboratories, Ltd. UK), anti-fibronectin (Sigma), anti-

prolyl 4-hydroxylase (5B5; DAKO, Denmark), anti-fibroblast surface protein (1B10; Sigma), anti-human CD31 (Dako, Denmark), α-smooth muscle actin (SMA) (1A4; Dako, Denmark), fluorescein isothiocyanate (FITC)-conjugated anti-Sca1 (BD PharMingen) and phycoerythrin (PE)-conjugated anti-CD31 (BD PharMingen). Antibodies for secondary staining were either anti-rabbit or anti-mouse IgGs conjugated with FITC or PE (Jackson Immunochemicals).

Immunohistochemistry

Tissues were incubated in 4% paraformaldehyde-PBS at 4°C for 48 hrs, followed by paraffin embedding. 4 μm tissue sections were generated and stained with hematoxylin and eosin (H&E). Immunohistochemistry was performed using the DAKO Animal Research Kit ARK (Dako, Denmark). Anti-α-smooth muscle actin (1A4; Dako, Denmark), anti-SDF-1 (K15C; generously provided by Dr. Fernando Arenzana-Seisdedos), anti-GFP (abcam, UK) and human specific anti-vimentin (Novocastra Laboratories, Ltd., UK) antibodies were used. After antibody staining, sections were slightly stained with hematoxylin. For double immunostaining of vimentin and GFP in MCF-7-ras tumor sections, the DAKO Envision Doublestain System (Dako) was used with anti-vimentin and anti-GFP antibodies.

Data analysis

Mixed effects models (Pinheiro and Bates, 2000) were used to conduct inference on different aspects of the relationship between cell types, growth rate of tumors formed by MCF-7-ras cells co-mingled various fibroblasts and activated property of fibroblasts measured by collagen gel contraction.

Evaluation of tumor growth rate (mm^3/day)-The basic model for the relationship between tumor volume y and cell type j (CAF, counterpart fibroblast or normal fibroblast) in donor i ($i = 1, \ldots, 6$) is

$$y_{ijklm} = \mu_{i(j)} + \beta_{i(j)} t_m + \gamma_{i(j)} x_{ij} + \delta_{i(j)} x_{ij} t_m + f_{ijkl}(t_m) + e_{ijklm}$$

where y_{ijklm} is the mth volume measurement on tumor l from donor i, cell type j, mouse k, obtained at time t_m. Parameter $\mu_{i(j)}$ is the marginal mean tumor volume averaged over all observations for which CAF for donor i was compared to cell type j for donor i, $\beta_{i(j)}$ is the average growth in volume per unit time for tumors with type j for

donor i, $\gamma_{i(j)}$ is the average difference in tumor volumes between CAF and cell type j, and $\delta_{i(j)}$ is the difference in growth rates between CAF and cell type j. The error term e_{ijklm} has mean zero and, given the values of the random effects to be described, are mutually independent with a constant variance. The random effects introduced by repeatedly measuring multiple tumors in different mice are captured in the (linear) random functions $f_{ijkl}(t_m)$, which are random tumor-specific growth curves specified by parameters that are subject to conventional constraints (conditionally independent mean zero Gaussian, with separate variances to be estimated by restricted maximum likelihood). The test of $H_0 : \delta_{i(j)} = 0$ is the test for common growth rates in donor i for CAF and type j cells.

Evaluation of activated property of CAFs-Activated property of CAFs were measured by collagen gel contraction. Repeated measurement of area (mm^2) of contracted collagen gels containing CAFs or counterpart fibroblasts were modeled as follows:

$$d_{ijkl} = \mu_{ij} + a_k + e_{ijkl}$$

where d is the area of the treated collagen gels, i indexes donor ($i = 1, \ldots, 6$), j indexes cell type (1 = CAF, 2= counterpart), l indexes replicates within experiments, and k indexes experiment (a pair of experiments was performed for donor 1; all other donors provided a single experiment). The parameters μ_{ij} are the type-specific mean areas. Again e_{ijkl} is a measurement error term with mean zero. The ratio of activated property of CAF (evaluated by areas of contracted collagen gels calculated relative to measurements of their cognate counterpart fibroblast) for donor i is $\hat{r}_i = \hat{\mu}_{i1}/\hat{\mu}_{i2}$. Small values of $\hat{r}_i$ therefore indicate significant activated property of CAF relative to counterpart.

Correlation between activated property of CAFs and the tumor-enhancing ability

The relationship between CAFs' activated property and their tumor-enhancing ability modeled using measurements of tumor volumes of MCF-7-ras tumors containing CAFs. The model used was

$$y_{ijkl} = \mu + \beta t_l + \gamma \hat{r}_i + \delta \hat{r}_i t_l + a_i + b_{ij} + c_{ijk} + e_{ijkl}$$

with i indexing donor, j indexing mouse, k indexing tumor, and l indexing repeated measurements on tumors. Here y denotes tumor volume, μ is overall average tumor

volume, and e_{ijkl} is an error term. Random effects a_i are donor-specific departures from the overall mean, b_{ij} are mouse-specific effects nested within donor, and c_{ijk} are tumor-specific effects nested within mouse. All random effects are conditionally independent mean zero Gaussian with separate variance parameters. Parameter δ measures the effect between activated property of CAFs and growth rate (mm^3/day) of tumors formed by MCF-7-ras cells co-injected with CAFs. The test of $H_0 : \delta = 0$ is the test for no effect between them.

All models are fit using restricted maximum likelihood (Pinheiro and Bates, 2000).

Preparation of Collagen Lattices and Measurement of Collagen Gel Contraction by human breast fibroblasts

Collagen lattices were prepared using type I collagen from rat tail tendon (BD bioscience, MA) adjusted to a final concentration of 2.0 mg/ml and pH 7.2 with 1X DMEM and 0.012N NaOH. $2X10^5$ fibroblasts were suspended in 300 μl of the prepared collagen lattices in 24-well plates. The collagen lattices were polymerized for 30 min in a humidified 5 % CO2 incubator at 37°C, followed by incubation in DMEM with 2% FCS. After 24 hrs, the collagen gels were gently released from the culture dish surface to initiate collagen gel contraction. The degree of gel contraction was determined after 24, 48 and 72 hrs. The major and minor axis diameters of 6 independent gels were measured for each type of fibroblast population, and areas were calculated using the formula (1/4)(π)(major diameter)(minor diameter).

Wound closure assay

$2X10^5$ fibroblasts were plated on 12-well plates and incubated in standard fibroblast medium (10% FCS in DMEM) for 3 hrs in 5% carbon dioxide at 37°C. The fibroblasts were then treated for an additional 3 hrs with mitomycin C (MMC) (Sigma) at a concentration of 10 μg/ml. After washing twice with PBS, the fibroblasts were incubated in DMEM+2% FCS for 24 hrs. The confluent fibroblast monolayers were disrupted by scraping with a 1000 μl pipette tip. Photomicrographs were taken at 0, 12, 24 hrs post-wounding.

Subcutaneous tumorigenicity assays

Eight- to twelve-week old athymic nude mice (NCR nude, nu/nu, Taconic Laboratories) were irradiated using a dual Cesium source with 400 rad 5 hrs prior to injection. 1 million GFP-labeled MCF-7-ras cells alone, or mixed with 3 million fibroblasts (CAFs, counterpart, or normal fibroblasts) were resuspended in 250 μl of DMEM+10% FCS with 50% Matrigel (BD biosciences). The cell mixtures were injected subcutaneously into isofluorane-anesthetized mice using a 1ml syringe equipped with a 27-gauge needle. Tumor size was measured every 3-4 days using precision calipers.

Plasmid construction and retroviral infection

A 0.8 kb cDNA fragment encoding GFP was cloned into the EcoRI site of the pWZL-Blasticidin retroviral expression construct. Amphotropic retroviruses were created by transient cotransfection of DNA into 293T cells. Briefly, 10 cm plates of 293T cells were cotransfected with 2 μg of the amphotropic packaging plasmid pCL-10A1 (Imgenex) and 2 μg of the GFP-pWZL-Blasticin vector using calcium phosphate precipitation. Viral supernatants were harvested at 48 hrs post-transfection and used to infect the MCF-7-ras cells in 8 μg/ml polybrene. Drug selection of the infected MCF-7-ras cells was performed with 30 μg/ml blasticidin S (Invitrogen) for 7 days.

Real Time PCR

$2x10^6$ fibroblasts were cultured in DMEM with 2% FCS on a 10 cm dish for 2 days prior to RNA isolation using Trizol reagent (In vitrogen). Quantitative real time RT-PCR analysis was performed using the iCycler apparatus (Bio-Rad) and SYBR Green PCR Core Reagents system (Perkin-Elmer Applied Biosystems). Results were evaluated with the ICYCLER IQ REAL TIME DETECTION SYSTEM SOFTWARE (Bio-Rad). Data were normalized relative to the expression level of β2-microglobin for each sample. Primers used for RT-PCR were SDF-1, 5'-CTAGTCAAGTGCGTCCACGA-3' (sense) and 5'-GGACACACCACAGCACAAAC-3' (antisense); and β2-microglobin, 5'-TGAGTGCTGTCTCCATGTTTGA -3' (sense) and 5'-TCTGCTCCCCACCTCTAAGTTG-3' (antisense).

Immunoassay for human SDF-1

1X 10^6 fibroblasts were cultured in DMEM with 2% FCS on a 10 cm culture plate for 2 days. The supernatants were harvested and SDF-1 levels were measured using a commercially available SDF-1 ELISA kit (R&D Systems).

Evaluation of angiogenesis in xenograft tumors

Vascular densities and volumes in stroma-reconstructed xenograft tumors at 55-58 days after injection were evaluated according to the following procedures. Serial sections (taken at 2 mm intervals) were prepared from various fibroblast-containing MCF-7-ras tumors. A total of 30 sections from 6 independent tumors of each type were immunostained using an anti-CD31 antibody. Microvessel density (i.e., the number of vessels per microscopic field) was assessed in the three most highly vascularized areas in each section, as described previously (Weidner et al., 1991). Briefly, highly vascularized areas were identified by scanning tissue sections at low power (x100). Microvessel density was then manually counted at high magnification (x400). After taking these counts, a 49-point Chalkley point eyepiece graticule (Klarmann Rulings, Inc., NH) was employed over the same tissue section and the number of graticular points (at x400 magnification) that fell within the lumen of vessels was counted (Fox et al., 1995).

Endothelial progenitor Assay

4X10^4 bone marrow-derived Sca1/CD31 double-positive cells were seeded onto CAF or normal fibroblast layers. After 5 weeks of co-culture in DMEM+2% FCS, Dil-labeled-acetylated-LDL was added to the culture medium and the cells was incubated (1μg/ml; Intracel) at 37°C for an additional 5 hrs. Cells were then fixed in 2% PFA for 10 min and incubated with FITC-conjugated *Ulex europaeus agglutinin* I (lectin) (10 μg/ml in 10 mM Hepes pH 7.5, and 150 mM NaCl) (Vector laboratories, Inc., CA) for 1 hr (Hatzopoulos et al., 1998). Adherent colonies positive for both acetylated-LDL-uptake and lectin-binding were visualized using a fluorescence microscopy and counted.

Flow Cytometry

10^5 mononuclear cells from mouse peripheral blood, or 10^6 cells dissociated from xenograft tumors were incubated for 20 min at 4°C with the following antibodies: Anti-FITC- or PE-conjugated Sca-1, anti-PE- or allophycocyanin (APC)-conjugated CD31, and anti-FITC-conjugated CXCR4 (BD PharMingen). For discrimination and exclusion

of dead cells, mononuclear blood cells were incubated with propidium iodide (5 ng/μl) (Becton Dickinson) and tumor-derived cells were incubated with 7-Amino-actinomycin D (7-AAD) (40 μl/10^6 cells) (BD PharMingen). Cells were analyzed in two or three color flow cytometry using a Coulter Elite flow cytometer (Beckman Coulter).

***In vitro* transmigration assay**

$1x10^5$ fibroblasts were seeded in the lower well of a 24-well chamber two days prior to co-culture. Whole bone marrow cells from GFP-transgenic mice (Ikawa et al., 1995) were incubated with anti-PE-conjugated-Sca1 and APC-conjugated-CD31 antibodies (BD PharMingen). GFP/Sca1/CD31 triple-positive cells were sorted using a BD flow cytometer and $4x10^4$ GFP/Sca1/CD31 triple-positive cells were seeded in DMEM+2% FCS in the upper well of a transwell chamber with a 5 μm pore size (Costar, MA). Control GFP-labeled Sca1/CD31-depleted populations were also seeded in an identical manner.

For antibody neutralizing experiments, an anti-SDF-1 neutralizing antibody (10 or 20 μg/ml) or control mouse IgG1 (20 μg/ml) (R & D Systems) was applied to the supernatant in the lower wells (n=4) 24 hrs prior to the co-culture. GFP-positive cells that migrated into the lower wells were counted under a microscope at 18 hrs after co-culture. All assays were performed in 4-5 independent wells. Three random fields were counted per well under a fluorescent microscope (magnification, x200). The chemotaxis index was calculated as the number of cells that migrated into the lower chamber, normalized in each experiment to the baseline value observed in the absence of any fibroblasts plated in the lower chamber.

ACKNOWLEDGMENTS

We would like to thank Dr. Todd R. Golub for help of DNA microarray experiment and critical reading of this manuscript, Dr. Fernando Arenzana-Seisdedos for anti-SDF-1 (K15C), Dr. Charlotte Kuperwasser for help of isolation of fibroblasts from human breast tissues, Drs Ittai Ben-Porath, Kimberly Hartwell, Nir Hacohen, Konrad Hochedlinger and Chengcheng Zhang for critical reading of this manuscript and Drs Paul Matsudaira, S.A. Mani, and Sridhar Ramaswamy for helpful experimental suggestions and data analysis and, members of R.A.W.'s laboratory for helpful comments and discussion. This work was supported by Merck/MIT (R.A.W.), the NIH/NCI grant R21CA87081-02 (R.A.W.), Uehara Memorial Foundation (A.O.), Sankyo Foundation of Life Science (A.O.), US Army Pre-doctoral Breast Cancer Fellowship DAMD17-02-1-0468 (P.G). R.A.W. is an American Cancer Society Research Professor and a Daniel K. Ludwig Cancer Research Professor.

References

Askari, A.T., Unzek, S., Popovic, Z.B., Goldman, C.K., Forudi, F., Kiedrowski, M., Rovner, A., Ellis, S.G., Thomas, J.D., DiCorleto, P.E., *et al.* (2003). Effect of stromal-cell-derived factor 1 on stem-cell homing and tissue regeneration in ischaemic cardiomyopathy. Lancet *362*, 697-703.

Barcellos-Hoff, M.H., and Ravani, S.A. (2000). Irradiated mammary gland stroma promotes the expression of tumorigenic potential by unirradiated epithelial cells. Cancer Res *60*, 1254-1260.

Berking, C., Takemoto, R., Schaider, H., Showe, L., Satyamoorthy, K., Robbins, P., and Herlyn, M. (2001). Transforming growth factor-beta1 increases survival of human melanoma through stroma remodeling. Cancer Res *61*, 8306-8316.

Bertolini, F., Paul, S., Mancuso, P., Monestiroli, S., Gobbi, A., Shaked, Y., and Kerbel, R.S. (2003). Maximum tolerable dose and low-dose metronomic chemotherapy have opposite effects on the mobilization and viability of circulating endothelial progenitor cells. Cancer Res *63*, 4342-4346.

Bissell, M.J., and Radisky, D. (2001). Putting tumours in context. Nat Rev Cancer *1*, 46-54.

Coussens, L.M., Tinkle, C.L., Hanahan, D., and Werb, Z. (2000). MMP-9 supplied by bone marrow-derived cells contributes to skin carcinogenesis. Cell *103*, 481-490.

Coussens, L.M., and Werb, Z. (2002). Inflammation and cancer. Nature *420*, 860-867.

Cunha, G.R., Hayward, S.W., Wang, Y.Z., and Ricke, W.A. (2003). Role of the stromal microenvironment in carcinogenesis of the prostate. Int J Cancer *107*, 1-10.

Dublin, E., Hanby, A., Patel, N.K., Liebman, R., and Barnes, D. (2000). Immunohistochemical expression of uPA, uPAR, and PAI-1 in breast carcinoma. Fibroblastic expression has strong associations with tumor pathology. Am J Pathol *157*, 1219-1227.

Elenbaas, B., Spirio, L., Koerner, F., Fleming, M.D., Zimonjic, D.B., Donaher, J.L., Popescu, N.C., Hahn, W.C., and Weinberg, R.A. (2001). Human breast cancer cells generated by oncogenic transformation of primary mammary epithelial cells. Genes Dev *15*, 50-65.

Fox, S.B., Leek, R.D., Weekes, M.P., Whitehouse, R.M., Gatter, K.C., and Harris, A.L. (1995). Quantitation and prognostic value of breast cancer angiogenesis: comparison of microvessel density, Chalkley count, and computer image analysis. J Pathol *177*, 275-283.

Fukumura, D., Xavier, R., Sugiura, T., Chen, Y., Park, E.C., Lu, N., Selig, M., Nielsen, G., Taksir, T., Jain, R.K., and Seed, B. (1998). Tumor induction of VEGF promoter activity in stromal cells. Cell *94*, 715-725.

Hanahan, D., and Folkman, J. (1996). Patterns and emerging mechanisms of the angiogenic switch during tumorigenesis. Cell *86*, 353-364.

Hasebe, T., Sasaki, S., Imoto, S., and Ochiai, A. (2000). Proliferative activity of intratumoral fibroblasts is closely correlated with lymph node and distant organ metastases of invasive ductal carcinoma of the breast. Am J Pathol *156*, 1701-1710.

Hatzopoulos, A.K., Folkman, J., Vasile, E., Eiselen, G.K., and Rosenberg, R.D. (1998). Isolation and characterization of endothelial progenitor cells from mouse embryos. Development *125*, 1457-1468.

Heissig, B., Hattori, K., Dias, S., Friedrich, M., Ferris, B., Hackett, N.R., Crystal, R.G., Besmer, P., Lyden, D., Moore, M.A., *et al.* (2002). Recruitment of stem and progenitor cells from the bone marrow niche requires MMP-9 mediated release of kit-ligand. Cell *109*, 625-637.

Hinz, B., Celetta, G., Tomasek, J.J., Gabbiani, G., and Chaponnier, C. (2001). Alpha-smooth muscle actin expression upregulates fibroblast contractile activity. Mol Biol Cell *12*, 2730-2741.

Iacobuzio-Donahue, C.A., Argani, P., Hempen, P.M., Jones, J., and Kern, S.E. (2002). The desmoplastic response to infiltrating breast carcinoma: gene expression at the site of primary invasion and implications for comparisons between tumor types. Cancer Res *62*, 5351-5357.

Ikawa, M., Kominami, K., Yoshimura, Y., Tanaka, K., Nishimune, Y., and Okabe, M. (1995). A rapid and non-invasive selection of transgenic embryos before implantation using green fluorescent protein (GFP). FEBS Lett *375*, 125-128.

Ishii, G., Sangai, T., Oda, T., Aoyagi, Y., Hasebe, T., Kanomata, N., Endoh, Y., Okumura, C., Okuhara, Y., Magae, J., *et al.* (2003). Bone-marrow-derived myofibroblasts contribute to the cancer-induced stromal reaction. Biochem Biophys Res Commun *309*, 232-240.

Jacobs, T.W., Byrne, C., Colditz, G., Connolly, J.L., and Schnitt, S.J. (1999). Radial scars in benign breast-biopsy specimens and the risk of breast cancer. N Engl J Med *340*, 430-436.

Kalka, C., Masuda, H., Takahashi, T., Kalka-Moll, W.M., Silver, M., Kearney, M., Li, T., Isner, J.M., and Asahara, T. (2000). Transplantation of ex vivo expanded endothelial progenitor cells for therapeutic neovascularization. Proc Natl Acad Sci U S A *97*, 3422-3427.

Kasid, A., Lippman, M.E., Papageorge, A.G., Lowy, D.R., and Gelmann, E.P. (1985). Transfection of v-rasH DNA into MCF-7 human breast cancer cells bypasses dependence on estrogen for tumorigenicity. Science *228*, 725-728.

Koukourakis, M.I., Giatromanolaki, A., Brekken, R.A., Sivridis, E., Gatter, K.C., Harris, A.L., and Sage, E.H. (2003). Enhanced expression of SPARC/osteonectin in the tumor-associated stroma of non-small cell lung cancer is correlated with markers of hypoxia/acidity and with poor prognosis of patients. Cancer Res *63*, 5376-5380.

Kurose, K., Gilley, K., Matsumoto, S., Watson, P.H., Zhou, X.P., and Eng, C. (2002). Frequent somatic mutations in PTEN and TP53 are mutually exclusive in the stroma of breast carcinomas. Nat Genet *32*, 355-357.

Lin, E.Y., Nguyen, A.V., Russell, R.G., and Pollard, J.W. (2001). Colony-stimulating factor 1 promotes progression of mammary tumors to malignancy. J Exp Med *193*, 727-740.

Lohr, M., Schmidt, C., Ringel, J., Kluth, M., Muller, P., Nizze, H., and Jesnowski, R. (2001). Transforming growth factor-beta1 induces desmoplasia in an experimental model of human pancreatic carcinoma. Cancer Res *61*, 550-555.

Lyden, D., Hattori, K., Dias, S., Costa, C., Blaikie, P., Butros, L., Chadburn, A., Heissig, B., Marks, W., Witte, L., *et al.* (2001). Impaired recruitment of bone-marrow-derived endothelial and hematopoietic precursor cells blocks tumor angiogenesis and growth. Nat Med *7*, 1194-1201.

Olumi, A.F., Grossfeld, G.D., Hayward, S.W., Carroll, P.R., Tlsty, T.D., and Cunha, G.R. (1999). Carcinoma-associated fibroblasts direct tumor progression of initiated human prostatic epithelium. Cancer Res *59*, 5002-5011.

Orimo, A., Tomioka, Y., Shimizu, Y., Sato, M., Oigawa, S., Kamata, K., Nogi, Y., Inoue, S., Takahashi, M., Hata, T., and Muramatsu, M. (2001). Cancer-associated myofibroblasts possess various factors to promote endometrial tumor progression. Clin Cancer Res *7*, 3097-3105.

Pablos, J.L., Amara, A., Bouloc, A., Santiago, B., Caruz, A., Galindo, M., Delaunay, T., Virelizier, J.L., and Arenzana-Seisdedos, F. (1999). Stromal-cell derived factor is expressed by dendritic cells and endothelium in human skin. Am J Pathol *155*, 1577-1586.

Pinheiro J. and Bates D., (2000). Mixed effects models in s and splus, NY: Springer.

Ronnov-Jessen, L., Petersen, O.W., and Bissell, M.J. (1996). Cellular changes involved in conversion of normal to malignant breast: importance of the stromal reaction. Physiol Rev *76*, 69-125.

Ronnov-Jessen, L., Petersen, O.W., Koteliansky, V.E., and Bissell, M.J. (1995). The origin of the myofibroblasts in breast cancer. Recapitulation of tumor environment in culture unravels diversity and implicates converted fibroblasts and recruited smooth muscle cells. J Clin Invest *95*, 859-873.

Ronnov-Jessen, L., Van Deurs, B., Nielsen, M., and Petersen, O.W. (1992). Identification, paracrine generation, and possible function of human breast carcinoma myofibroblasts in culture. In Vitro Cell Dev Biol *28A*, 273-283.

Sappino, A.P., Skalli, O., Jackson, B., Schurch, W., and Gabbiani, G. (1988). Smooth-muscle differentiation in stromal cells of malignant and non-malignant breast tissues. Int J Cancer *41*, 707-712.

Serini, G., and Gabbiani, G. (1999). Mechanisms of myofibroblast activity and phenotypic modulation. Exp Cell Res *250*, 273-283.

Shao, Z.M., Nguyen, M., and Barsky, S.H. (2000). Human breast carcinoma desmoplasia is PDGF initiated. Oncogene *19*, 4337-4345.

Sieweke, M.H., Thompson, N.L., Sporn, M.B., and Bissell, M.J. (1990). Mediation of wound-related Rous sarcoma virus tumorigenesis by TGF-beta. Science *248*, 1656-1660.

Silzle, T., Randolph, G.J., Kreutz, M., and Kunz-Schughart, L.A. (2004). The fibroblast: sentinel cell and local immune modulator in tumor tissue. Int J Cancer *108*, 173-180.

Skobe, M., and Fusenig, N.E. (1998). Tumorigenic conversion of immortal human keratinocytes through stromal cell activation. Proc Natl Acad Sci U S A *95*, 1050-1055.

Tlsty, T.D. (2001). Stromal cells can contribute oncogenic signals. Semin Cancer Biol *11*, 97-104.

Tokunou, M., Niki, T., Eguchi, K., Iba, S., Tsuda, H., Yamada, T., Matsuno, Y., Kondo, H., Saitoh, Y., Imamura, H., and Hirohashi, S. (2001). c-MET expression in myofibroblasts: role in autocrine activation and prognostic significance in lung adenocarcinoma. Am J Pathol *158*, 1451-1463.
Tuxhorn, J.A., McAlhany, S.J., Dang, T.D., Ayala, G.E., and Rowley, D.R. (2002). Stromal cells promote angiogenesis and growth of human prostate tumors in a differential reactive stroma (DRS) xenograft model. Cancer Res *62*, 3298-3307.
Weidner, N., Semple, J.P., Welch, W.R., and Folkman, J. (1991). Tumor angiogenesis and metastasis--correlation in invasive breast carcinoma. N Engl J Med *324*, 1-8.